SPRAY REGIME OPERATION OF SIEVE PLATES

A thesis submitted for the degree of

Doctor of Philosophy of the University of London

and for the Diploma of Imperial College

by

M. MANICKAMPILLAI B.Sc. (Eng.)

March 1980

Department of Chemical Engineering and Chemical Technology

Imperial College of Science and Technology

London, S.W.7.

ABSTRACT

A critical re-examination was conducted of the work on the spray regime operation of a sieve plate column by employing systems other than air-water. In the course of these investigations it was found that, although the effect of surface tension was adequately incorporated by some of the previous workers, there was a strong effect of viscosity which went undetected. This affected the drop projection velocity, mean drop diameter, entrainment and transition point. As a result existing correlations were modified and a new correlation developed for the froth-spray transition by analogy to a flooding correlation.

A study was also conducted on the effect of colloidal suspensions on dispersion hydrodynamics. No effect was observed in either the foam or the froth regimes so that the reports received from industry could be discounted.

Finally, an attempt was made to develop a model for the relation between point and plate efficiency. The so-called 'forward-jump' model correlated existing data better than the existing model and was also able to accommodate the liquid throughput on the plate.

ACKNOWLEDGEMENTS

I am extremely grateful to Professor H. Sawistowski for his precious advice and encouragement during the course of this work.

Valuable assistance from the technical staff of the department is gratefully acknowledged, in particular from Messrs. A. Harrup and R. Wood.

My thanks are also due to the Science Research Council for their financial support.

TABLE OF CONTENTS

		Page
CHAPTER ONE	INTRODUCTION	1
CHAPTER TWO	LITERATURE SURVEY	3
	2.1 Hydrodynamic Characteristics of Sieve Plates	3
	2.1.1 Introduction	3
	2.1.2 Hydrodynamic Regimes	3
	2.1.3 Foam Characteristics	9
	2.1.4 Froth Characteristics	11
	2.1.5 Spray Characteristics	12
	2.1.5.1 Droplet Formation	12
	2.1.5.2 Droplet Trajectory	16
	2.1.5.2.1 Initial Projection Velocity	16
	2.1.5.2.2 Trajectory	16
	2.1.5.3 Drop Size Distribution	19
	2.1.6 Froth-Spray Transition	21
	2.1.6.1 Transition Determination	22
	2.1.6.2 Transition Correlations	28
	2.2 Performance Characteristics of Sieve Plates	29
	2.2.1 Concept of Performance	29
	2.2.2 Basic Definitions	29
	2.2.3 Mass Transfer Relationships	30
	2.2.4 Effect of Surface Tension on Plate Performance	33
	2.3 Modelling of the Spray Regime	36
	2.3.1 Fluidization Model	36
	2.3.2 Free Trajectory Model	36
	2.4 Entrainment	39

		Page
CHAPTER THREE	EXPERIMENTAL	42
3.1	Introduction	42
3.2	Test Rig - 1	44
3.2.1	Description	44
3.2.2	Experimental Procedure	44
3.3	Test Rig - 2	49
3.3.1	Description	49
3.4	Gamma Radiation Technique to Measure the Dispersion Density Profile	52
3.4.1	Principle	52
3.4.2	Description	54
3.4.3	Calibration of the Gamma Ray Traverse System	54
3.5	Light Transmission Technique	57
3.5.1	Principle	57
3.5.2	Description	61
3.6	Experimental Procedure	61
CHAPTER FOUR	RESULTS	64
4.1	Introduction	64
4.2	Effect of Colloidal Suspension on Foaming	65
4.3	Transition Point	65
4.4	Parameters Affecting Dispersion	69
4.4.1	Effect of Viscosity	69
4.4.2	Effect of Surface Tension	72
4.5	Effect of Operating Variables	75
4.6	Effect of Colloidal Suspensions	75
4.7	Entrainment	80

		Page
CHAPTER FIVE	INITIAL PROJECTION VELOCITY	83
	5.1 Introduction	83
	5.2 Mechanism of Droplet Formation	84
	5.3 Total Pressure Drop	85
	5.4 Residual Pressure Drop	87
	5.4.1 Liquid Shearing	87
	5.4.2 Formation of Interfacial Area	89
	5.4.3 Projection of Droplets	90
	5.4.3.1 Effect of Hole Diameter	90
	5.4.4 Momentum Transfer	91
	5.5 Proposed Correlation	93
CHAPTER SIX	EFFICIENCY PREDICTION	98
	6.1 Introduction	98
	6.2 Description of Model	99
	6.3 Formulation of Models	100
	6.3.1 Model 1	100
	6.3.2 Model 2	103
	6.4 Discussion of Models	107
	6.4.1 Effect of Varying the Number of Pools on Efficiency	108
	6.4.2 Effect of Change in Non-Atomised Fraction of Liquid Flow on Efficiency	112
	6.4.3 Effect of Variation in mG/L on Efficiency	112
	6.5 Determination of the Volumetric Liquid Flowrate	119
	6.5.1 Droplet Trajectories	119
	6.5.2 Experimental Dispersion Density Profile	120
	6.5.3 Height-Velocity-Residence Time Relation	121

Page

6.5.4 Volume Flowrate in Spray 123

6.5.5 Volume Flowrate on Tray Floor 124

6.5.6 Mass Transfer 125

6.6 Testing of the Models 126

CHAPTER SEVEN DISCUSSION 129

7.1 Introduction 129

7.2 Factors Affecting Dispersion in the Foam Regime 129

7.3 Factors Affecting Phase Transition 131

7.4 Factors Affecting Dispersion in the Spray Regime 132

7.5 Efficiency Prediction 135

CHAPTER EIGHT CONCLUSIONS 137

8.1 Conclusions 137

8.2 Future Work 138

NOMENCLATURE 139

BIBLIOGRAPHY 142

APPENDIX 1 APPARENT FOAM DENSITY BY THE γ-RADIATION ABSORPTION TECHNIQUE 151

APPENDIX 2 EXPERIMENTAL RESULTS 154

APPENDIX 3 PROGRAM LISTINGS 176

CHAPTER ONE

INTRODUCTION

Sieve plates are widely used in process industries on account of their low cost, simplicity of construction and flexibility in operation. Furthermore, considerable research on sieve plates has shown that their turndown ratio is satisfactory even for large industrial columns.

It is well established that the hydrodynamic regime in which the plate is operating has a significant influence on the mass transfer performance of the plate. This depends on the process variables, design parameters and systems physical properties. Apart from the investigation of the effect of colloidal suspensions main interest in this work was confined to spray regime and its delineation. This regime is present at high gas or vapour velocities when liquid is continuously atomised at the plate floor and the droplets thus produced present the major contribution to interfacial area for mass transfer.

Most of the fundamental work on the spray regime, in particular on its delineation and on the formulation of equations for projection velocity, was based on the system air/water. This may have produced correlations of limited applicability, disguised some important effects and even led to the acceptance of wrong models. For this reason it was decided to employ systems which cover a range of variations in physical properties, particularly viscosity and surface tension, considered to be the two most important properties in the drop formation stage. It was intended to re-examine the existing correlations in the light of the results obtained.

A further limitation of the existing work is the lack of a suitable relation between point and plate efficiencies. Although the free-trajectory model has been successfully applied to point efficiencies, its extension to the prediction of plate efficiencies has proved largely unsatisfactory since the proposed models were unable to accommodate the proven liquid-handling capacity of the tray. The second objective of the work was therefore the development of a model relating point to plate efficiency in the spray regime.

Finally, it was decided to investigate the effect of the presence of colloidal suspensions on plate performance. For industrial reasons this aspect was given a wider context and the effect studied both under foam and spray conditions.

CHAPTER TWO

LITERATURE SURVEY

2.1 Hydrodynamic Characteristics of Sieve Plates

2.1.1 Introduction

A short description of the different hydrodynamic regimes is given. Attention is mainly focussed on the spray regime and its delineation. This is followed by a discussion of different hydrodynamic models proposed and their role in predicting mass transfer performance. A short review of relevant mass transfer concepts and the present state of knowledge of point efficiency and its relation to plate efficiency is discussed.

2.1.2 Hydrodynamic Regimes

The type of dispersion formed on a sieve plate is dependent on various factors such as design parameters, operating variables and physical properties of the phases. The different hydrodynamic regimes in which a particular tray is operating for varying gas flowrates may be illustrated by the variation of the volumetric fraction of liquid in the dispersion (dispersion density) with gas flowrate, as shown in Fig. 2.1.

Region a-b. Free bubbling exists in this region and the dispersion density falls rapidly as the gas flowrate increases.

Region b-c"-c With increasing gas flowrate bubbles begin to accumulate at the surface forming a closely packed structure, the height of which is determined by the dynamic equilibrium between the rate of bubble

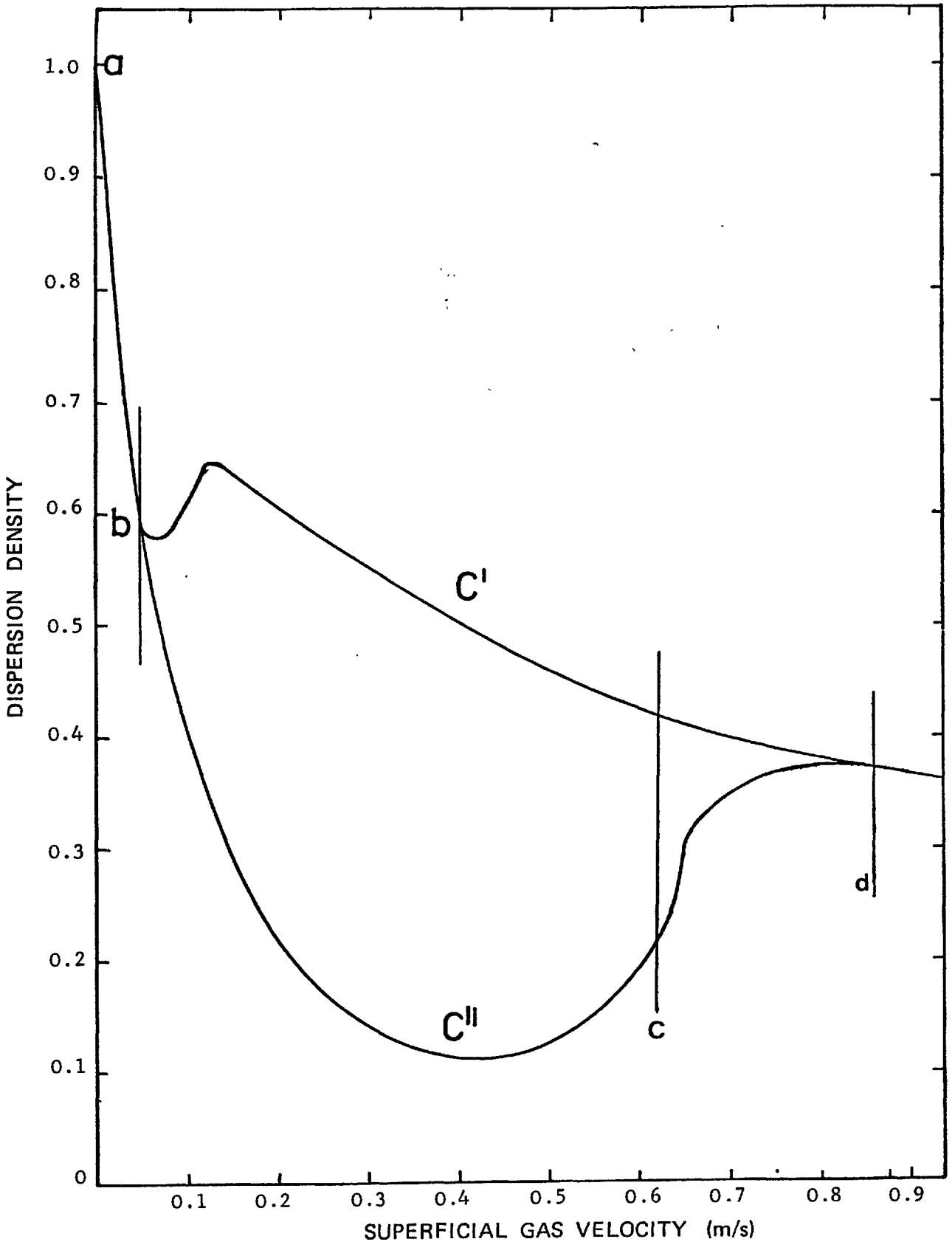


Fig. 2.1 Flow regime diagram.

coalescence at the free interface and their arrival at the bottom of the foam layer. This gives the cellular foam regime. Bubbles move upwards in counter-current to the liquid which is being drained through the separating lamellae. The rigid structure of the cellular foam breaks down with further increase in gas flowrate and the foam becomes mobile. The liquid lamellae thicken and the dispersion density increases.

Region c-d — With gradual increase in gas flowrate the foam degenerates into froth. Froth can be defined as a turbulent gas-liquid dispersion in which liquid is the continuous phase. Bubbles of different sizes are formed including the appearance of large bubbles, known as gas voids, at higher gas rates. Formation of gas voids can be regarded as a stage towards intermittent jetting.

Region d-e — With further increase in gas flowrate phase inversion occurs leading to spray regime where gas is the continuous phase and liquid is the dispersed phase. The system thus described (path taken abc"cde) is typical of a surface tension positive system. This is a system in which surface tension increases with decreasing concentration of more volatile component in the reflux.

Region b-c'-c — There are systems which do not follow the flow pattern described above. These are the surface tension negative systems. A negative system is one in which

the surface tension decreases with decreasing concentration of the more volatile component. In such a case the rate of bubble coalescence is too rapid to allow for foam formation and there is a direct transition from free bubbling to froth and then to spray.

The regimes previously described are arbitrary and the transition between them not clearly defined. Thus Muller and Prince[24], who also studied the transition between regimes in terms of liquid holdup and vapour flowrate, divided the flow regime into six different types by relating it to phenomena at bubble formation.

At high liquid holdup and low gas velocities discrete bubbles are formed. This they called perfect bubbling and it corresponds to the free bubbling regime as previously described. With increasing gas flowrate bubbles became distorted leading to deformed bubbling with severe circulation and turbulence. This corresponds to the froth regime. In these two regimes because of the high liquid holdup bubbles could be formed fully at the orifice and detach before breaking the surface. At low liquid holdup and low gas velocities imperfect bubbling was observed. Bubbles break the surface before they are fully formed. At very low liquid holdup vapour jets through the orifice forming a liquid meniscus. Liquid is held to the plate by surface tension forces. With further increase in gas velocity, gas interacts with the liquid, stripping off droplets from the thin liquid film dragged up by the gas. This leads to steady jetting. Increasing the liquid holdup at constant gas velocity results in a pulsating jet regime. As the jet expands liquid enters the jet and as it contracts

liquid is thrown upwards in the form of sheets which break into droplets. From these studies Muller and Prince constructed a diagram showing the transition between various regimes [Fig. 2.2]. Free bubbling, meniscus flow and steady jetting are not considered to be of practical importance under normal operating conditions.

Hofhuis and Zuiderweg[3] studied the flow regimes on sieve trays using the gamma ray absorption technique and identified four regimes. These are spray, free bubbling, emulsified flow and mixed froth respectively (Fig. 2.3). They defined emulsified flow as the regime in which large proportion of the gas is emulsified by the high liquid velocity. This regime was observed at high liquid-vapour ratio. In the mixed froth regime both bubbling and spraying occur simultaneously. The two regimes of importance for industrial applications are froth and spray.

It was shown by Fane and Sawistowski[1], who measured the dispersion density profile using the gamma ray absorption technique, that each regime has associated with it its own characteristic dispersion density profile (Fig. 2.4). It is clear from the diagram that the dispersion density profile for various operating regimes is a function of height above the plate floor[4,5], thus explaining the non-homogeneity of the dispersion. In the foam regime, there is a steady decrease in dispersion density with increasing height due to thinning of the lamellae, where froth is characterised by a zone of constant density at a short distance from the plate floor indicating a region of almost perfect mixing.

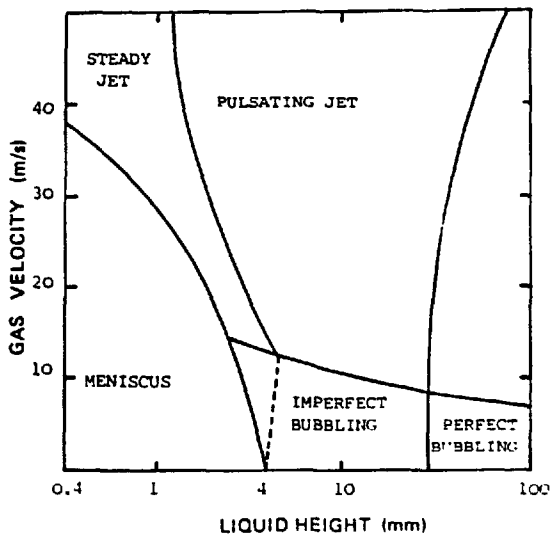


Fig. 2.2

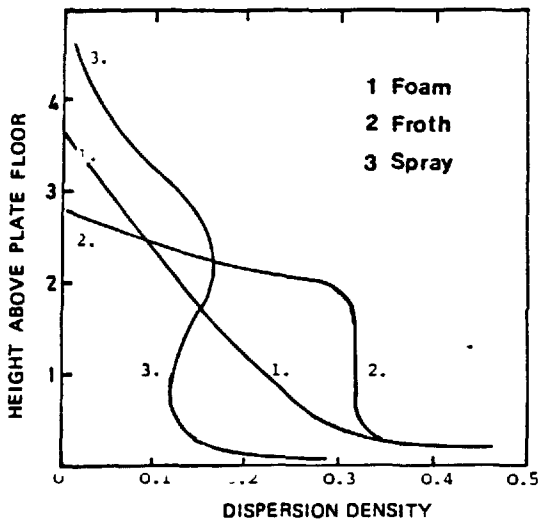


Fig. 2.4

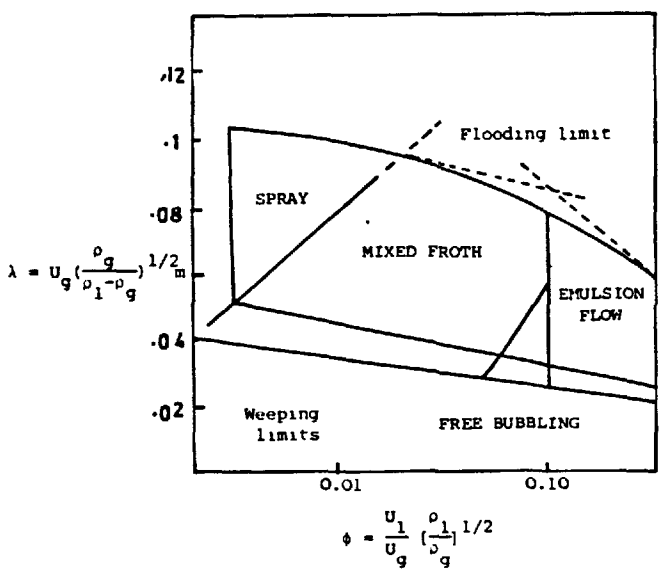


Fig. 2.3 FLOW REGIME DIAGRAM

FIOW REGIME DIAGRAMS

Fig. 2.2 Muller and Prince

Fig. 2.3 Hofhuis and Zuiderweg

Fig. 2.4 Fane and Sawistowski

2.1.3 Foam Characteristics

Foaming in distillation columns can have disastrous effects on performance, due to the following reasons:

1. flooding of the column
2. entrainment of the liquid
3. contamination of the product
4. low throughput, i.e. below design capacity.

Calderbank & Rennie[7] described foam as large cellular relatively stable bubbles in close proximity. The cellular structure of the bubbles is the unique feature of this regime observed by all the investigators who studied it.

The ability of a liquid to form a stable film is the criterion which decides whether the given system will operate in the foam regime at low gas flowrates. It is a known fact that pure liquids cannot sustain a stable foam. The presence of a surface active agent in pure liquids gives the film its stability and hence a stable foam. The surface activity of a solute is defined as its ability to lower the surface or interfacial tension of the solvent. Foam stability can be explained by means of the Gibbs adsorption equation[8].

The Gibbs function is given by

$$dG = VdP - SdT - \gamma dA \qquad (2.1)$$

where γ = surface tension of the liquid

A = surface area

$$\gamma = \left(\frac{\partial G}{\partial A}\right)_{P,T} \qquad (2.2)$$

integrating equation 2 gives

$$\Delta G = \gamma \Delta A \qquad (2.3)$$

where

ΔG = change of the free energy at constant temperature and pressure.

Equation 2.3 gives an explanation why pure liquids cannot sustain a stable foam. There is a decrease in the Gibbs function, when foam collapses because of the decrease in area. Hence a foam composed of a pure liquid is thermodynamically unstable. Presence of a surface active agent brings in an additional free energy term required in equation 2.3 to ensure thermodynamic stability of the foam. This comes from the work that must be done to transfer the solute molecules from the surface to the bulk phase, bearing in mind that surface or interfacial tension can only be lowered, if the solute is positively adsorbed at the surface or interface. When bubbles coalesce there is a reduction in surface area and simultaneous transfer of solute from the surface to the bulk. If the loss in free energy resulting from the $\gamma\Delta A$ term as a result of foam collapse, is greater than the gain in the free energy as a result of the transfer of the solute, then spontaneous coalescence will not occur and the foam will be thermodynamically stable.

Kitchener and Cooper[9] pointed out that the property which distinguishes foaming from non-foaming liquids is the ability to resist excessive localized thinning of a membrane of liquid, while a controlled general thinning proceeds.

Foam stabilization due to Marangoni effect can be explained as follows. Wherever a region of higher surface tension is created,

contraction of the surface at that point immediately begins and the surrounding areas of lower surface tension are pulled in towards this point until the difference is equalised.

Stabilisation of the foam as a result of mass-transfer-induced surface tension gradient is discussed in detail in section 2.2.4. In general, surface tension positive systems[1] favour cellular foam buildup. de Goederen[10] came to the conclusion that decrease in the absolute value of surface tension aids foam stabilisation. Effect of plate characteristics on foaming was studied by Rennie and Evans[11]. They found small diameter holes, large free area and low liquid flow-rates to encourage foaming. Schroter[12] found that the presence of foam baffles, high overflow weirs, and the side walls acted in the same way.

Presence of impurities are also known to have an effect on foaming[13], by their influence on interfacial forces. There has been some suggestions from industry[14] that the presence of traces of colloidal substances resulting from corrosion of mild steel and aluminium columns caused severe foaming. This phenomenon is discussed later.

2.1.4 Froth Characteristics

Froth can be described as a turbulent gas liquid dispersion in which liquid is the continuous phase. For a long time froth was thought[15-18] to be composed of bubbles of approximately constant size of 4.5 mm in diameter and was regarded independent of operating conditions and physical properties. In large columns operating at high throughput large bubbles known as gas voids were, however observed[19] of diameters 20-30 mm. This variation in size distribution

of bubbles was explained by Sawistowski[20] as due to the phase shift in the time dependence of bubble growth at different holes on account of constancy of pressure below a plate. This disturbs the flow pattern of liquid across the plate and leads to its oscillatory behaviour. Local fluctuation of the liquid seal leads to the formation of bubbles of different sizes. Large bubbles can be assumed to have a constant residence time equal to the time of vertical rise through the dispersion. Since most of the gas passes through the plate in the form of large bubbles, their effect is to decrease the plate efficiency in the froth regime. This reduction in plate efficiency in the froth regime with increasing gas flowrate has led to the introduction of baffles which increased plate efficiency by suppressing liquid oscillation and thus reducing or eliminating bubble voids[21].

2.1.5 Spray Characteristics

2.1.5.1 Droplet Formation

Understanding of the mechanism of droplet formation and hence the formation of interfacial area is critical because the mass transfer performance of the plate is proportional to the surface area of the droplets. Surface tension forces are known to affect the formation of interfacial area differently in the froth and spray regimes, and hence has an important effect on the magnitude of the interfacial area and consequently on plate performance. It is independent of surface tension in the froth[10] and inversely proportional to it in the spray[1,10,59]. Therefore the understanding of the orifice behaviour which holds the key to the understanding of the mechanism of droplet formation, is essential in order to formulate a mathematical model for the spray.

Lindsey and Sawistowski[85] carried out extensive photographic studies on drop formation above both a single orifice and a multi-orifice sieve plate using still and cine photography. Although single orifice behaviour is not representative of a multiorifice plate, it gives some indication of the mechanism of droplet formation.

According to the photographic studies of Lindsey and Sawistowski the mechanism of droplet formation is a cyclic process. As the bubble grows, the film stretches, and the liquid outside drains by gravity. Thinning causes the upper surface of the bubble to burst, producing very fine droplets. The resulting conical liquid sheet breaks up into vertical ligaments and the ligaments break-up into relatively large drops as a result of hydrodynamic instability. Lindsey failed to observe continuous jetting as described by Prince[49] for the range of hole velocities and liquid submergence studied.

The cyclic nature was also observed on the multiorifice sieve plate. However, due to bubble interaction and smaller chamber pressure fluctuations, the frequency of bubble formation was increased.

Among others who studied the mechanism of drop formation are Spells[25-27], Muller and Prince[24], Nielson et al[28], Newitt[29] and Teller and Rood[30]. Spells and Bakowski investigated the mechanism of bubble formation by means of high speed cinematography, both in rectangular single slots and multiple slots. They observed two distinct mechanisms of droplet formation depending on liquid holdup. Deep mechanism, where discrete bubbles were formed, occurred when the liquid holdup exceeded a critical value. Shallow mechanism, where vapour channelling was observed, occurred for holdup less than this critical value. This shallow mechanism corresponds to chain bubbling or the pulsating jet regime of Muller and Prince[24], who

described the pulsating jet behaviour of the orifice from high speed cine photography as follows:

As the gas expands due to shearing of the liquid, the pressure within the jet increases. The trapped liquid segments are pushed upwards and then break into drops, thus lowering the pressure. The process is repeated cyclically causing the pulsation effect.

From photographic studies of single orifices Nielsen et al[28] postulated continuous vapour channelling through the orifice at high gas flowrates. As a result of momentum transfer due to vapour-liquid interaction, liquid was dragged up in the form of an inverted hollow cone which broke into ligaments and then into drops.

Mechanism of drop formation as a result of bubble interaction on a multiorifice plate was the subject of study of Teller and Rood[30]. They observed that bubbles were formed individually at each orifice and as the bubbles grew they coalesced, producing a large stream of gas which on release caused sheet disintegration and ligament breakup.

Newitt et al[29] carried out experiments using air-water system and glass capillary orifices to produce bubbles. They also observed two distinct mechanisms of drop formation. As the bubbles reached the surface, liquid drained and thinning of the surface caused bubble rupture, producing very fine droplets of size less than 40 μ, leaving a well defined bubble crater. As the crater fills in the momentum of the inflowing liquid produces a jet which breaks into larger drops of the size range of several hundred microns. This behaviour is probably characteristic of drop formation in the free bubbling regime.

Pinczewski and Fell[31] monitored the hydrodynamic behaviour of a single orifice on a sieve plate, to locate the transition from froth to spray. They observed intermittent flume formation close to the

froth to spray transition, like Teller and Rood[30] and Spells[25]. From orifice studies Banerjee et al[32-33] came to the conclusion that there is a change in mechanism of drop formation from discrete bubbling to channelling with increasing gas flowrate.

CONCLUSION

It follows from these studies that different mechanisms of drop formation are responsible for droplet formation in the froth and the spray regime. In the froth regime drops result from bubble break-up whereas in the spray regime the impact of the gas jet on the liquid, which periodically covers the orifice, throws up the liquid in the form of conical sheets which disintegrate into ligaments and then into drops as the result of hydrodynamic instability.

2.1.5.2 Droplet Trajectory

It is now well established from high speed photographic studies that break-up of bubbles responsible for droplet formation in the froth and jetting is the mechanism of droplet formation in the spray. These orifice mechanisms are unique to their particular regimes.

As the high velocity vapour rushes through the orifice the liquid is dragged up in the form of conical sheets which break into ligaments and then into droplets under hydrodynamic instability. Part of the energy transferred from the gas to the liquid, as the vapour jets through the orifice is utilized for the projection of the droplets. They thus acquire an initial projection velocity and follow a well defined trajectory. Lindsey's[23] photographic studies have confirmed these trajectories to be parabolic, and he found no evidence of droplet coalescence or break-up in flight. In order to formulate a mathematical model for the spray a knowledge of the initial projection velocity and its trajectory is vital.

2.1.5.2.1 Initial Projection Velocity

Aiba and Yamada[34], Akselrod and Yusova[35], and Cheng and Teller[36], estimated the initial projection velocity by impacting drops on coated slides at various distances from the plate floor. From this information it is possible to determine the height to which a drop of a particular size would rise, and then to compute the initial projection velocity. Fane and Sawistowski[1] correlated the data of Aiba and Yamada for initial projection velocity, and utilized it in their free trajectory model. Their equation was

$$V_P = A\, d_p^{B} \qquad (2.4)$$

Nielson et al[28] proposed a model for the initial projection velocity taking into account the momentum transfer between gas and liquid. The vapour velocity in the vapour channel was related by a friction factor to the velocity of the liquid in the inverted cone from which the drops are formed. However the values of friction factor used in the model were of the order of 10 which is unrealistically high. According to Pinczewski and Fell[37], Nielson had failed to account for the momentum transfer after sheet breakup.

Pinczewski and Fell's model is based on momentum transfer after sheet break-up. Their equation for the initial projection velocity is

$$V_P = \frac{3\rho_G}{4d_P\rho_L} \int_0^t C_D V_h^2 dt \qquad (2.5)$$

where t is duration of the vapour rush and can be estimated from the size of the largest droplet formed. According to Jeronimo and Sawistowski[38] this model explains the upper envelope of projection velocities of drops in the spray regime.

Jeronimo and Sawistowski[38] correlated the initial projection velocity in terms of the relative velocity between the gas and the jet, and its break-up time following the suggestions put forward by Levich[79]. Empirical values were obtained by analysing the data of Pinczewski[80]. Their correlation was

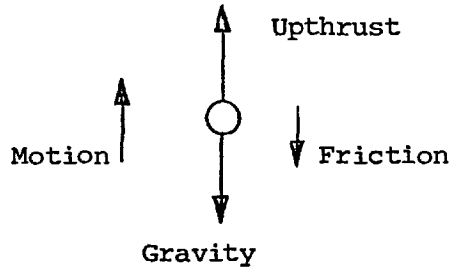
$$We_L = 207 We_G^3 \, Bo^{-1} A_f^{-2} \qquad (2.6)$$

where

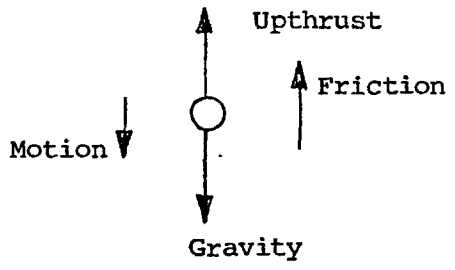
$$We_L = V_P^2 \rho_L d_H/\gamma, \quad We_G = F_S^2 d_H/\gamma \quad \text{and} \quad Bo = g\rho_L d_H^2/\gamma.$$

2.1.5.2.2 Trajectory

By taking a force balance on the droplet in the rising vapour stream, the droplet trajectory can be described. Forces acting on the droplet are



For motion upwards



For motion downwards

Force balance on the droplet gives the following equation.

For motion upwards:

$$\frac{\pi d_P^3}{6}\rho_P V\frac{dv}{dh} = \frac{\pi d_P^3}{6}\rho_G g - \frac{\pi d_P^3}{6}\rho_P g - C_D\frac{\pi d_P^2}{4}\rho_G\frac{(v-v_s)^2}{2} \qquad (2.7)$$

For motion downwards:

$$\frac{\pi d_P^3}{6}\rho_P V\frac{dv}{dh} = \frac{\pi d_P^3}{6}\rho_P g - \frac{\pi d_P^3}{6}\rho_G g - C_D\frac{\pi d^2}{4}\rho_G\frac{(v+v_s)^2}{2} \qquad (2.8)$$

where

v - vertical component of the droplet velocity

v_s - superficial velocity

ρ_P - droplet density

ρ_G - gas density

d_P - droplet diameter

C_D - drag coefficient

$$C_D = f(Re) \quad \text{where} \quad Re = \frac{d_p(v-v_s)\rho_G}{\mu_G}$$

$$\begin{aligned} Re < 2.0 \qquad & C_D = 24/Re \\ 2.0 < Re < 1000 \qquad & C_D = 18.5/Re^{0.6} \\ Re > 1000 \qquad & C_D = 0.3 \end{aligned}$$

The above correlations are taken from Hughes and Gilliland[39]. However, Jeronimo and Sawistowski[84] have shown that the effect of drag on drop trajectory is negligible. This will be discussed later.

2.1.5.3 Drop Size Distribution

An accurate knowledge of drop size distribution is of prime importance for determination of interfacial area, entrainment etc. As the high velocity vapour jets through the orifice, the liquid is thrown up in the form of cylindrical sheets, which break into ligaments and then into droplets under hydrodynamic instability. Such a complex mechanism of ligament formation and break-up imposes severe difficulties on the prediction of drop size distribution above a sieve plate and its experimental determination. However, many techniques have been developed which include

1. light-transmission and light-scattering techniques
2. impacting drops on coated slides
3. drop freezing
4. conductivity measurements
5. charge detection
6. photography
7. holography
8. automatic image analysis

Drop size distribution can often be mathematically represented by a distribution function and two parameters one of which is a mean diameter and the other a measure of the dispersion of the spray[40]. There is experimental evidence[30,34,36] to suggest that the drop size distribution above a multiorifice plate can be represented either by normal or log normal distribution function. The normal distribution function is expressed as:

$$f(x) = \frac{1}{S_n\sqrt{2\pi}} e^{-(x-\bar{x})^2/2S_n^2} \qquad (2.9)$$

where

$x = d_p$; $\bar{x} = d_{Pm}$ - mean drop size

S_n - measure of the dispersion, i.e. standard deviation

S_n^2 - variance.

For the log-normal distribution the equation is

$$f(x) = \frac{1}{xS_g\sqrt{2\pi}} e^{-(\ln x-\ln \bar{x}_{ng})^2/2S_g^2} \qquad (2.10)$$

where

x_{ng} - number geometric mean drop size

S_g - geometric standard deviation.

Empirical Distribution Functions

Drop size distribution has been correlated empirically by

1. Rosin-Rammler
2. Nukiyama and Tanasawa
3. Tate and Marshal

Mugele and Evans[41] critically examined the various distribution functions; calculated the mean diameter from drop size distribution

data and compared the means so calculated with the various means computed from the distribution functions. From this they formulated an upper-limit function, which is the log-normal distribution function, taking into consideration that there is an upper limit to the drop size.

$$f(x) = \frac{1}{S_g x\sqrt{2\pi}} e^{-\ln\left(\frac{x_m - x}{\bar{x}_n}\right)^2 / 2S_g^2} \qquad (2.11)$$

where

x_m - the maximum drop size of the spray.

2.1.6 Froth-Spray Transition

It is extremely important, from the design point of view, to determine the point at which transition occurs. This has been studied by a number of investigators in recent years. Froth to spray transition is a gradual process starting with gas breakthrough at one hole and ending with all the holes jetting. This poses the problem of the exact location of the point of phase inversion and this is far from clearcut. To overcome this problem Sawistowski[42] defined an interfacial criteria based on the effectiveness of mass transfer. He defined transition as the point which corresponds to a gas velocity above which the surface area of drops contributes significantly more to the interfacial area for mass transfer than the surface area of bubbles.

However, in order to decide whether the given system will operate in the froth or spray regime its transition point has to be determined experimentally. Techniques used to determine the transition point include:

1. optical transmittivity
2. residual pressure drop
3. frequency of liquid bridging
4. entrainment
5. acoustic analysis

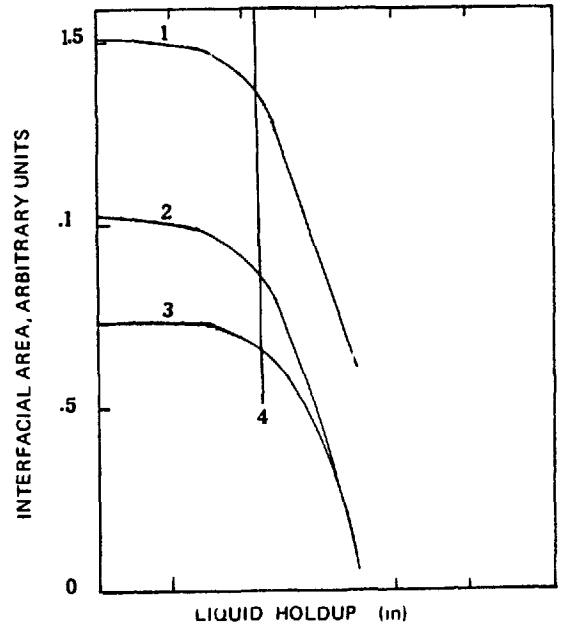
2.1.6.1 Transition Determination

Optical Transmittivity.

Porter and Wong[43] used this technique to measure the transition point, by passing a light beam through the dispersion, and measuring the change in the transmitted light intensity under spray and froth conditions. They carried out their experiment on a static sieve plate, i.e. one without liquid cross flow. By keeping the gas flowrate constant liquid was slowly added to the test plate until the dispersion changed from spray to bubbly. This was accompanied by a sharp increase in the amount of light transmitted (Fig. 2.5) as the dispersion changed from spray to froth. Jeronimo and Sawistowski [86] recalculated the data of Porter and Wong in terms of interfacial area and found that the transition point quoted by Porter and Wong was well within the fully developed interfacial area of spray. Hence, the transition velocity should be lower than predicted by these workers.

Pressure Drop:

Pressure drop as the criterion to locate the transition was utilized by Shakhov et al[45], and Burgess and Robinson[46]. Shakhov et al carried out their experiment on a large sieve plate with liquid cross flow. They observed a sharp change both in pressure drop and entrainment at the transition point. They also noted hysteresis effect (Fig. 2.6).



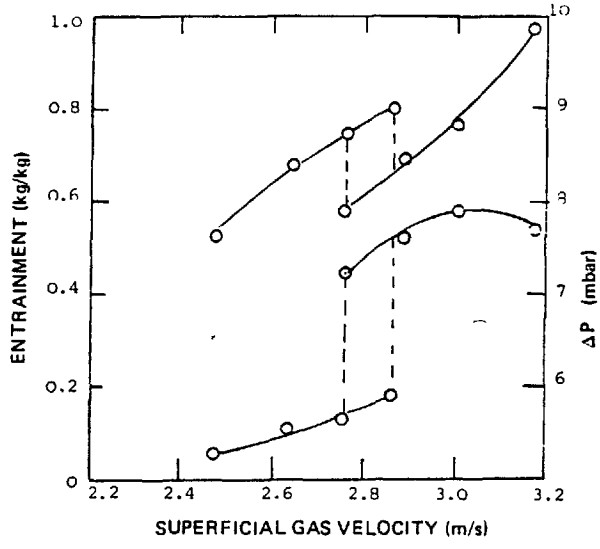
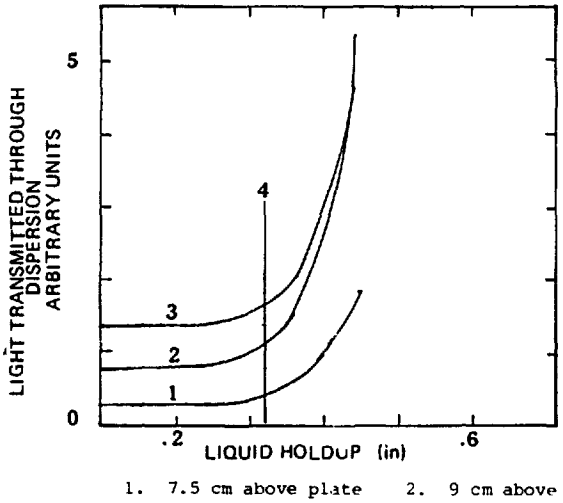


Fig. 2.6 Variation of entrainment and pressure drop with superficial gas velocity at constant liquid rate. O Pressure drop; ⊙ Entrainment.



1. 7.5 cm above plate 2. 9 cm above plate
3. 10 cm above plate

Fig. 2.5 Determination of transition from spray to bubbling by the light transmission technique at constant hole velocity[44]

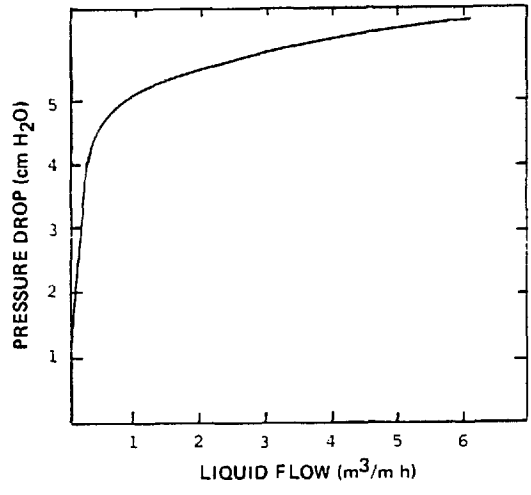


Fig. 2.7 Variation of plate pressure drop with liquid crossflow at constant superficial gas velocity.

Burgess and Robinson studied the variation of pressure drop with liquid rate on sieve plates with liquid cross flow. They observed a rapid initial rise in pressure drop at low liquid flowrates and a gradual change in pressure drop at high liquid flowrates. It was concluded that the rapid rise was due to spray regime and the slow rise due to bubbly regime (Fig. 2.7). They did not observe a sudden step change in pressure drop as observed by Shakov[45] et al.

Payne and Prince[47] conducted their experiment in a similar way to Porter and Wong[43] on a static sieve plate. They used a single orifice and a multiorifice plate to study phase transition. Residual pressure drop is the result of momentum transfer between gas and liquid, and represents the difference between the total pressure drop and the sum of the dry plate pressure drop and the liquid head. They observed a maximum in the residual pressure drop curve which according to them corresponded to the point of phase inversion (Fig. 2.8). Simultaneous measurements of optical transmittivity indicated that the residual pressure drop criterion predicted phase transition at a higher holdup and thus lower gas velocity than proposed by Porter and Wong. From cine observations of a single hole Payne and Prince found at transition, as defined by the maximum in the residual pressure drop, that 70% of the holes were jetting and the remaining 30% of the holes were bubbling at any instant of time.

Frequency of liquid bridging:

Pinczewski and Fell[31] used an electrical resistance probe to monitor the bubbling behaviour of an orifice in a sieve plate. They placed the probe centrally in the orifice protruding approximately 0.6 cm above the plate. No current was passing when the tip of the probe is surrounded by gas whilst maximum current was expected when

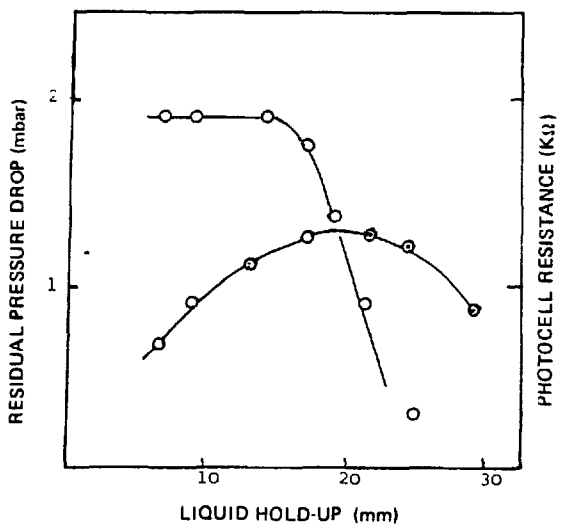


Fig. 2.8 Variation of residual pressure drop and optical transmittivity, expressed as photocell resistance with head of liquid on plate at constant hole velocity

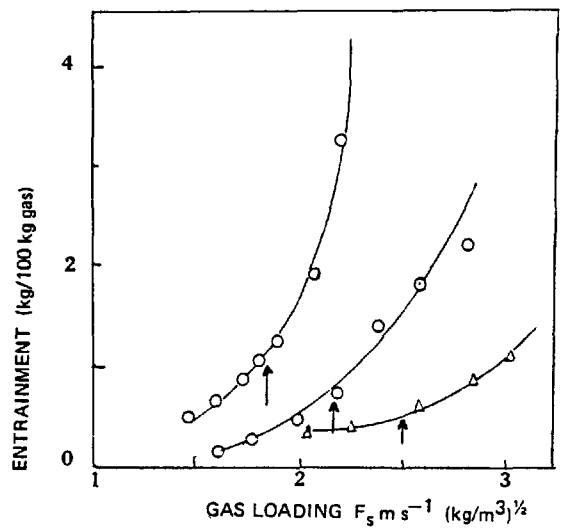


Fig. 2.10 Effect of phase inversion on entrainment

Arrows - transition points. L = 15 m^3 h^{-1} m^{-1}

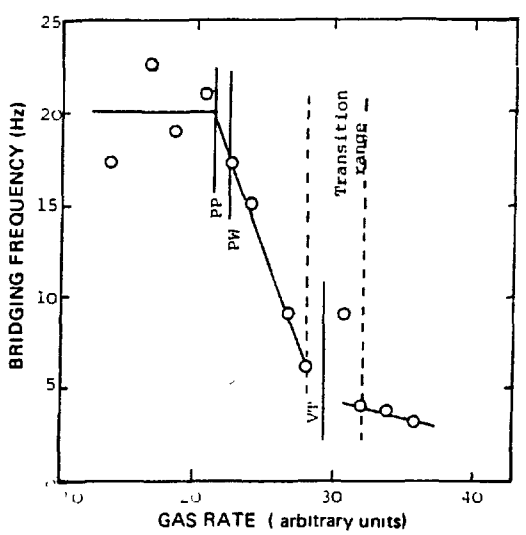


Fig. 2.9 Variation of bridging frequency with gas velocity
VT - Visual transition
PW - Transition according to Porter and Wong
PP - Transition according to Payne

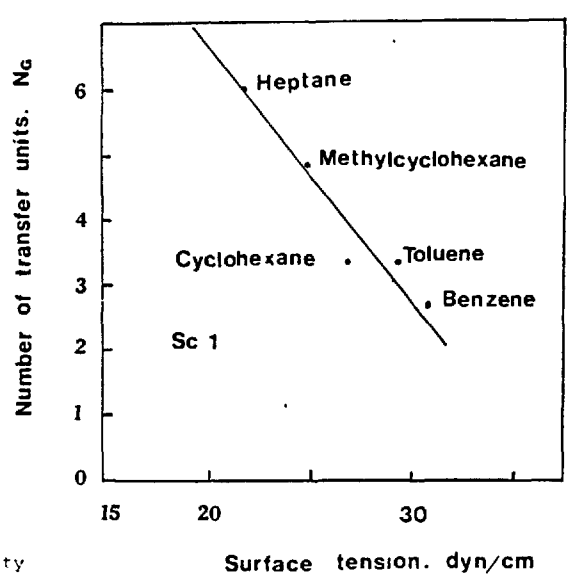


Fig. 2.11 Dependence of performance on surface tension

there was a liquid bridge across the tip. Periodic bridging was observed under bubbling conditions with the bridging frequency dropping to a very low value at high gas flowrates. At the transition point bridging frequency increased due to oscillations on the tray (Fig. 2.9). This point corresponded to simultaneous jetting of all holes. From similar experiments Payne and Prince located the transition point to correspond to initial decrease in bridging frequency. According to Jeronimo and Sawistowski the point of initial decrease in the bridging frequency agrees with their interfacial area measurements and with those of Prince and Payne obtained by the residual pressure drop method.

Entrainment:

Entrainment as a criterion to detect the transition point was employed by Shakhov et al[45], by Banerjee et al[32-33], and by Pinczewski[48]. Entrainment can be measured by an impingement process on a plate and collection of the liquid or by mass balance of a non-volatile compound, e.g. a salt, added to the liquid flowing down the column. When entrainment is plotted as a function of gas velocity on a log-log paper a change in slope occurs at transition (Fig. 2.10).

Acoustic analysis:

The noise pattern generated when a gas flows through an orifice changes at transition. This change in the noise pattern can be observed in an oscilloscope connected to a transmitter. Banerjee et al[32-33] used this technique to detect the transition point. They observed that at low velocities the wave pattern exhibited was smooth with low frequency wavelength. With increasing gas velocity the smooth pattern changed into irregular wave lengths and amplitudes.

At high velocities the pattern was smooth again but with high frequency and uniform amplitude.

CONCLUSION

Therefore in conclusion it can be said that froth to spray transition occurs when the hydrodynamic behaviour of the plate changes as a result of the change in the orifice behaviour. Bubbling at the orifice is the phenomenon in the froth regime and jetting at the orifice is the mechanism in the spray regime. According to Jeronimo and Sawistowski[84] if the light transmission technique is used to determine the transition point, then transition point should be taken somewhere midway of the sudden increase in transmittivity. If the frequency of liquid bridging method is used then the point of initial decrease in the bridging frequency should be taken. Then all the techniques discussed above will give approximately the same answer and will be in accordance with the interfacial area criterion.

2.1.6.2 Transition Correlations

Correlations to predict the froth to spray transition have been proposed by several workers[49-51]. They all require the knowledge of liquid holdup at transition to predict the velocity at transition. In order to overcome this difficulty Jeronimo and Sawistowski[52] correlated the data of Pinczewski and Fell[31] in terms of hole velocity at transition. Starting with the approach of Kutateladze and Styrikovich[50] they presented the following equation

$$We_t^o = 0.429\ Bo^{1/3}\ /A_f^2 F_c^2 \qquad (2.12)$$

where

We_t^o - Weber number at transition

F_c - correction factor for cross flow of liquid

$$F_c = 1 + 0.000104\ L_v^{-0.59}\ A_f^{-1.79}$$

This equation gives the upper transition limit beyond which the froth regime does not exist. The lower limit below which the spray will not exist can be obtained by multiplying the transition velocity by a factor of 0.75.

2.2 Performance Characteristics of Sieve Plates

2.2.1 Concept of Performance

A knowledge of the actual number of stages required to give a desired separation is of prime importance in the design of any mass transfer equipment. The concept of efficiency allows one to calculate the behaviour of an actual column from the knowledge of the behaviour of an ideal column which has hypothetical equilibrium stages. By definition an equilibrium stage produces an exit vapour stream in thermodynamic equilibrium with the exit liquid stream on a plate.

2.2.2 Basic Definitions

Murphree[54] expressed this approach to equilibrium as the ratio of actual change in vapour composition to that which would have occurred if the vapour had actually reached thermodynamic equilibrium with the exit liquid

$$E_{MV} = \frac{y_n - y_{n-1}}{y_n^* - y_{n-1}} \qquad (2.14)$$

where

y_n and y_{n-1} are the compositions of the vapour entering and leaving the plate

y_n^* is the composition of the vapour in equilibrium with the exit liquid concentration x_n.

Murphree efficiency can also be expressed in terms of liquid composition

$$E_{ML} = \frac{x_{n+1} - x_n}{x_{n+1} - x_n^*} \qquad (2.15)$$

x_{n+1} and x_n liquid concentration entering and leaving the plate

x_n^* is the liquid concentration in equilibrium with exit vapour y_n.

Point efficiency is a fundamental concept and is taken as the Murphree efficiency which applies to a vertical line through vapour liquid dispersion.

$$E = \frac{y - y_{n-1}}{y^* - y_{n-1}} \qquad (2.16)$$

where

y and y_{n-1} are composition of vapour below and above the dispersion

y^* - composition of vapour in equilibrium with the liquid in the dispersion assumed to be perfectly mixed in the vertical direction.

The basic approach to the prediction of tray efficiencies involve:

1. The prediction of point efficiencies from mass transfer characteristics of the phases and design parameters of the tray,
2. Relating the point efficiencies to plate efficiencies by means of a liquid and vapour mixing models, using some simplyfing assumptions. Plate efficiency can then be related to the overall column efficiency by

$$E_O = \frac{\log [1 + (\lambda-1)E_{mv}]}{\log \lambda} \qquad (2.17)$$

2.2.3 Mass Transfer Relationships

The 'two film' concept of Whitman[55] is widely used as a design basis. The model assumes that the rate of transfer is controlled by the magnitude of two resistances which are in series, one on each side of the interface. The interface itself offers no resistance. The overall resistance is the sum of the two individual resistances, which are the reciprocals of the mass transfer coefficients but, since

equilibrium is assumed at the interface, they are related by the equilibrium constant. Each resistance can be evaluated separately because it depends on the physical properties of its own phase.

$$\frac{1}{K_{OG}} = \frac{1}{K_G} + \frac{m}{K_L} \tag{2.18}$$

where

K_{OG} is the overall gas phase mass transfer coefficient

K_G and K_L are the individual mass transfer coefficients of the two phases.

In terms of transfer unit, the concept introduced by Chilton and Colburn[56], this becomes

$$\frac{1}{N_{OG}} = \frac{1}{N_G} + \frac{mG/L}{N_L} \tag{2.19}$$

where

N_{OG}, N_G and N_L are overall and individual transfer units.

The relation between mass transfer coefficient and transfer unit is given by

$$N_{OG} = K_{OG} \cdot S/G$$

In turn the point efficiency may be related to the number of transfer units by

$$E = 1 - \exp(-N_{OG}) \tag{2.20}$$

Point efficiency is related to the tray efficiency by means of a liquid mixing model. For a perfectly mixed liquid, point efficiency is equal to the plate efficiency.

$$E = E_{mv} = \frac{y_n - y_{n-1}}{y_n^* - y_{n-1}} \tag{2.21}$$

For plug flow of liquid Lewis[57] derived the following relationship

$$E_{mv} = \frac{1}{\lambda}\,[\exp(\lambda E) - 1] \tag{2.22}$$

For partial liquid mixing, A.I.Ch.E. Research Committee developed the following equation based on the eddy diffusion concept,

$$E_{mv} = \frac{1 - \exp[-(\eta+N_{pe})]}{(\eta+N_{pe})\,[1+(\eta+N_{pe})/\eta]} + \frac{\exp(\eta) - 1}{\eta[1+\eta/(\eta+N_{pe})]} \tag{2.23}$$

where

$$\eta = \frac{N_{pe}}{2}\left[\sqrt{1 \quad \frac{4\lambda E}{N_{pe}}} - 1\right]$$

$$\lambda = mG_m/L_m.$$

N_G and N_L values can be corrected for physical properties using the Chilton and Colburn[56] analogy between heat, mass and momentum transfer. j-factor for mass transfer is given by

$$(j_D)_G = \frac{K_G.S}{G}\,(Sc_G)^{2/3} = f(Re_G) \tag{2.24}$$

From equation 2.24

$$\frac{(N_G)_1}{(N_G)_2} = \left(\frac{Sc_2}{Sc_1}\right)^{2/3} \tag{2.25}$$

For the liquid phase

$$\frac{(N_L)_1}{(N_L)_2} = \left(\frac{D_{L1}}{D_{L2}}\right)^{1/2} \tag{2.26}$$

In all the above relations for plate efficiency it was assumed that the vapour approaching the plate is perfectly mixed.

2.2.4 Effect of Surface Tension on Plate Performance

Surface tension affects plate performance in two ways: by its absolute value and by the effect of mass transfer on surface tension gradient (Marangoni effect).

Bainbridge and Sawistowski[59] first brought to attention the influence of absolute value of surface tension on the interfacial area formed, its stability and hence on mass transfer performance. They found from vaporization studies with pure liquids that efficiency increased with decrease in absolute value of surface tension. The variation of plate performance expressed in terms of N_G, with surface tension, is shown in Fig. 2.11. This was later confirmed by de Goederen[10]. Later Fane and Sawistowski[1] experimentally confirmed the findings of Bainbridge. Because of the stabilising influence of surface tension, small diameter drops are easily formed in a low surface tension system, which explains the large interfacial area responsible for high plate efficiency.

Zuiderweg and Harmens[58] found surface tension positive systems to have a tendency to operate in the foam regime and have higher efficiencies than negative or neutral systems which under similar hydrodynamic conditions tend to operate in the spray regime. This they explained as due to the Marangoni effect. Thus in the foam regime, the liquid lamellae become saturated with the less volatile component relatively rapidly and hence increasing the surface tension locally. This causes expansion of the surrounding areas which are of lower tension surface. The resulting flow counteracts the thinning of

the trapped film, coalescence is opposed, and the liquid film is stabilised resulting in high interfacial area. The opposite behaviour applies to a negative system, which favours the spray regime. The rupture of the lamellae between the bubbles is accelerated. These findings are only applicable to the foam regime operating at low gas flowrates as pointed out by Bainbridge and Sawistowski[59]. These authors also found that for columns operating in the spray regime, at high gas flowrates, surface tension negative systems gave higher efficiencies than positive systems. This tendency of the negative system to spray was explained by them by means of a necking model.



Schematic illustration of the necking model.

a. - positive system.

b. - negative system.

In the negative system the neck becomes depleted of the more volatile component and this reduces the surface tension locally, surrounding areas of high surface tension contract thus rupturing the neck. In the positive system surface tension is higher in the neck and the Marangoni effect counteract the rupture. They have shown for negative systems the mean drop diameter, $d_{pm} \propto \gamma^{0.25}$ and for positive systems, $d_{pm} \propto \gamma^{0.55}$. It can be said that negative systems assist droplet formation and positive systems discourage droplet formation. In both cases, the plate performance expressed in terms of transfer units was found to depend on surface tension in the following way.

$$N_G \propto \gamma^{-1.10} \qquad \text{(Negative system)}$$

$$N_G \propto \gamma^{-0.90} \qquad \text{(Positive system)}$$

2.3 Modelling of the Spray Regime

There are only two hydrodynamic models formulated for the spray regime. They are:

1. Fluidization Model
2. Free Trajectory Model

2.3.1 Fluidization Model

Porter and Wong[43], Ho et al[49], and Andrew[51] all considered spray as a fluidized bed of droplets. There is a critical velocity at which the drops are just suspended in the vapour stream and this is known as the minimum fluidization velocity. In the fluidization model it is assumed that a gas-liquid bed starts forming once the local gas velocity exceeds this minimum fluidization velocity. This is accompanied by a considerable increase in the residence time of drops in the dispersion and hence a significant shift of liquid holdup from the froth to the spray. Although plausible, there is little experimental evidence to support such a model. Instead it was observed that droplets take well defined trajectories in the interplate space. In any case this model was used only for an explanation of phase inversion. The free trajectory model is now commonly accepted for mass transfer performance calculations.

2.3.2 Free Trajectory Model

In the free trajectory model proposed by Fane and Sawistowski[1] it is assumed that the droplets produced by the jetting mechanism follow a trajectory in the interplate space. Using the equation of motion to describe the trajectory, they obtained a height-velocity-residence time map for each drop size at chosen height intervals.

This information together with a known drop size distribution produces the dispersion density profile. They also determined a mean drop diameter and the standard deviation of the spray by a two parameter fit of dispersion density profiles, calculated from the model to the experimentally determined dispersion density profile. From this information area available for mass transfer in each height increment and the contribution of each height increment to the plate performance could be evaluated. This approach to modelling the spray regime and predicting the efficiency was successful. Free trajectory model is now widely accepted as the only model for mass transfer prediction[60,61].

However, the model requires the knowledge of initial projection velocity of drops and their drag coefficients to solve the equation of motion, of spray characteristics and liquid holdup to produce the dispersion density profile. Estimation of spray characteristics by parameter fitting involves numerical techniques and it is rather tedious. Hence, Jeronimo and Sawistowski[84] attempted to simplify the model. They assumed

a) drag effect to be negligible

b) contribution to dispersion density and superficial area came only from drops at maximum level

c) equation for initial projection of drops was of the form $v_p = Ad_p^B$ with A and B as constants

d) drop size distribution was log normal.

They proved that the error in the profiles of dispersion density, interfacial area and sauter mean diameter introduced by taking drag coefficient as zero was almost negligible. Hofhuis and Zuiderweg[3] also found, drag has negligible effect on the dispersion density profile. Following these assumptions the hydrodynamic model was described

analytically by nine independent relations in terms of fourteen variables. From experimental dispersion density profiles and surface area profiles it is possible to establish such analytical relationships between spray parameters and experimental values. Each of the profiles will be characterised by its maximum value M_L and M_a the location of the maximum above the plate floor, Z_{Lm} and Z_{am}, as well as the standard deviation of the corresponding property σ_L and σ_a (subscripts L,a refer to dispersion density and specific surface area profiles respectively). The spray at formation will be characterised by d_m, σ and there will also be a specific maximum height, h_m, attained by a drop of diameter d_m. Holdup of drops, H_D, its total interfacial area, A_D, and the number of projected drops per unit time, N_P, and the constants in the projection velocity equation A and B. Hence the total number of variables is 14. Since it was possible to set up nine equations to relate these variables five parameters had to be determined experimentally.

Jeronimo and Sawistowski selected V_P (i.e. A and B), d_m, M_L and σ as the unknown parameters and correlated them as follows.

$$V_P = 0.38\ (0.004/d_p)^{0.83} \tag{2.27}$$

$$d_m = 0.006\ (10\ A_f)^{0.56} F_s^{-2} \tag{2.28}$$

$$M_L = (0.17 + 0.07 \log L_v)(F_s/2)^{-2}(0.00317/d_h)^{0.37}(10\ A_f) \tag{2.29}$$

$$\sigma = 0.19\ (F_s/F_{st})^{1.5} \tag{2.30}$$

where F_s is F - factor = $u_G \rho_G^{1/2}\ (kg^{1/2} s^{-1} m^{-1/2})$

and F_{st} is F - factor at transition.

2.4 Entrainment

It becomes more and more important, from the design point of view, to understand the mechanism of entrainment and the factors that affect it. Research has been carried out by a number of workers on entrainment under various operating conditions. Nielson[28] has given a brief literature survey on this subject. Among the few who studied entrainment on sieve plates[62-64] are Jeronimo and Sawistowski [84], Pinczewski et al[48] and Banerjee et al[32,33].

Jeronimo and Sawistowski[84] found entrainment to be proportional to $F_s^{9.1}$ and inversely proportional to $L_v^{0.49}$, whereas Banerjee et al[32,33] found entrainment to be proportional to $F_s^{4.44}$ for single orifice and 6.66 for a multiorifice plate.

It has been said that, operating the column in the spray regime for negative systems yields higher efficiencies. However, there is a limit to which the gas flowrate can be increased, with tolerable amount of entrainment, in the spray regime. Therefore it can be said that entrainment fixes the upper limit for spray regime operation. The effect of entrainment on efficiency can be shown by Colburn's[65] equation,

$$E_a = \frac{E_{mv}}{1 + \frac{e_m}{R} E_{mv}} \qquad (2.31)$$

where

E_{mv} - dry Murphree plate efficiency

E_a - Murphree plate efficiency corrected for entrainment

e_m - moles of entrained liquid per mole of dry vapour

R - reflux ratio.

Standart et al[83] pointed out that E_{mv} is the Murphree efficiency for the actual vapour and liquid concentrations around the n^{th} tray of a column which is operating with no entrainment and E_a is a tray efficiency defined in terms of a hypothetical vapour composition Y_n corrected for entrainment

$$Y_n = \bar{y}_n - e_m(\bar{x}_{n+1} - \bar{x}_n) \qquad (2.32)$$

to give a simple operating line for an equivalent dry column without entrainment. The equilibrium vapour $y_n^*(\bar{x}_n)$ used in defining E_a is the same as for E_{mv}. Standart's main criticism was centred on the inability to simulate a set of operating conditions for a dry column without entrainment as in an actual column which would give a tray efficiency equal to E_{mv} without affecting the mass transfer on the trays. In view of this he defined a reduced tray efficiency E_{mv}^r, in terms of reduced liquid flowrate (the vapour flowrate is unchanged while the reduced liquid flowrate is the actual one diminished by the entrainment from the tray below),

$$\dot{L}_n^r = \dot{L}_n - \dot{E}_{n-1}^+ \qquad (2.33)$$

reduced liquid composition corrected for entrainment

$$\dot{L}_n^r \bar{x}_n^r = \dot{L}_n \bar{x}_n - \dot{E}_{n-1}^+ \bar{x}_{n-1} \qquad (2.34)$$

and reduced equilibrium composition, $(y_n^* \bar{x}_n^r)$.

He then proposed for a mid-column tray with perfectly mixed liquid and equal flows from tray to tray

$$(E/E_{mv}^r)^2 - [1 - E(\lambda^r - 1 - e^r)](E/E_{mv}^r) - E(\lambda^r - 1)(1 + e^r) = 0 \qquad (2.35)$$

where $\lambda^r = kv/L^r$, $e^r = E^+/L^r$,

E - Point efficiency.

If $e^r = 0$, then $E^r_{mv} = E$.

For unmixed liquid crossing the tray but uniform vapour (and entrainment) entering it from below as from a reboiler and equal flows from tray to tray

$$E^r_{mv} = [\exp((E\lambda^r + e^r)/(1+e^r) - 1](E\lambda^r+e^r) \quad (2.36)$$

which reduces to the Lewis[57], solution for $e^r = 0$.

Summary

It can be concluded that under fully developed spray regime, efficiency is higher for negative systems than positive systems, which is the result of the higher interfacial area. It is clear from the above studies that ligament formation and their subsequent disintegration produces droplets. These ligaments will differ in size and a negative system will be more prone to assist disturbances leading to sheet rupture producing higher proportion of thin filaments which in turn break into small drops thus giving higher interfacial area in negative systems. Factors which influence the spray regime operation are large diameter holes, low free area and high hole velocities. Efficiency is independent of weir height in the spray regime.

CHAPTER THREE

EXPERIMENTAL

3.1 Introduction

The main aim of this work was the study of vapour-liquid dispersions formed on sieve plates and the extent to which they are influenced by physical properties and impurities.

The hydrodynamic behaviour of the plate changes from that of liquid continuous-gas dispersed to gas continuous-liquid dispersed with increasing gas flowrates. Two sets of experiments were carried out: one to study the foaming behaviour and the effects of colloids on foaming, the other to investigate the spray behaviour, both on a multiorifice sieve plate.

The first set of experiments was initiated from communications[14] received from Union Carbide and the Canadian Atomic Energy Commission in which they reported severe foaming in the H_2S-H_2O exchange columns and ascribed it to the presence of traces of colloidal substances (10 to 100 ppm) resulting from corrosion of mild steel columns. Similar observations concerning U.K. operation of aluminium columns, were also quoted.

Some preliminary experiments were conducted as part of a final year B.Sc. research project and of an M.Sc. project[66]. In both cases water-insoluble dyes were employed to produce colloidal suspensions of the right concentrations. The dyes used were Orasol Black, Orasol Yellow, Orasol Red, Neozapan Orange and Neozapan Red. The experiments were carried out on a static plate, that is there was no crossflow of liquid. The results obtained have shown a marked influence on foaming even at a concentration of 10 ppm. In general,

the foaming was stronger than that produced by an equal concentration of a surfactant, Teepol. Subsequent measurement of surface tension has shown, however, that the colloids were surface active, i.e., they resulted in significant lowering of surface tension. Commercially available colloidal substances are usually chemically treated and it is probable that this effect was the result of the presence of other components. In addition, dye particles are hydrophobic. They affect surface mobility and hence give the foam greater stability than that produced by surfactants alone.

In view of this it was decided to critically assess whether foaming was due to the colloids themselves or the effect of the presence of other substances in the colloidal suspension. It became obvious, therefore, that the work cannot be conducted using commercially available colloids. The colloids had to be prepared in situ under carefully controlled conditions, and, in such a case, it was decided to use hydrous ferric oxide sol. and hydrous aluminium oxide sol. as these two substances were mentioned in the original communication.

Spray regime has received much attention in the past few years and most of the work carried out so far was on the air-water systems. It was therefore intended to extend this work to systems other than air-water, paying particular attention to the upper limit of the liquid continuous phase, i.e. the transition from froth to spray and its dependence on physical properties and the extent to which the presence of colloids influences this transition point.

3.2 Test Rig - 1

3.2.1 Description

A schematic diagram of the test rig in which the foaming studies were carried out is shown in Fig. 3.1. The column was made of three Q.V.F. flanged glass sections of 0.228 m diameter. The sieve tray and the air distributor tray were fitted between the sections, the upper plate forming the test plate and the lower serving as the air distributor. The constructional details of the test plate is shown in Fig. 3.2 and given in table 3.1. The bottom Q.V.F. section fitted directly on to the air distributor which terminated in a conical section fitted with a drain valve. The distributor consisted of an inner tube and an outer concentric tube. Air supply from the high pressure air line was stepped down to 25 psig using a reducing valve and admitted to the column through the outer section of the air distributor. Air flowed down through the annulus into the inner tube and up the column through the distributor plate. Air flow was controlled by a needle valve and metered by a type 65-A rotameter. The liquid was pumped around using a Tuxan centrifugal pump and the flow was monitored by two rotameters set up in parallel to achieve fine control over the range of flowrates studied.

3.2.2 Experimental Procedure

Commercially available colloidal substances are usually chemically treated and to avoid contamination, the colloids were prepared in situ under controlled conditions. Hydrous ferric oxide sol. and hydrous aluminium oxide sol. used in these studies were prepared according to Hauser and Lynns[67] specification.

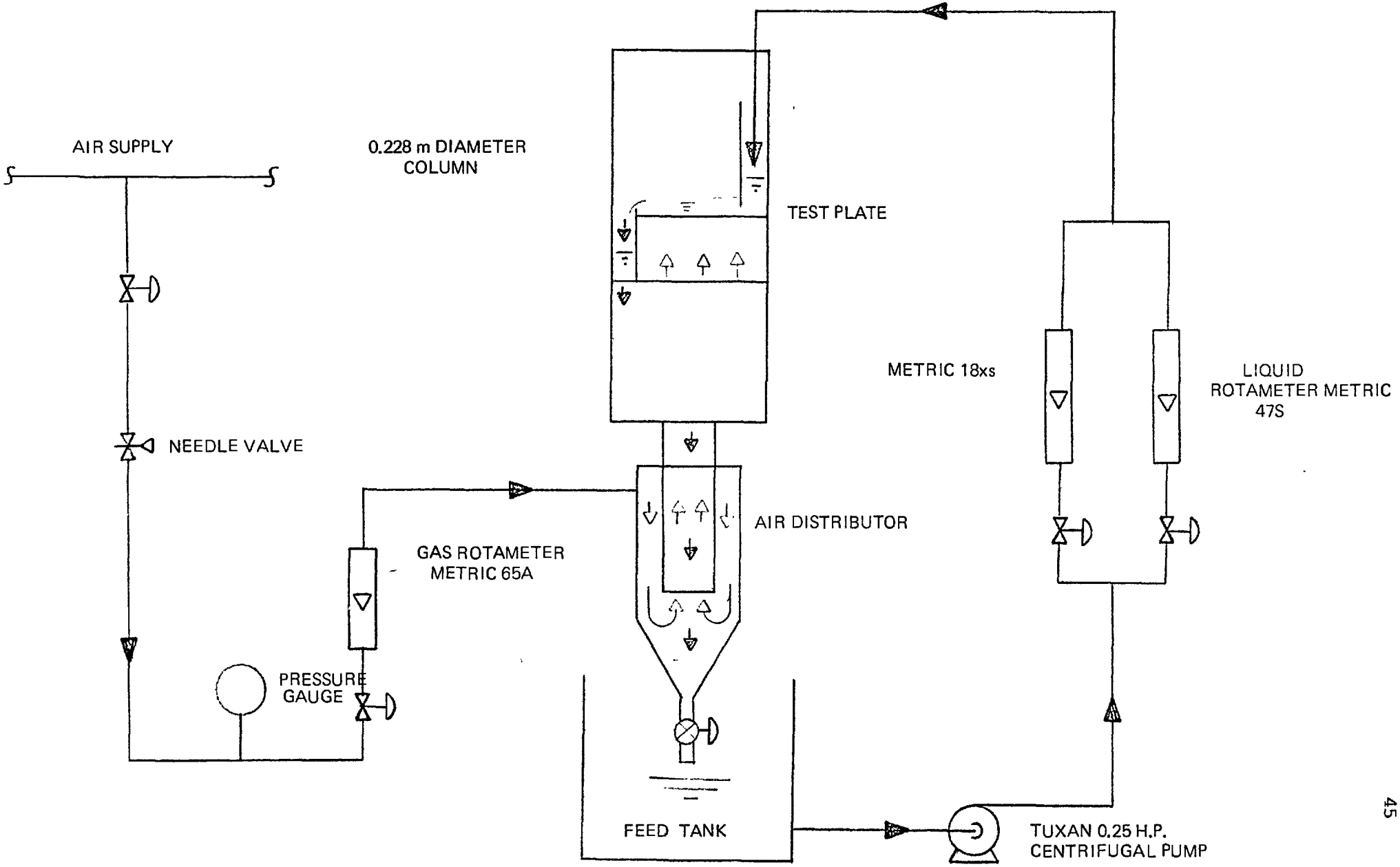
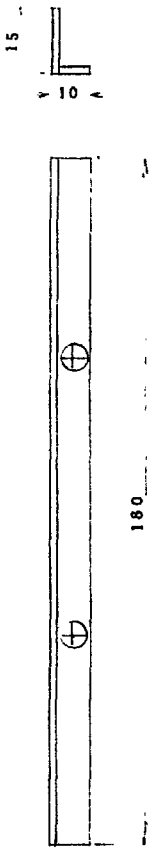
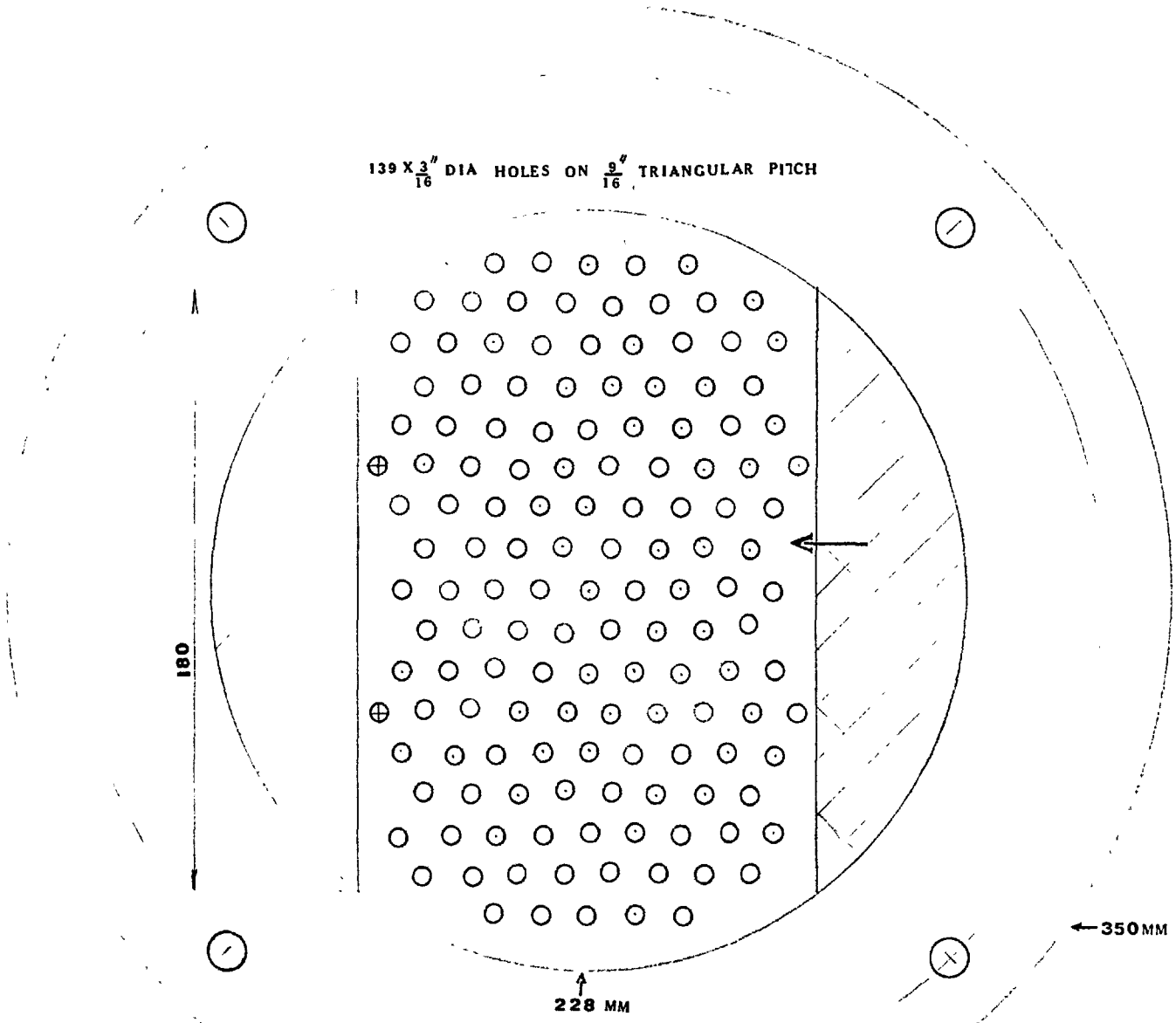


Fig. 3.1 Line diagram of test rig 1.



WEIR



TEST PLATE

Fig 3.2

TABLE 3.1

Test Plate Specifications

Cross-flow Plate:	
Hole diameter (mm)	4.76
Pitch (equilateral triangular) (mm)	14.29
Number of holes	139
Free area (% of active area)	10
Weir height (mm)	12.7
Weir length (mm)	180
Plate thickness (mm)	9.525
Static Plate:	
Hole diameter (mm)	3.175
Pitch (equilateral triangular) (mm)	12.7
Number of holes	247
Free area	4.76
Plate thickness	9.525

TABLE 3.2

Range of Operating Variables

air flowrate (m^3/h)	12 -112.5
F_S-factor ($m/s\ (kg/m^3)^{1/2}$)	0.089- 0.84
F_H-factor ($m/s\ (kg/m^3)^{1/2}$)	1.521- 15.21
Liquid flowrate (m^2/h)	3.3 - 23.3

Hydrous aluminium hydroxide sol. was prepared by warming 10 cm^3 of a 10 per cent aluminium acetate solution in 200 cm^3 of water on a water bath until the odour of acetic acid disappeared. The evaporated water was replaced from time to time to keep the volume constant. This took several days. The solution was then filtered to obtain a clear hydrous aluminium hydroxide sol.

Hydrous ferric oxide sol. was prepared by boiling 25 cm^3 of a 2 per cent ferric chloride solution in 250 cm^3 of boiling water and boiling was continued until a clear red sol. was obtained. The water lost by evaporation was replaced from time to time.

The first series of experiments was carried out with water to obtain a reference set of results for comparative purposes. Air flowrate was set to prevent weeping during the initial introduction of liquid. Height of dispersion was measured for the range of operating variables shown in Table 3.2. Each data point was obtained after operating the column under steady state conditions.

The experimental procedure was repeated with hydrous ferric oxide sol. and hydrous aluminium oxide sol. Concentrations of 10 ppm, 100 ppm, 1000 ppm were injected into the column. Experiments were repeated with aluminium oxide sol. prepared at 30 ^{o}C, 40 ^{o}C, 50 ^{o}C, and 60 ^{o}C to observe the effect of particle size which is temperature dependent. There was no evidence of foaming.

Since there was no evidence of foaming in the crossflow tray it was decided to repeat the experiment in a static plate. A static plate has significantly higher holdup and in order to magnify any occurrence of foaming a plate with much smaller free area was necessary. Consequently a plate of dimensions given in Table 3.1 was used. The experiment was repeated with the same concentrations of hydrous ferric

oxide sol. and hydrous aluminium oxide sol. and under the same operating range for gas flowrates as for the crossflow tray but for a fixed liquid holdup of 1000 cm^3. Surface tension, viscosity and density measurements were taken in all cases. Again there was no evidence of foaming.

3.3 Test Rig - 2

3.3.1 Description

A line diagram of the test rig in which the spray characteristics were studied is shown in Fig. 3.3. The two columns A and B were of identical specifications, with rectangular cross-section 0.11 m by 0.19 m. Constructional details of column A are given by Fane[68] and of column B by Lindsey[23].

Experimental studies were carried out in column A which was fitted with two trays. The upper plate was the test plate and the lower one was used as an air distributor. Both the test plate and the air distributor were of the same design as given in table 3.3 and shown in Fig. 3.4. This set-up made it possible to operate the column in close circuit. Saturated air was circulated through the column. Dispersion density and surface area measurements were taken on the test plate.

TABLE 3.3

Test Plate Specification

Hole diameter (mm)	3
Pitch (equilateral triangular) (mm)	9.5
Number of holes	148
Free area (% of active area)	10
(% of superficial area)	7
Weir height (mm)	19
Weir length (mm)	70

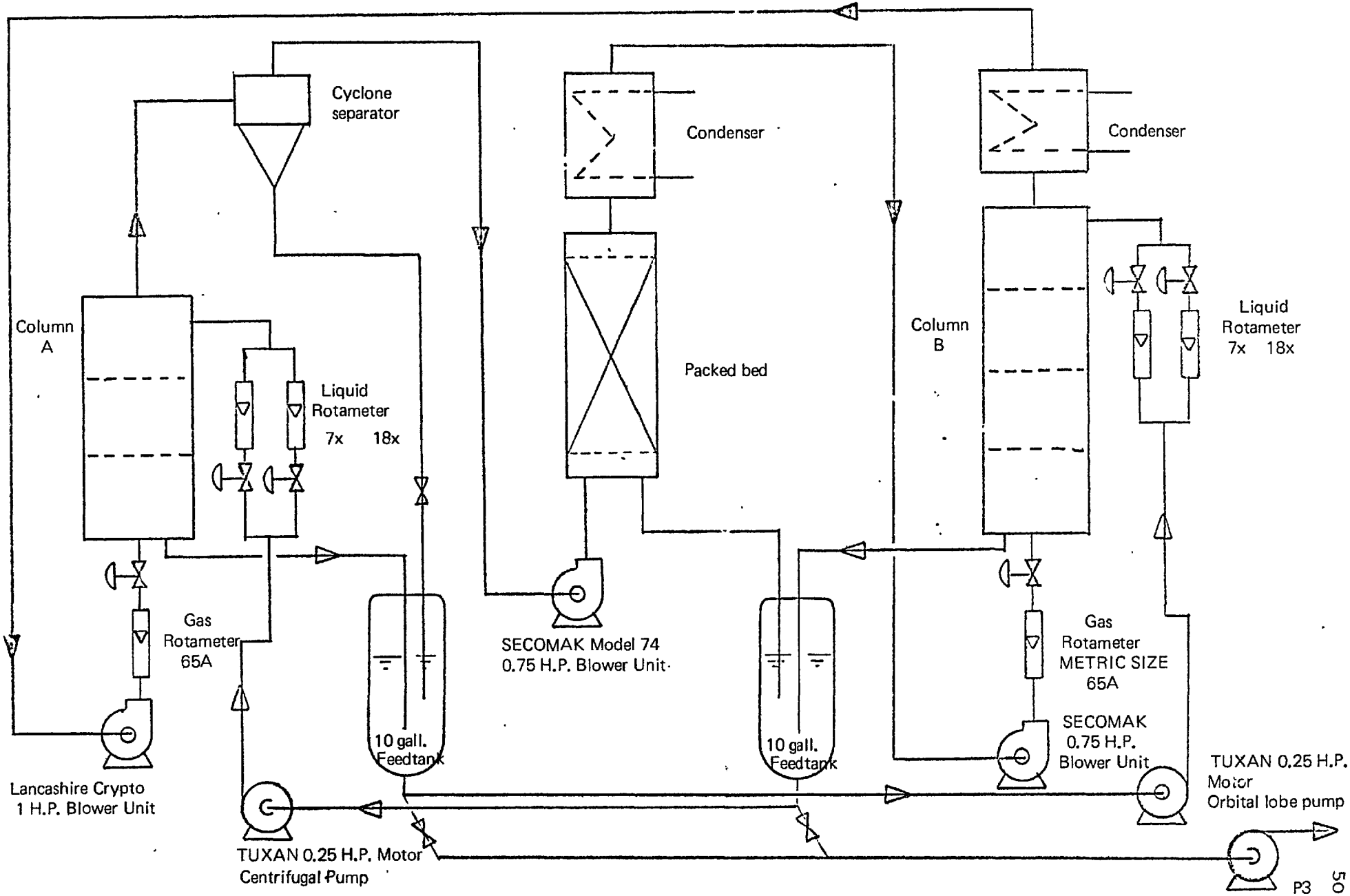


Fig. 3.3 Line diagram of test rig 2.

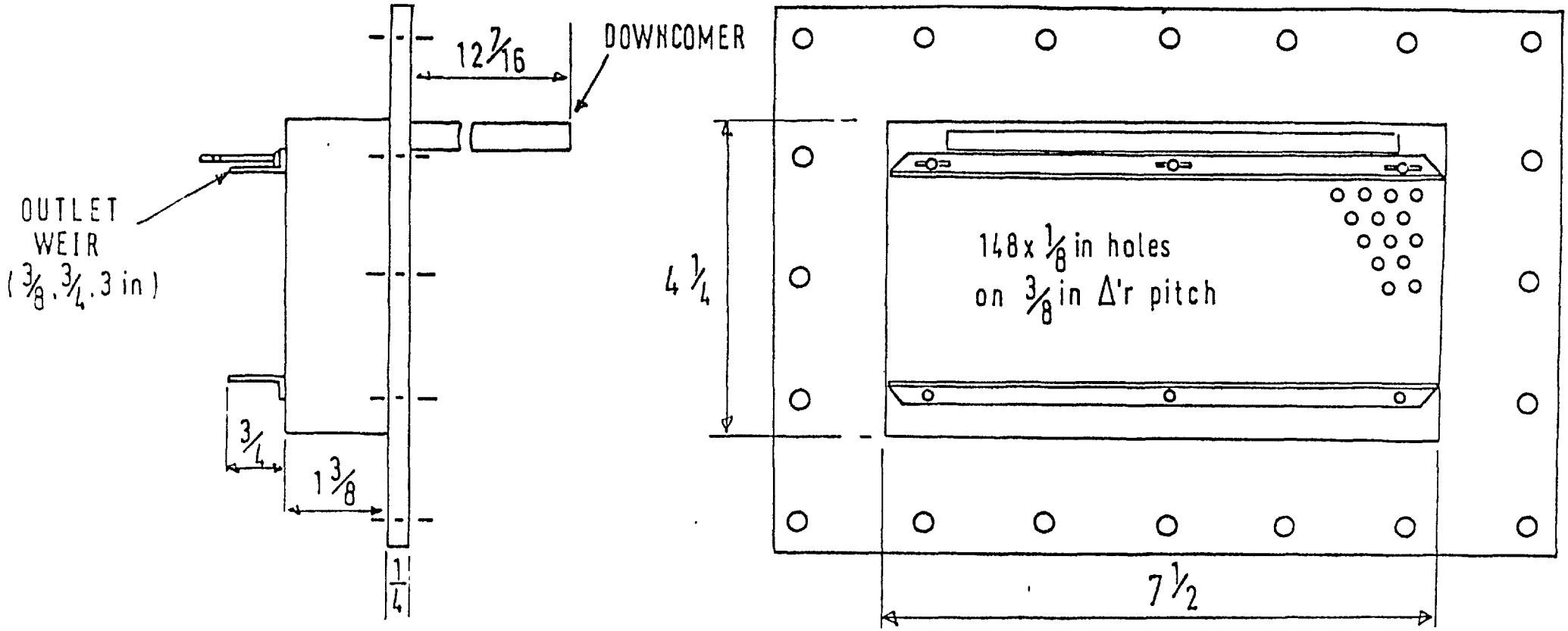


Fig.3.4 DETAIL OF TEST PLATE

3.4 Gamma Radiation Technique for Measurement of Dispersion Density Profile

3.4.1 Principle

Several investigators have successfully employed this technique to measure the dispersion density profile. The technique is based on the principle that the absorption of a parallel, mono-energetic beam of gamma radiation by a homogeneous medium of density ρ and thickness x obeys an exponential law, given by

$$I = I_o e^{-\mu\rho x} \qquad (3.1)$$

where I_o and I are the intensities of the incident and transmitted radiation and μ is the mass absorption coefficient of the medium.

Based on this principle the dispersion density profile can be measured accurately by determining

(i) The intensity of the radiation transmitted through the empty column.

(ii) The intensity of the radiation transmitted through the column filled with the liquid, and

(iii) The intensity of the radiation transmitted through the column containing the dispersion.

From this information the density can be either calculated or read off from the calibration chart of count rate versus density.

Number of counts recorded in a fixed time, or time taken to record a fixed number of counts, gives a measure of the intensity of the transmitted beam. If the number of counts recorded in a fixed time are used then

$$I \propto N$$

Equation 3.1 can then be written as

$$N = N_o e^{-\mu\rho x} . \qquad (3.2)$$

where N is the number of counts recorded in a fixed time.

If the time taken to record a fixed number of counts is used as a measure of the intensity, then

$$I \propto \frac{1}{t}$$

and equation 3.1 becomes

$$t = t_o e^{\mu\rho x} \qquad (3.3)$$

where t is the time taken to record a fixed number of counts.

Errors that are likely to be encountered in this method of density determination include forward scattering and errors due to non-homogeneity of dispersion. Errors due to forward scattering of radiation can be made negligible by adequate collination of the source and the scintillation counter. Errors due to non-homogeneity[69] in dispersion result in the measurement of the average of the point densities, but fluctuations with time during the counting period result in the measurement of an apparent time average density of smaller magnitude than the true density (see Appendix 1). In order to average out fluctuations and eliminate errors in the counting device sufficiently large numbers of counts are necessary. From statistical point of view, timing for 10,000 counts must be determined in order to achieve 99% accuracy in the count rate from a radioactive source. The number of counts obtained for 100 secs were in the range of 18,000 in this study and this was thought to be sufficient to average out random fluctuations of the density and provide good timing

accuracy. Random decay of radio-isotope follows a Poisson distribution and the number of counts recorded in 100 secs should result in a 97% probability that a single data point is within 1% of the true value.

Calderbank[16] has shown that a collimated mono-energetic beam of radiation from caesium 137 obeys a linear relationship between log I and density whereas a multienergetic beam from thalium 170 does not obey the linear relationship.

3.4.2 Description

Caesium 137 of strength 0.8 millicurie giving a monoenergetic beam of radiation of gamma energy 0.662 MeV and half life of about 30 years was used as the radioactive source. The gamma ray source and the scintillation detector were mounted vertically on a three-armed beam. An hydraulic ram attached to the base plate and acting through the centre of gravity of the three-armed beam allowed the dispersion to be scanned in a vertical direction. A Ladgear D4133 directional scintillation counter with built-in photomultiplier tube was used to detect the radiation. The EHT was supplied from a Dynatron N103 power unit. The count rate was recorded with a scaler which was coupled to an automatic timer.

3.4.3 Calibration of the Gamma Ray Traverse System

A schematic diagram of the units of the counting equipment is shown in Fig. 3.5. For accurate determination of the dispersion density the optimum setting for each unit had to be established. The voltage to be applied to the photomultiplier was determined from the variation of the count rate with the EHT supplied to the scintillation counter. Optimum setting of 1100 V was chosen because the variation

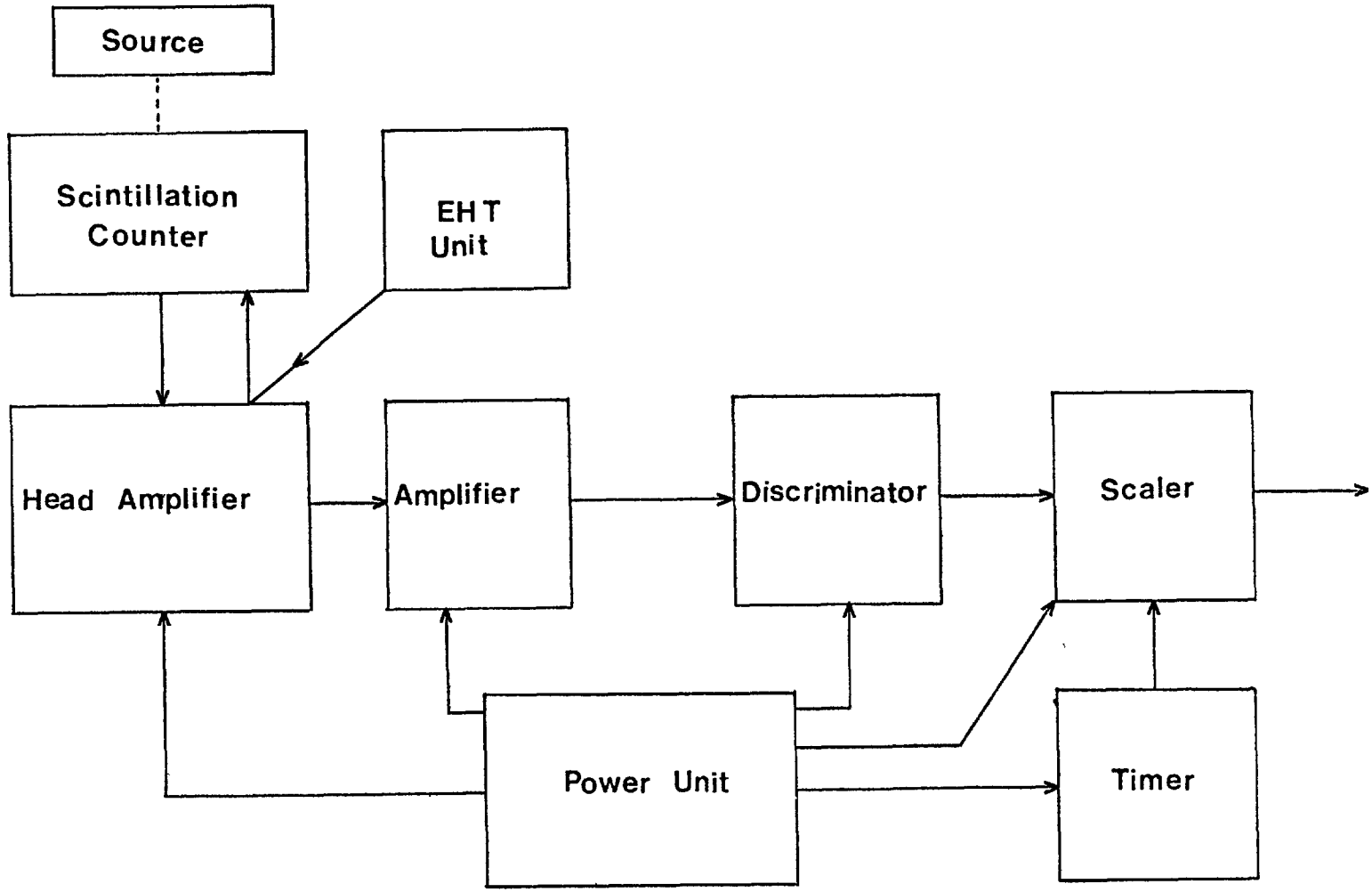


Fig. 3.5 COUNTING EQUIPMENT

of count rate with EHT was very small at this voltage. Other settings were determined using an oscilloscope and are given in Table 3.4.

Adequate collimation of the source and the counter are necessary to eliminate any errors due to forward scattering. A check on this can be made by calculating the effective path length through the dispersion,

$$D = 2.303 \log \left(\frac{N}{N_o}\right) \mu^{-1} \qquad (3.4)$$

and comparing it with the actual path length. Mass absorption coefficient for water is 0.085 cm^2/g. The count rate can be corrected for dead time by the following equation

$$N = \frac{n}{1 - ntd} \qquad (3.5)$$

where

N - count rate corrected for dead time of scaler

n - observed count rate (s^{-1})

t_d - dead time of scaler.

Dead time is the time after the production of a pulse during which another pulse cannot be recorded.

Intensity of the transmitted beam was measured by the number of counts recorded in 100 s for an empty column (N_o) and column filled with liquid (N). A straight line can be drawn through these two points on a semilog paper (ln N_o, ρ_o and ln N, $\rho = 1$). The density of the dispersion can then be determined by measuring the number of counts recorded in 100 s and reading the density directly from the calibration chart.

TABLE 3.4

Counting Equipment Settings

EHT	1100 volts
Head amplifier time constant	100 μs
Main amplifier:	
gain	29.5 dB
differentiator	1 μs
integrator	1 μs
Discriminator	
level	0.16 V
dead time	10 μs

3.5 Light Transmission Technique

3.5.1 Principle

The light transmission technique to measure the drop size of dispersions is a widely used method and the fraction of light transmitted through the dispersion is a function of its characteristics. Consider a rectangular volume of the vapour-liquid dispersion of the spray, (Fig. 3.6), the dimensions of which are w, h, and ℓ.

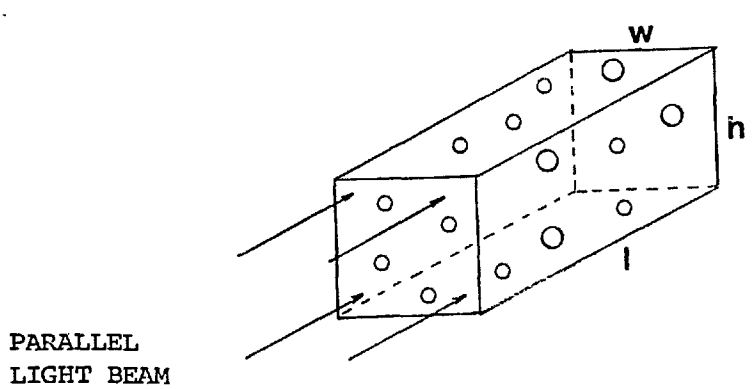


Fig. 3.6 Light transmission through a dispersion.

Fraction of the liquid in the dispersion (ϕ) is given by

$$\phi = \frac{\pi \sum_{i=1}^{n} d_i^3}{6wh\ell} \tag{3.6}$$

Interfacial area per unit volume of dispersion (a) is

$$a = \frac{6\phi}{\bar{d}} \tag{3.7}$$

where $\bar{d}$ is the Sauter mean diameter of the drops.

$$\bar{d} = \frac{\sum_{i=1}^{n} d_i^3}{\sum_{i=1}^{n} d_i^2} \tag{3.8}$$

Fraction of light transmitted through the dispersion can be determined using the probability theory[70], provided the drops are randomly distributed. The probability (P) that an arbitrary ray of light does not strike the i^{th} drop is

$$P = 1 - \frac{\pi d_i^2}{4wh} \tag{3.9}$$

Probability that the ray does not strike the i^{th} or j^{th} drop is

$$P = (1 - \frac{\pi d_i^2}{4wh})(1 - \frac{\pi d_j^2}{4wh}) \tag{3.10}$$

Probability of the ray not striking any of the drops is the fraction of light (f) transmitted through the dispersion

$$f = \sum_{i=1}^{n} (1 - \frac{\pi d_i^2}{4wh}) \tag{3.11}$$

From equations 3.6, 3.7, 3.8 and 3.11, fraction of light transmitted is a function of the dropsize distribution, interfacial area, Sauter mean diameter, volume fraction and optical path length. For log-normal drop size distribution fraction of light transmitted is given by

$$f = \exp\left[-1.5 \frac{a\ell}{6}\right]. \tag{3.12}$$

and

$$a = \frac{-4 \ln f}{\ell} \tag{3.13}$$

This relationship will only hold if the following conditions are satisfied.

1. transparent continuous phase;
2. random drop locations;
3. drops greater than 0.10 mm in diameter;
4. drops are subject to random orientation in the light beam;
5. drops have no concave surfaces;
6. the light source emits a incoherent parallel light beam; and
7. the light detector receives only parallel light.

When a light beam is passed through a dispersion, it is scattered by diffraction, refraction, absorption, and reflection as shown in the Fig. 3.7. The net effect of this can be determined by means of a scattering coefficient of the drop which is a function of the size of the drop relative to the wave length of the incident light and the refractive index of the two phases,

$$a_s = k_s a_p$$

where a_s - scattering cross-section of the drop

a_p - geometric cross-section of the drop

k_s - scattering coefficient of the drop, defined by $\alpha\ell/6$.

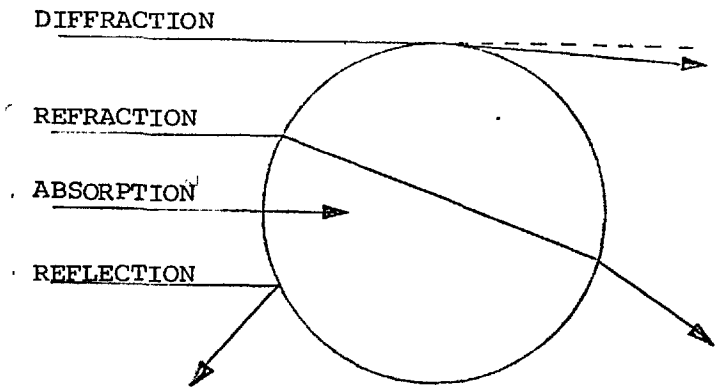


Fig. 3.7 The four mechanisms of light attenuation.

$\infty = \pi d/\lambda$

λ - wave length of the incident light.

For drops greater than 0.1 mm in diameter k_s is a function of the refractive index ratio only. k_s can be made equal to unity by allowing only parallel light to reach the detector. Multiple scattering of the light beam would result in detector receiving an excessive amount of light. Error due to this can be made negligible if the detector has a high angular resolution. Thus for a properly constructed light probe the scattering cross-section of the drops will be equal to the geometric cross-section, and the light transmission technique proves to be a very simple method of interfacial area determination.

3.5.2 Description

A schematic diagram of the light probe is shown in Fig. 3.8. A gentle stream of air was blown through the probe to prevent liquid droplets entering the horizontal section of the probe and wetting the mirrors. In addition, the horizontal section was provided with Teflon baffles and any liquid that entered was discharged through the longitudinal slit in the bottom of the tubing, Fig. 3.9. A high pressure mercury vapour lamp (Wotam, ref. HBO.50 W/3) was chosen as the light source and it was fed by direct current from a stabilized power supply built in the department. Fraction of the light transmitted through the dispersion was received by the photomultiplier, fed by an EHT power unit (A.E.R.E. type 1359A), which was set at a negative voltage of 600 volts.

Electrical output of the phototube is a measure of the fraction of light transmitted through the dispersion. This output was amplified using a photomultiplier amplifier which had the facility for zero adjustment when no light reached the tube and full scale deflection when all the light arrived there. In this way the intensity of the light transmitted could be read directly. In addition, the output was directed to a Hitachi-Perkin-Elmer model 159 flat bed recorder. The light probe was fixed to the hydraulic lifting system and this made it possible to move the light probe and gamma-ray traverse system simultaneously, to scan the dispersion vertically.

3.6 Experimental Procedure

The main objective of this work was to study the behaviour of a sieve plate in the spray regime. In order to operate the column in the fully developed spray regime the transition point had to be determined. This was established using the light probe. Pre-saturated

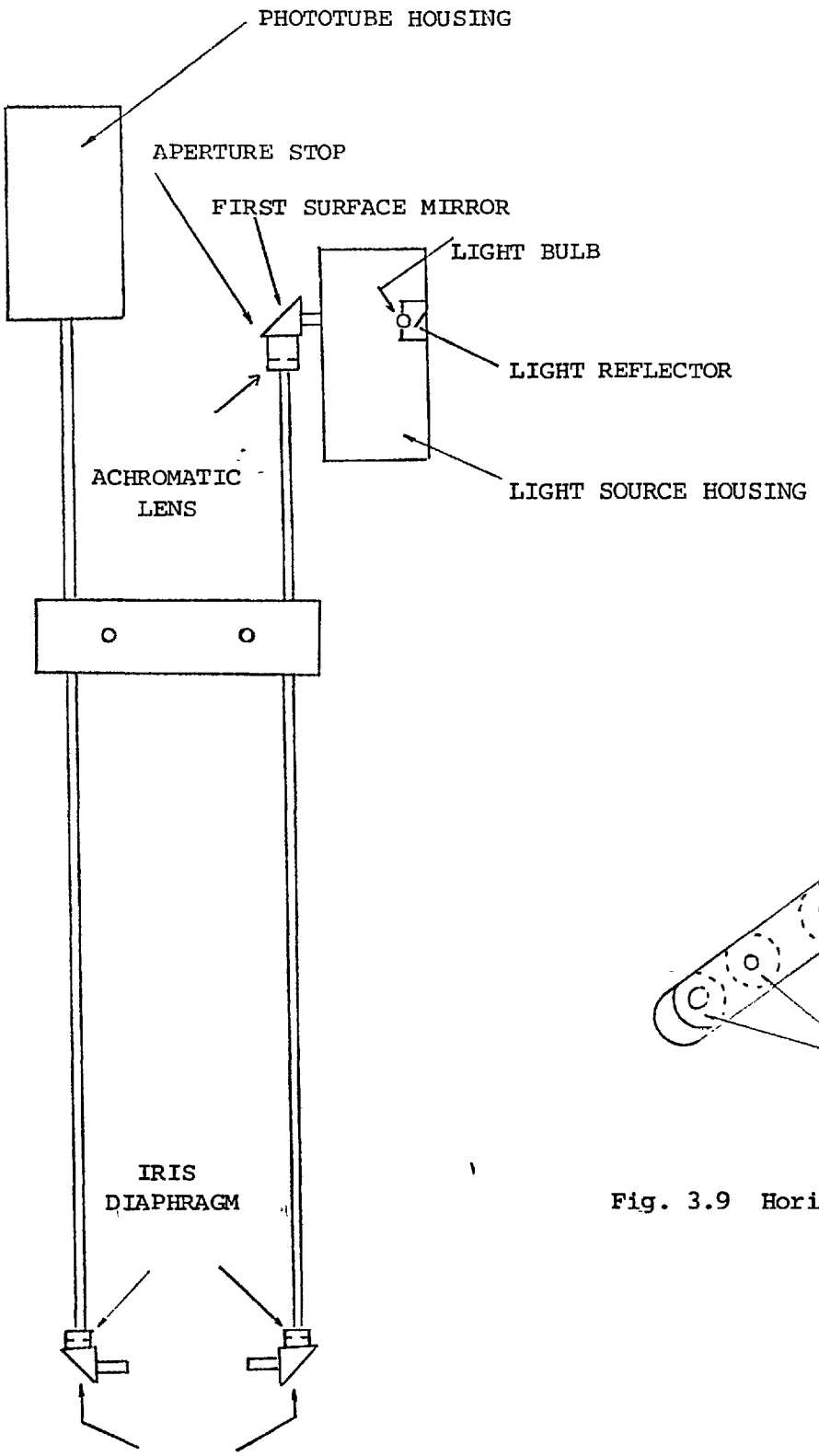


Fig. 3.8 The experimental light probe

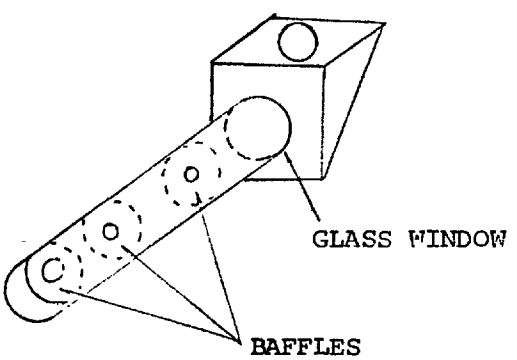


Fig. 3.9 Horizontal section.

air was circulated through the column and the air flowrate was set to prevent weeping during the initial introduction of liquid. Keeping the air flowrate constant, liquid flowrate was gradually increased until the dispersion changed from spray to bubbly. This procedure was repeated for different gas flowrates. Once the boundary was located, the column could be operated in the fully developed spray regime. Dispersion density and the fraction of light transmitted through the dispersion were measured at different heights above the sieve plate. The following systems were studied:

	density ρ kg/m^3	surface tension γ N/m	viscosity μ Ns/m^2
1. Butanol	809	24.6×10^{-3}	2.950×10^{-3}
2. Methanol	792	22.60×10^{-3}	0.597×10^{-3}
3. Water	998	71.97×10^{-3}	1.00×10^{-3}
4. 1000 ppm hydrous ferric oxide in water	AS WATER		
5. 1000 ppm hydrous aluminium oxide in water			

CHAPTER FOUR

RESULTS

4.1 Introduction

As discussed previously the parameters which influence the nature of dispersion formed on sieve plates are

1. Vapour and liquid physical properties
2. Vapour and liquid flowrates
3. Design variables - hole diameter and plate free area.

Among the physical properties, which have an influence on the type of dispersion formed, the effect of viscosity and surface tension has been investigated. In addition, the effect of operating variables on the nature of dispersion formed has been studied. Experimental work also included the study of the effects of colloids on the hydrodynamic behaviour of the plate. Since the main interest in this investigation lies in the spray regime, this regime was delineated in terms of operating variables using a light transmission technique.

In the fully developed spray regime, the fraction of liquid in the dispersion at various heights above the plate floor was measured to obtain the dispersion density by means of the gamma ray attenuation technique. Fraction of light transmitted through the dispersion was used to provide the surface area profile.

4.2 Effect of Colloidal Suspension on Foaming

The flow pattern that exists at low gas flowrates is cellular foam and colloidal suspensions were found to have negligible effect on the foaming behaviour of sieve plates for the concentrations employed. This is discussed later in Chapter 7.

4.3 Transition Point

Transition results are graphically presented in Fig. 4.1 for methanol, butanol and water. Methanol and butanol have similar physical properties except for viscosity which is about five times higher for butanol than for methanol. Fig. 4.1 clearly illustrates that viscosity has a significant influence on the transition point. It also shows that gas flowrate at transition increases with increased liquid loading.

Based on the correlation of Kutateladze and Styrikovich Jeronimo and Sawistowski[52] proposed a correlation for hole velocity at transition:

$$u_h^t = \frac{0.655(g\Delta\rho\gamma^2/d_H\rho_G^3)^{1/6}}{A_f F_c} \qquad (4.1)$$

where F_c is a correction factor for liquid flow.

Using the data of Pinczewski and Fell[31] Jeronimo found F_c to be given by

$$F_c = 1 + 0.000104 L_v^{-0.59} A_f^{-1.79} \qquad (4.2)$$

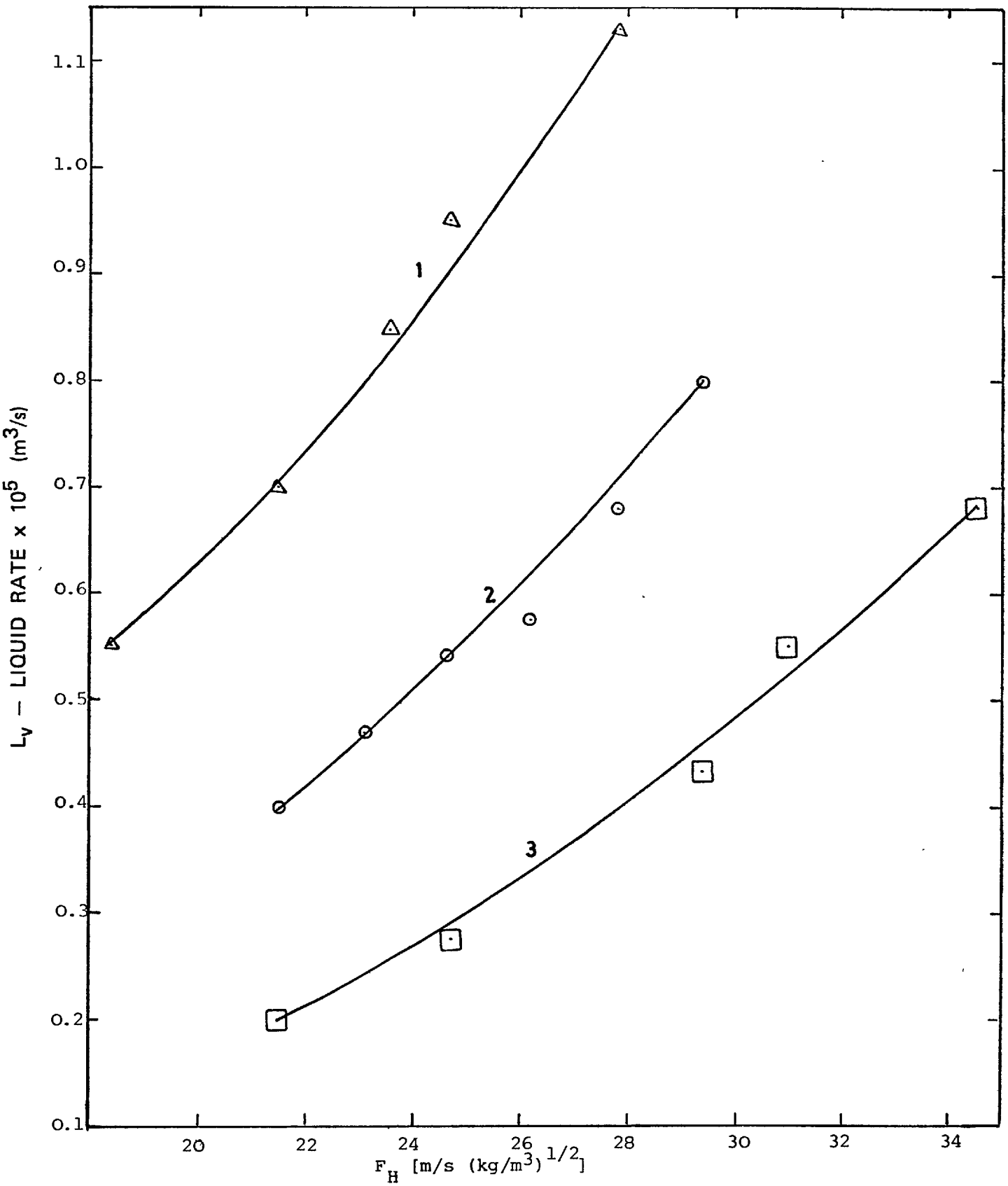


Fig. 4.1 The effect of viscosity on the transition from spray to bubbling. (1: butanol, 2: methanol, 3: water)

However, Fell's results do not show a strong dependence on liquid flowrate. For example a liquid flowrate of 10 m^3/hr m weir needs an F_H factor of 20 for transition whereas a liquid flowrate of 56 m^3/hr m weir needs only an F_H factor of about 24 for transition for a tray having a free area of 10.7%. Therefore the correction term introduced for liquid crossflow is negligible and equation 4.1 reduces to

$$U_h^t = \frac{0.655}{A_f} \left(\frac{g\Delta\rho\gamma^2}{d_H\rho_G^3}\right)^{1/6} \qquad (4.3)$$

It can be noticed that Jeronimo's correlation did not include the effect of viscosity which indicates a fundamental weakness in the model on which it is based. A correlation of the transition point must therefore incorporate the effect of viscosity and of the liquid rate which proved to be much more significant than previously predicted.

Nevertheless in establishing a new correlation it was decided to retain the group $\frac{1}{A_f}\left(\frac{g\gamma^2}{d_H}\right)^{1/6}$, and represent the effect of the liquid and gas flowrate by using the flow parameter $(L/G)(\rho_G/\rho_L-\rho_G)^{1/2}$ by analogy to flooding correlation in packed columns and empirically establishing the influence of viscosity. The flow parameter used here is similar to the flow parameter $(L/G)(\rho_G/\rho_L-\rho_G)^{1/2}$ employed by Porter and Jenkins[53]. The final correlation obtained is

$$U_h^t = \frac{const}{A_f}\left(\frac{g\gamma^2}{d_H\mu^2}\right)^{1/6} \frac{L}{G}\left(\frac{\rho_G}{\rho_L-\rho_G}\right)^{1/2} \qquad (4.4)$$

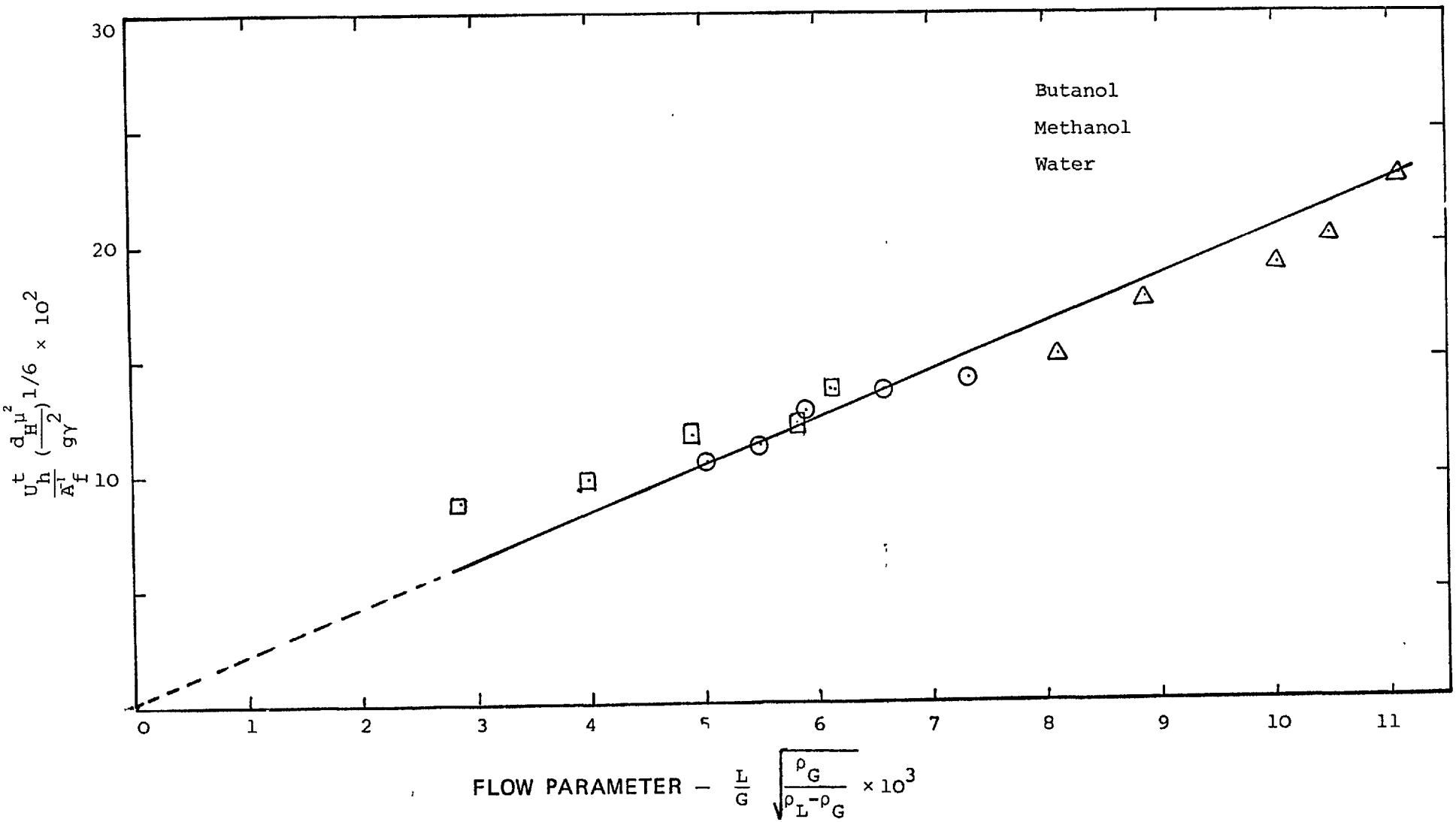


Fig. 4.2 Transition Correlation

The constant is equal to 20.05 if SI units are used throughout (Fig. 4.2). It seems significant that hold-up data of Porter and Wong[43] at constant U_h^t indicate holdup to be proportional to $(\rho_G/\Delta\rho)^{1/2}$.

4.4 Parameters Affecting Dispersion

Experimental dispersion density measurements and the fraction of light transmitted through the dispersion are tabulated in the Appendix 2 and represented graphically in Figs 4.3-4.6 as

1) Fraction of liquid in dispersion as a function of height above plate floor

2) Specific surface area as a function of height above plate floor.

4.4.1 Effect of Viscosity

The systems chosen to study the effect of viscosity were methanol and butanol. In these two systems surface tension and density are similar but the viscosity is about five times higher for butanol than for methanol. It is clear from the dispersion density profiles presented in Fig. 4.3 that the two systems behave differently in the fully developed spray regime. This can be attributed to the effect of viscosity. The height at which the maximum occurs in the profile is higher for methanol than for butanol and the maximum increases with increasing viscosity for the same gas and liquid flowrates. This maximum is the characteristic feature of the spray regime. Profiles also suggest that there is more liquid held at higher levels of dispersion for methanol than for butanol.

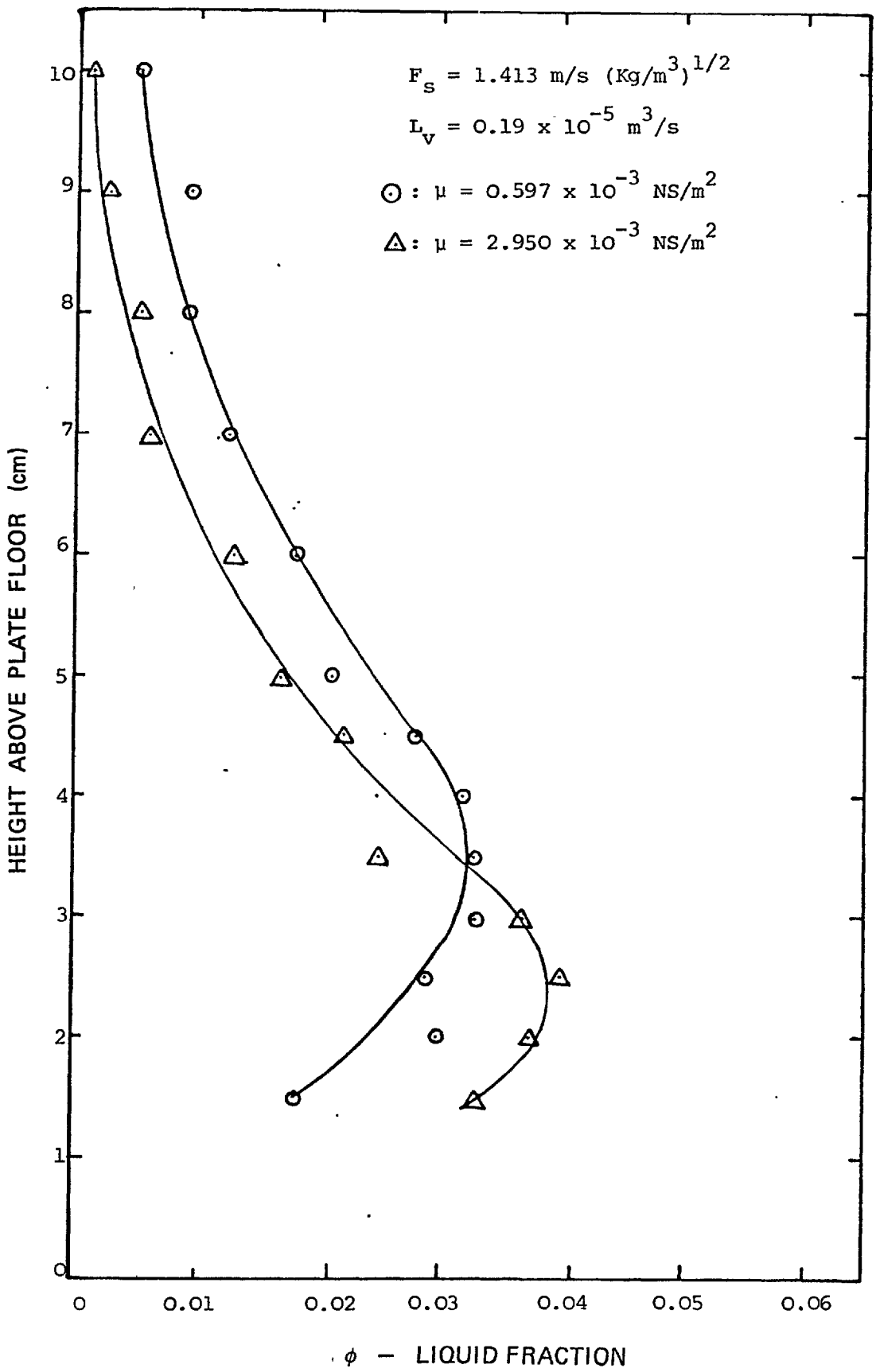


Fig. 4.3 Dispersion-density profiles

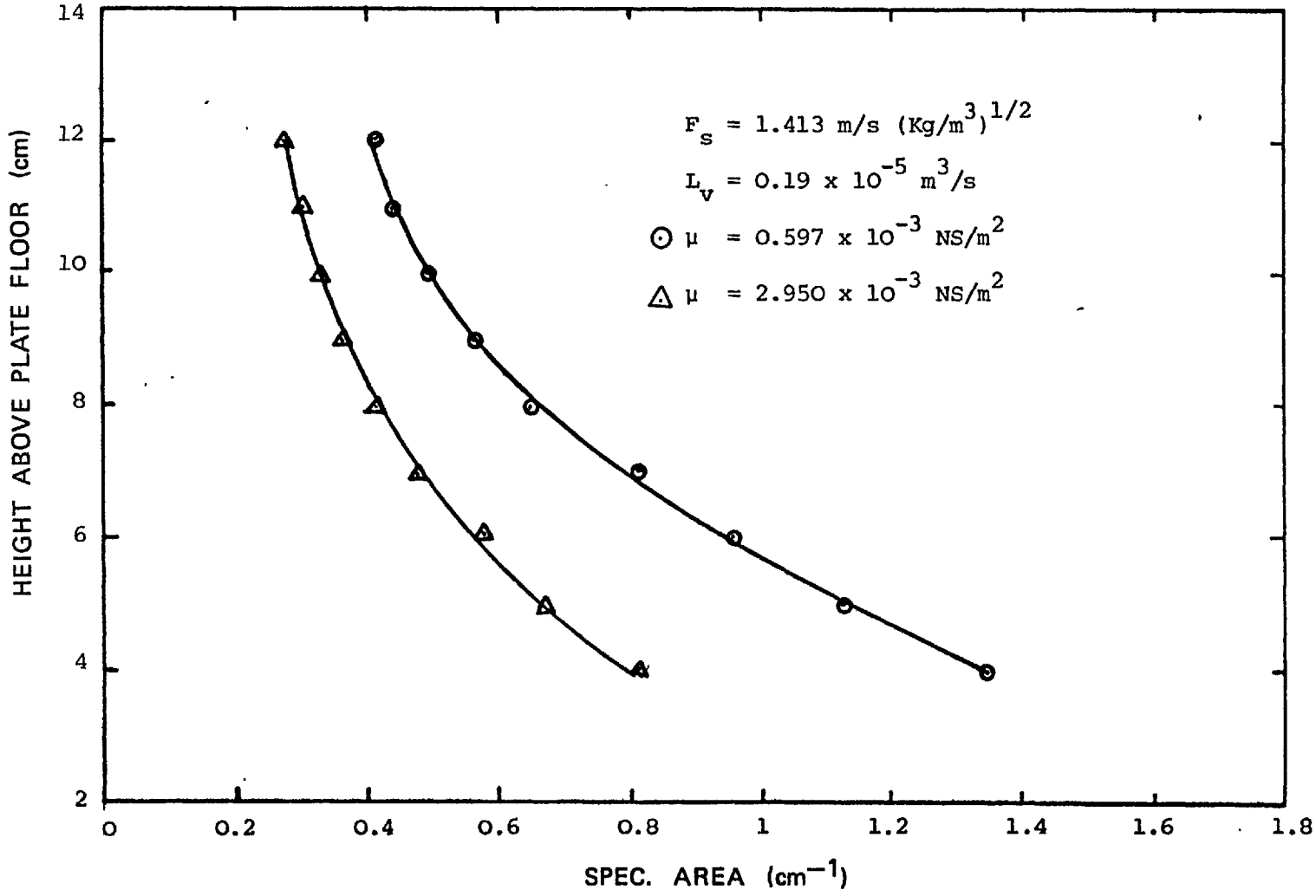


Fig. 4.4 Specific surface area profiles

It can be seen from the surface area profiles in Fig. 4.4 that butanol has lower surface area than methanol. This suggests that comparatively larger drops are formed in the case of butanol than for the less viscous methanol. This agrees with the visual observation which indicated the presence of smaller drops for methanol with a consequent increase in entrainment.

4.4.2 Effect of Surface Tension

It is difficult to ascertain accurately the effect of surface tension on dispersion density profiles from the work carried out because in the systems employed surface tension was not constant. However, a rough comparison was made between water and methanol. Water has a surface tension about 70% higher than methanol and the viscosity about 40% higher. Density of water is about 20% higher than that of methanol. It is clear that the effect of surface tension is stronger between the two systems and any difference in behaviour between the two systems can be attributed primarily to the effect of surface tension.

Comparison of the two profiles for water and methanol (Fig. 4.5) indicates that the maximum in the profile for methanol is higher than for water and more liquid is held at upper levels of dispersion.

The surface area profiles (Fig. 4.6) indicate that methanol has larger surface area. This suggests that small diameter drops are formed in methanol. Again this is in agreement with visual observation. The maximum in the profile increases with increasing surface tension with a corresponding decrease in height at which this maximum occurs for the same operating conditions.

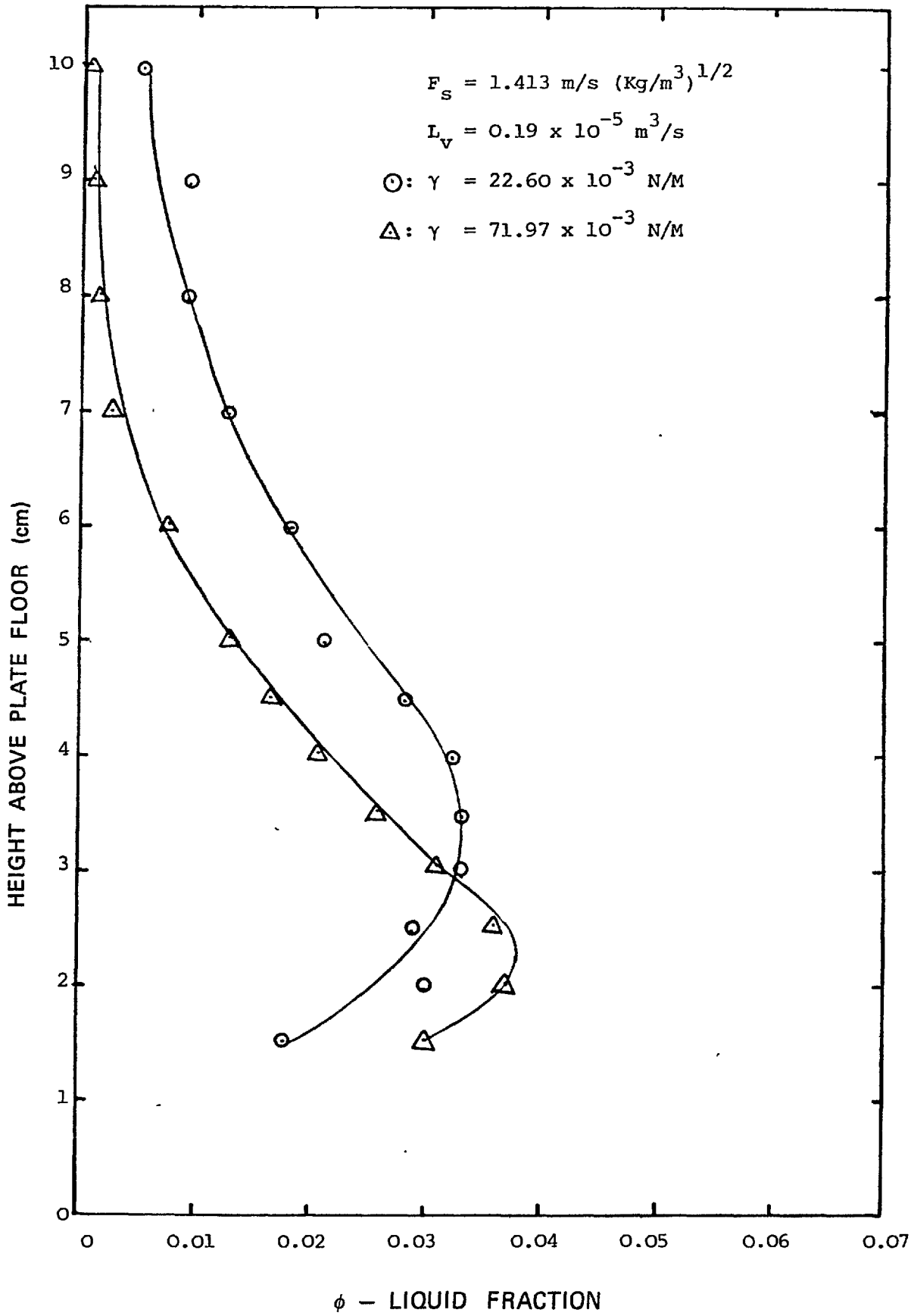


Fig. 4.5 Dispersion-density profiles.

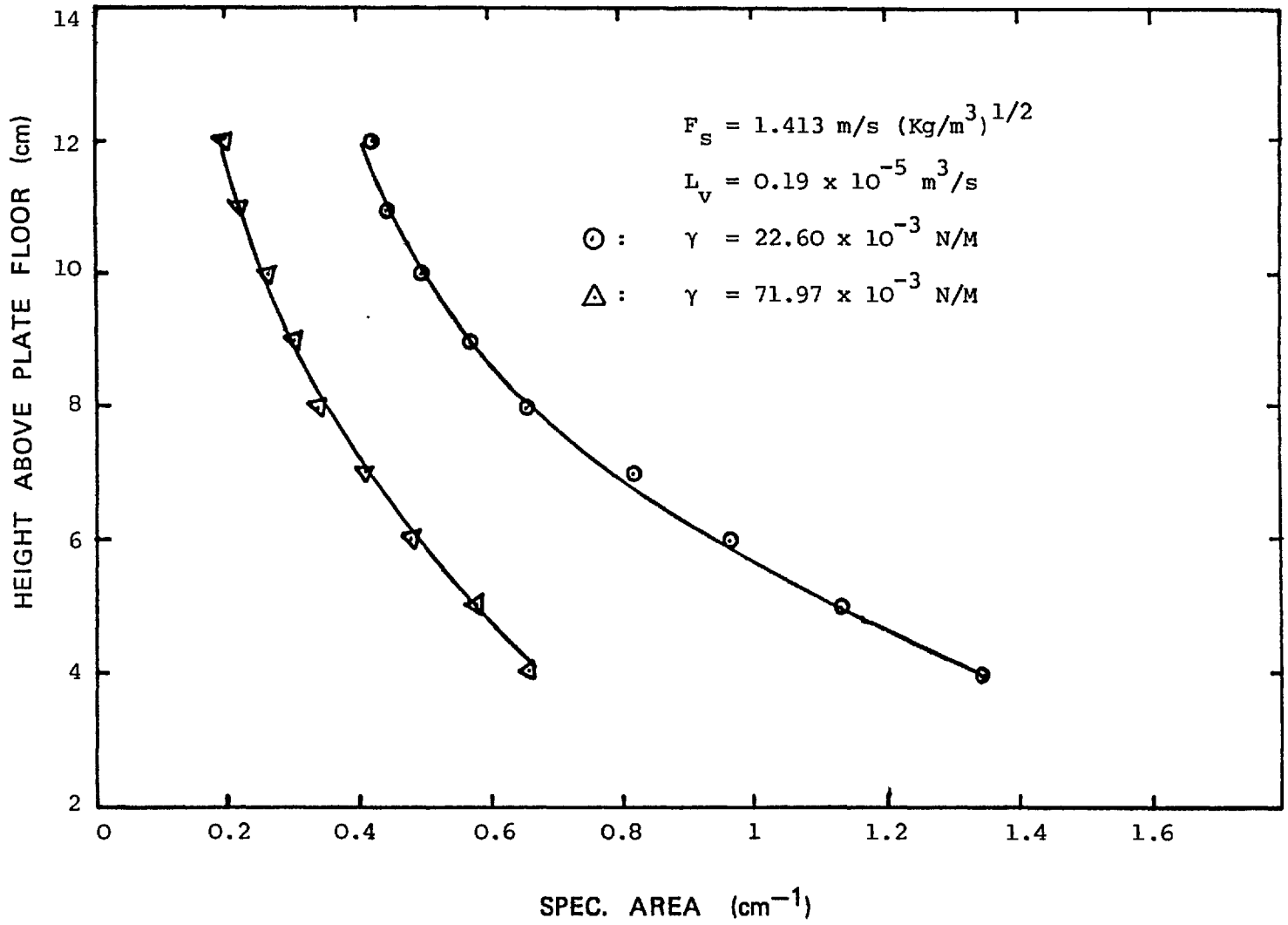


Fig. 4.6 Specific surface area profiles

Jeronimo[44] studied the effect of surface tension on dispersion density profiles using the systems air/dilute aqueous methanol solution. In such a system it is possible to obtain large surface tension variations with small changes of physical properties. The above results are roughly in agreement with those predicted by Jeronimo.

4.5 Effect of Operating Variables

Figs 4.7 and 4.8 illustrate the effect on the dispersion density profile of increasing the gas flowrate at constant liquid flowrate. The maximum in the profile decreases with increasing gas flowrate in all the systems studied. The corresponding height at which this maximum occurs in the profile increases with increasing gas velocity. Also at high gas velocities more of the liquid is held in the upper levels of the dispersion.

The effect of increasing the liquid rate at constant gas rate is shown in Fig. 4.9. The maximum of the profile and the corresponding height increases with increasing liquid flowrate. Also it can be seen that the dispersion density increases at all levels due to more liquid being atomised. This of course is only valid up to a critical flowrate at which phase transition occurs.

4.6 Effect of Colloidal Suspensions

Presence of colloids did not show any significant effect on the dispersion density profile in the fully developed spray regime for the concentrations studied (see Fig. 4.10).

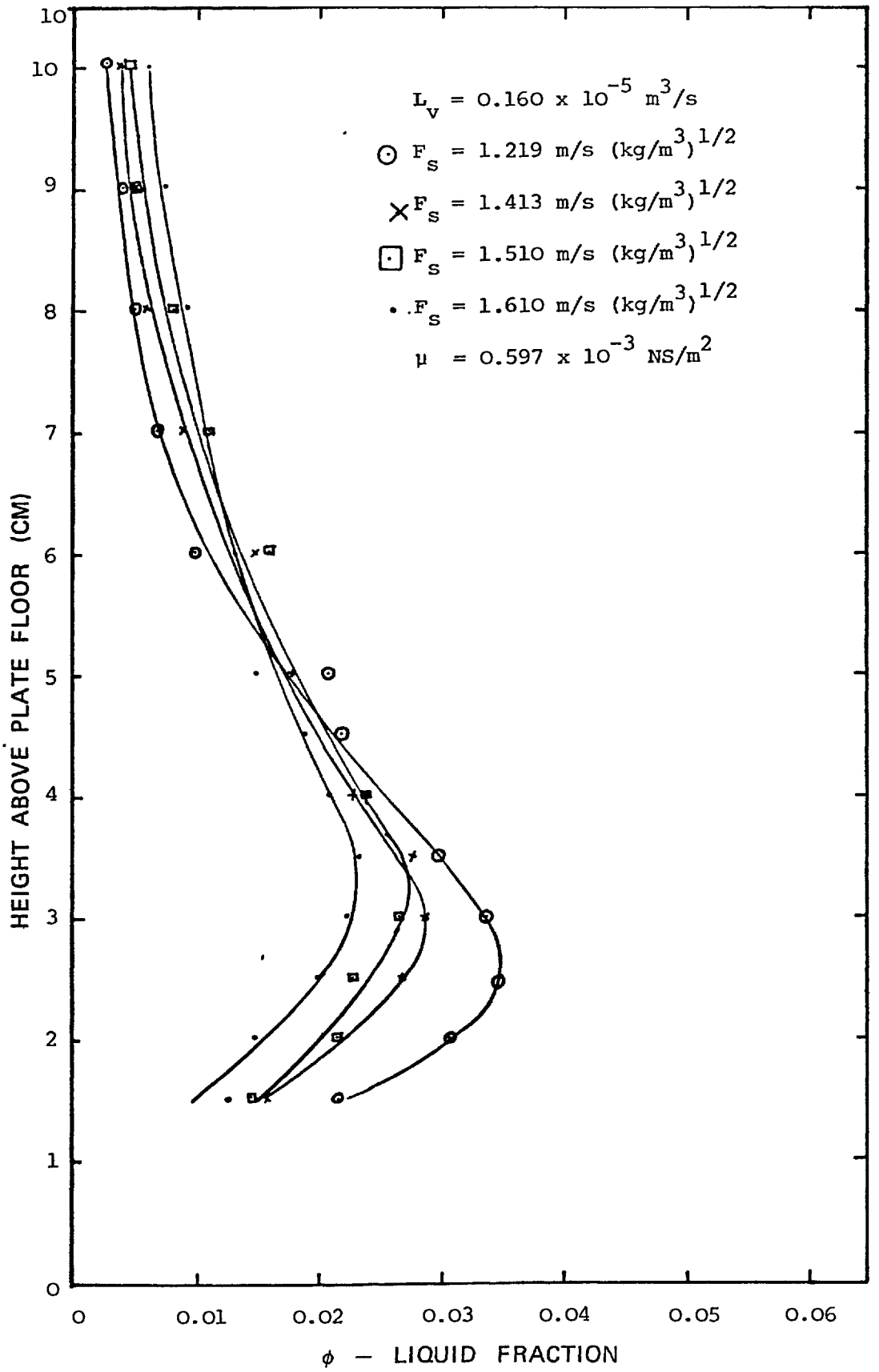


Fig. 4.7 Dispersion-density profiles.

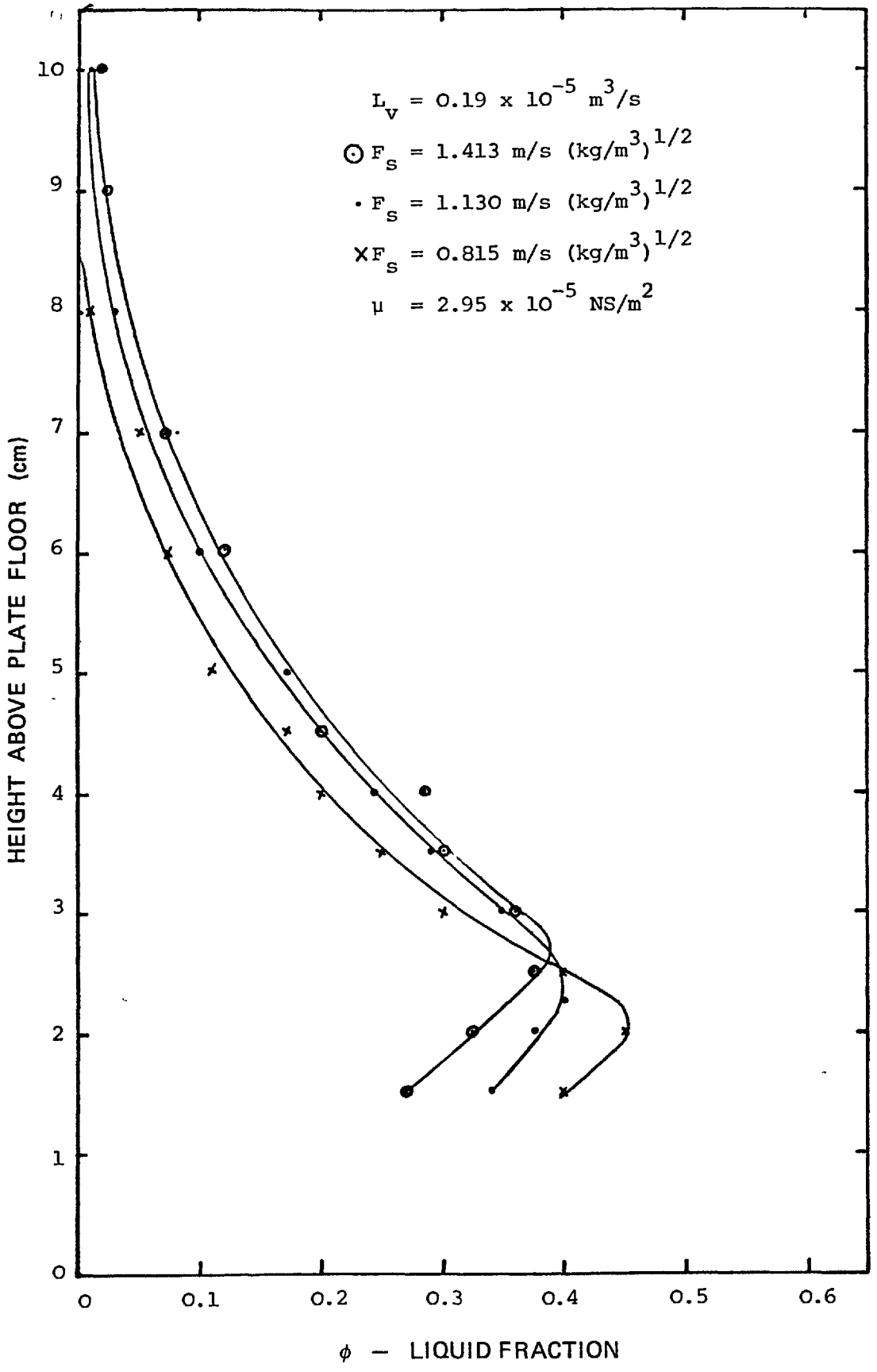


Fig. 4.8 Dispersion-density profiles

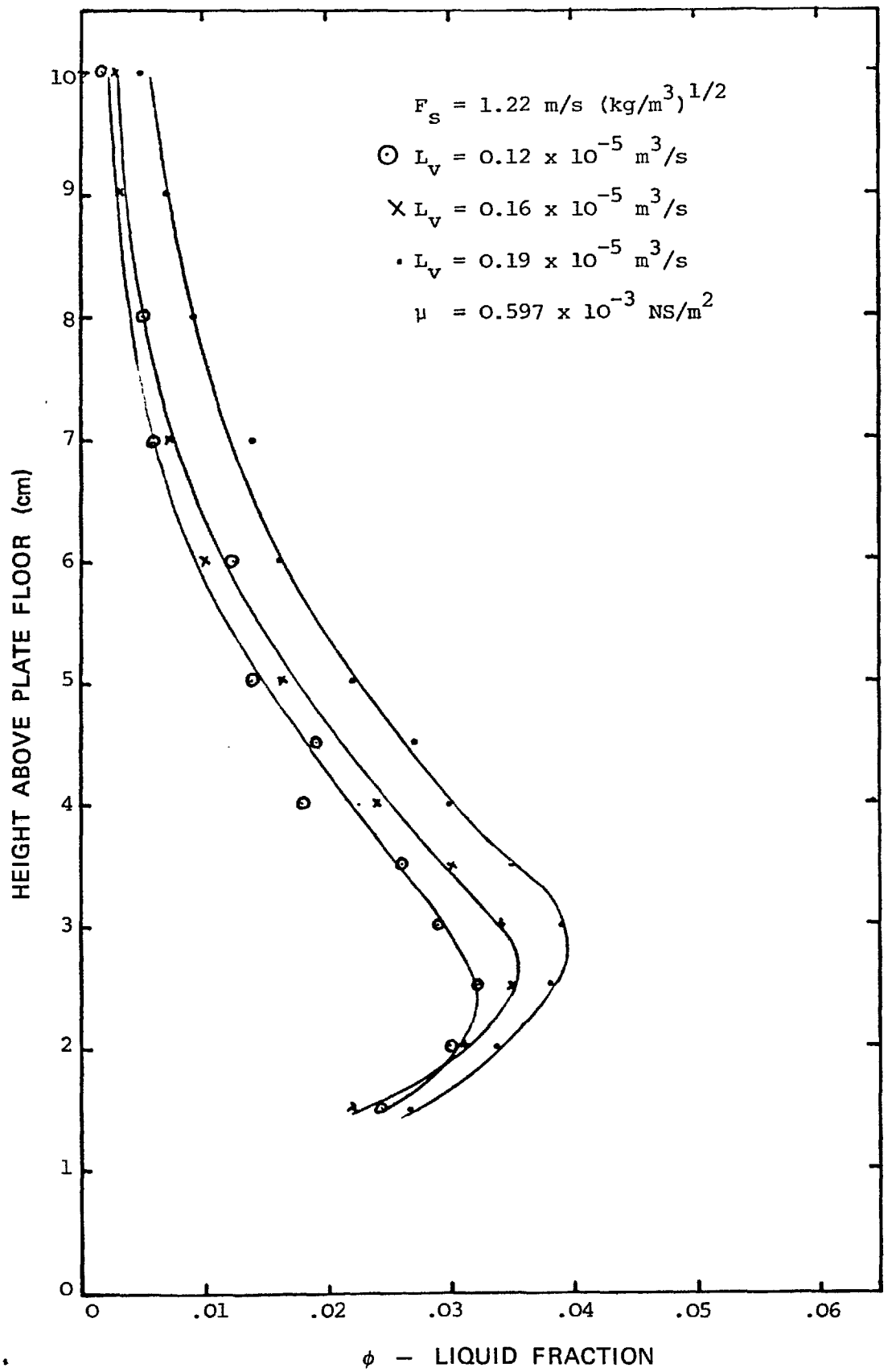


Fig. 4.9 Dispersion density profiles.

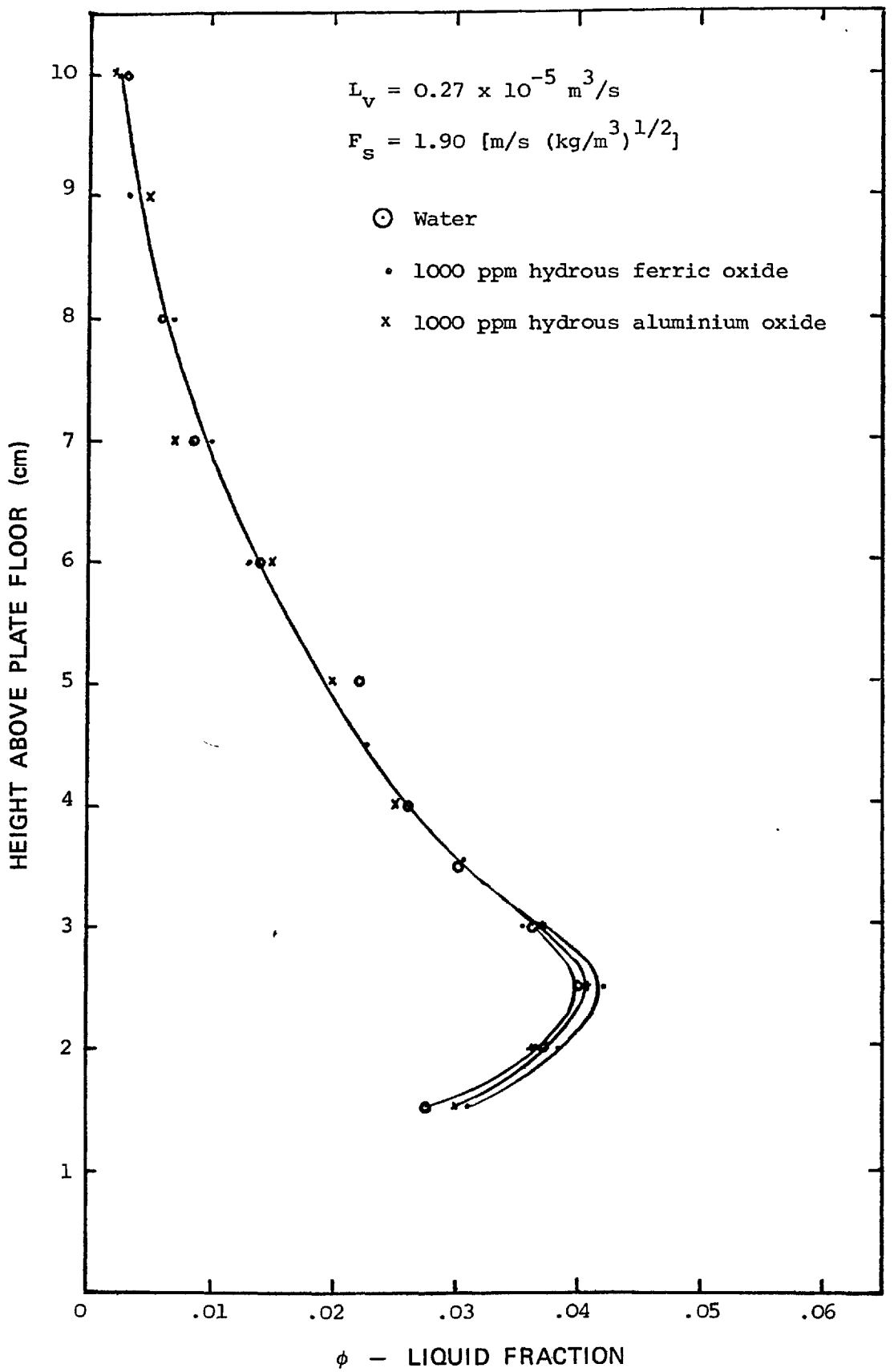


Fig. 4.10 Dispersion density profiles

4.7 Entrainment

It is clear that the lower the viscosity and surface tension of a liquid the greater is the tendency to produce smaller droplets and thus increase the entrainment. This is in agreement with atomisation studies. Garner et al[78] has explained the relationship between viscosity of liquid and the size of droplets as follows: The time of formation of droplets from a filament of liquid was very short, and the rate of deformation of the liquid was high. If the viscosity were increased the viscous forces became large and larger droplets would be formed. Therefore the entrainment would probably decrease.

Entrainment values were calculated by parameter fitting of dispersion density profiles. The computer program is listed in the Appendix 3. The entrainment can be correlated by

$$e \propto \mu^{-0.2} \gamma^{-0.3} \qquad (4.5)$$

Jeronimo and Sawistowski[44] showed the dependence on gas velocity and liquid flow-rate

$$e \propto F_s^{9.1} L_v^{-0.49} \qquad (4.6)$$

Fell's[48] data for entrainment in the spray regime (Fig. 2.10) suggests that entrainment is strongly influenced by free area. On correlating his results

$$e \propto A_f^{-2.45} \qquad (4.7)$$

Yoshida[82] found $e \propto H^{-1.45}$ but this is obviously only applicable to conditions where the plate spacing is smaller than the distance reached by drops whose terminal falling velocity is larger than the superficial velocity. In the present work it was found from the

analysis of dispersion density profiles that $e \propto H^{-1.2}$ (Fig. 4.11). On taking into account the effect of physical properties, operating variables and design parameters, as predicted by other workers, the following correlation was obtained:

$$e = 5.86 \times 10^{-8} \frac{F_s^{9.1}}{A_f^{2.45} L_v^{0.49} H^{1.2}} \left(\frac{\gamma_W}{\gamma_L}\right)^{0.3} \left(\frac{\mu_W}{\mu_L}\right)^{0.2} \left(\frac{\rho_G}{\rho_L}\right)^{1/2} \quad (4.8)$$

For this equation

e	- entrainment	(kg/kg gas)
F_s	- superficial F factor $U_s\sqrt{\rho_G}$	$(ms^{-1}(kg/m^3)^{1/2})$
L_v	- volumetric liquid rate per unit length of weir	(m^2/s)
H	- tray spacing	(m)
γ_W and γ_L	- surface tension of water and liquid	(N/m)
μ_W and μ_L	- viscosity of water and liquid	$(N\ s/m^2)$
ρ_G and ρ_L	- density of air and liquid	(kg/m^3)

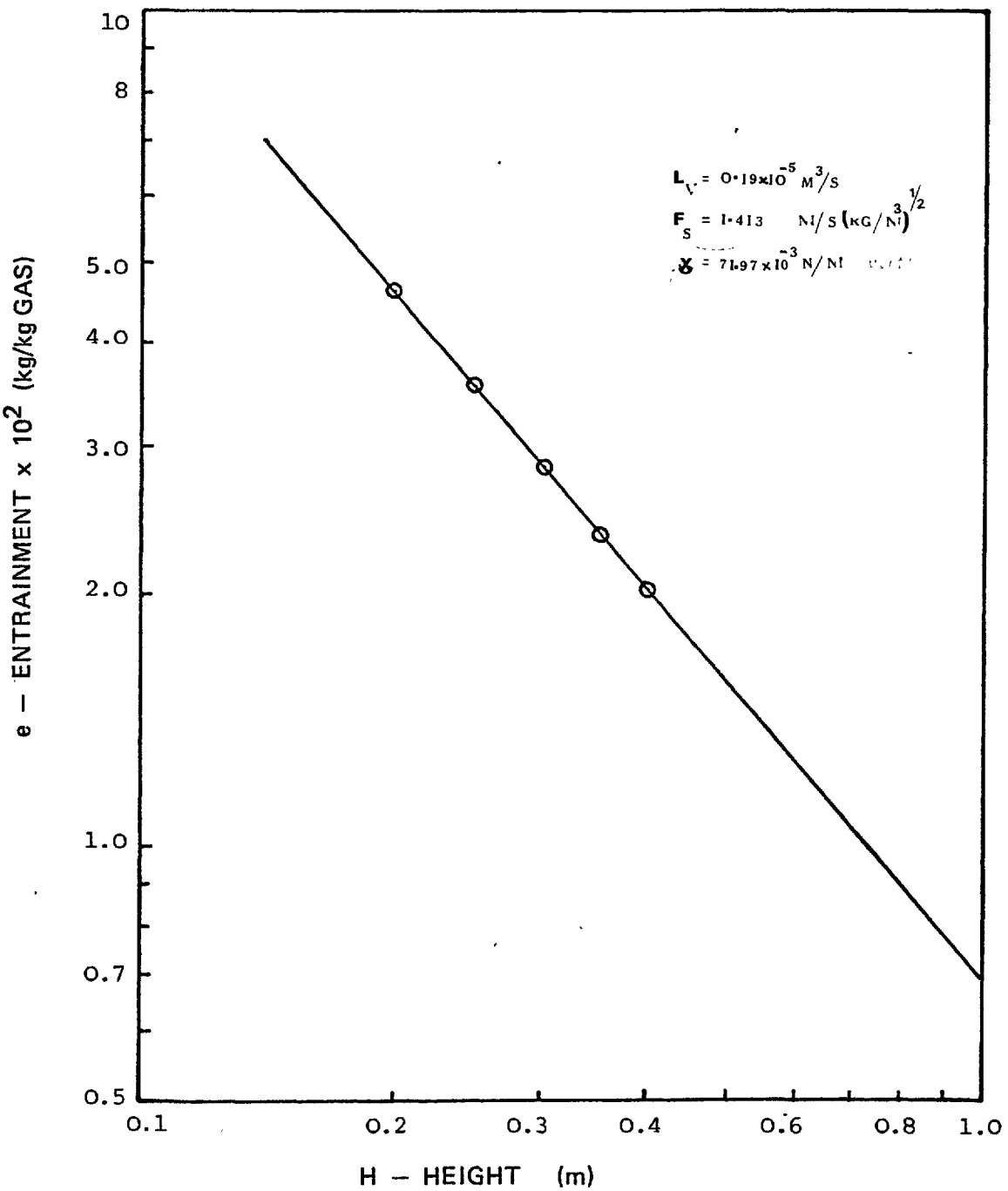


Fig. 4.11 Variation of entrainment with height.

CHAPTER FIVE

INITIAL PROJECTION VELOCITY

5.1 Introduction

In the spray regime the liquid is continuously atomised near the plate floor. The droplets produced are projected upwards with an initial projection velocity and follow clearly defined trajectories. The initial projection velocity is thus an important parameter in modelling of the regime. It determines the residence time of the drop in the intertray space and hence the mass transfer performance of the plate. There is only limited amount of information available in the literature on initial projection velocity. Fane and Sawistowski[1] correlated the data of Alba and Yamada[34] as

$$V_p = 0.4 \left(\frac{0.004}{d_p}\right)^{0.93} = 2.355 \times 10^{-3} \, d_p^{-0.93} \qquad (5.1)$$

With the aid of this correlation they successfully predicted the mass transfer performance of a small-scale sieve plate. Later Fell et al[37] proposed an equation of the form

$$V_p = \frac{3\rho_G}{4 d_p \rho_L} \int_0^t C_D V_h^2 \, dt \qquad (5.2)$$

where t is the vapour rush time.

The duration of the vapour rush was estimated from the knowledge of the largest droplet size produced. This requires separate data for similar dynamic conditions to be available to give the breakup time of the ligament that will produce droplets of this size. Apart from the need for separate experimental study to evaluate the vapour rush time, Fell et al have claimed agreement[37][61] between

their results and the Fane and Sawistowski correlation. This strengthens the validity of equation 5.1. This is further confirmed by the experimental results of Jeronimo and Sawistowski[84] who assumed A and B to be adjustable parameters in the relation $V_p = Ad_p^B$ and determined A and B by parameter fitting of dispersion density and specific surface area profiles. They also conducted a sensitivity analysis on effects of variations of A and B on interfacial area and plate efficiency. The effect on the latter tended to be small. However, in spite of this agreement there is little doubt that the equation oversimplifies the mechanism of droplet formation. Therefore an attempt was made to extend the Fane and Sawistowski correlation to take into account physical properties, design parameters and operating variables without losing the simplicity of the original correlation.

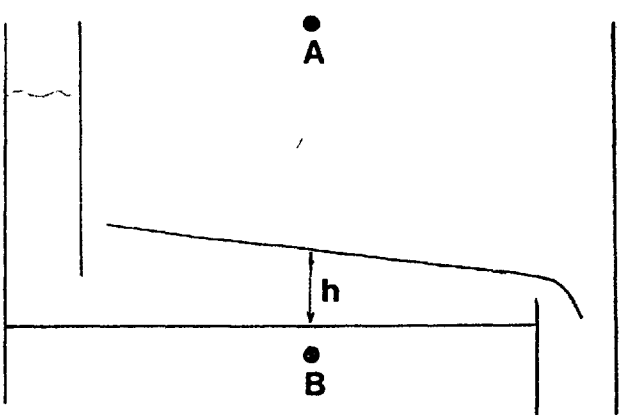
5.2 Mechanism of Droplet Formation

The mechanism of droplet formation is now fairly well established from high speed photographic studies and confirmed by visual observation. Liquid is sheared as the high velocity vapour jets through the orifice and dragged up in the form of sheets which subsequently rupture into ligaments and then break up into drops as a result of hydrodynamic instability. Size of the drops form depends on the thickness of the ligament at the instant of ligament breakup which occurs as a result of the drag force exceeding the surface tension force. The breakup of the bulk of liquid, that is liquid shearing and ligament breakup (formation of interfacial area) as well as the projection of droplets, require energy. It is therefore obvious that the primary consideration in predicting the initial projection

velocity should involve energy and momentum transfer. Initial projection velocity depends therefore on the physical properties of the two phases involved, on plate and column geometry, and on the operating variables. Because of the complex mechanism of droplet formation and the number and nature of the variables involved, theoretical prediction of the initial projection velocity is hardly possible. A semitheoretical approach based on energy and momentum transfer is therefore adopted in this work.

5.3 Total Pressure Drop

Energy transferred to the liquid by the high velocity vapour jet is proportional to the drop in pressure across the plate.



The pressure drop across the plate from point B to point A known as the wet plate pressure drop is the sum of

1. Dry plate pressure drop,
2. Hydrostatic head, h ,
3. Residual pressure drop, i.e. pressure drop corresponding to energy losses resulting from:
   (i) liquid shearing,
   (ii) formation of interfacial area,

(iii) projection of droplets,

(iv) losses such as turbulence, expansion, etc.

The dry plate pressure drop is that pressure drop which would occur if the vapour passed through the holes without liquid on the plate. This can be calculated from the orifice equation[75]

$$v_2 = \frac{C}{Y}\sqrt{\frac{2g(\Delta P_{3,1})}{\rho_1[1 - (\frac{A_2}{A_1})^2]}} \tag{5.3}$$

where C = average orifice coefficient

Y = average expansion factor for the fluid

A = cross-sectional area

subscripts

1 = condition upstream from orifice

2 = condition in the orifice

3 = condition downstream from orifice

This is the flow equation for a single orifice. For a perforated plate assuming that the fluid flowing is equally distributed among all holes the equation of continuity can be written as

$$A_D v_D = (\text{no of holes})(A_d)(v) = A_f v \tag{5.4}$$

where subscripts d refers to the orifice and D to the column. v is the average fluid velocity in the orifice.

Therefore the flow equation for a perforated plate becomes

$$v = \frac{C}{Y}\sqrt{\frac{2g(\Delta P)}{\rho_D[1 - (\frac{A_f}{A_D})^2]}} \tag{5.5}$$

The presence of liquid on the tray creates a static head. Residual pressure drop is the difference between the total pressure drop across the plate less the dry plate pressure drop and liquid head. This way of calculating the residual pressure drop is not strictly correct because in a dry plate the expansion losses would be high. When the gas encounters liquid on the tray, part of this becomes useful energy which has not been accounted for previously. One would expect the residual pressure drop to be a significant factor in the fully developed spray regime because liquid shearing, formation of interfacial area, i.e. of droplets, and their projection take up a substantial amount of energy.

5.4 Residual Pressure Drop

5.4.1 Liquid Shearing

The liquid is atomised by the jetting action of the high velocity vapour stream. The force required to overcome the viscous forces in the liquid phase is the shearing force and this depends mainly on viscosity.

Experimental work carried out with methanol and butanol, i.e. liquids of almost the same surface tension and density but with large viscosity difference, under the same operating conditions, have indicated that with methanol - the low viscosity liquid - the surface area generated (Fig. 4.4) was significantly larger than for butanol, thus suggesting a smaller dropsize at formation. The dispersion density profiles (Fig. 4.3) show the maximum at a higher level for methanol than for butanol with higher liquid holdup at higher levels above the plate floor. This again suggests a smaller dropsize at formation, since smaller drops reach greater heights, or, alternatively,

a higher initial projection velocity. This can be explained in terms of the energy transfer process as methanol, being less viscous needs less energy for shearing and more energy is therefore available for formation of interfacial area and droplet projection. This availability of additional energy for interfacial area formation explains the higher surface area and hence the presence of small drops with higher projection velocities, i.e. viscosity affects the projection velocity not only through drop size as could be deduced from equation 5.1. This in turn indicates formation of a large number of thin ligaments which consequently breakup into small drops. The above finding is also in agreement with atomisation studies.

Atomisation studies have predicted a dependence on viscosity for drop size. For sprays Mugele[76] proposed an equation based on dimensional analysis for mean drop size

$$\frac{\bar{x}}{D} = A \left(\frac{D\rho_L V_R}{\mu_L}\right)^B \left(\frac{\mu_G V_R}{\gamma}\right)^C \qquad (5.6)$$

where

$\bar{x}$ - mean or maximum drop diameter

D - characteristic linear dimension of the equipment

V_R - relative phase velocities at formation.

He suggested for the mean diameter the values of A, B, and C as 5.0, -0.35, -0.20 respectively and 57, -0.48, -0.18 for the maximum diameter. This is also in agreement with Hinze's[77] theory.

The effect of gas viscosity follows from the equation for continuity of shear stress at the interface

$$\mu_G \frac{dU_G}{d\ell} = \mu_L \frac{dU_L}{d\ell} \qquad (5.7)$$

From the above analysis it is reasonable to assume that the initial projection velocity and the droplet diameter are both functions of viscosity,

$$V_p = f(\mu_G, \mu_\ell)$$

5.4.2 Formation of Interfacial Area

Surface tension is important in the formation of interfacial area and therefore the provision of surface energy is a significant factor in the energy transfer process. Nielson[28] explained that ligaments become unstable under the influence of surface tension forces and neck down to form individual drops. Bainbridge and Sawistowski[59] and de Goederen[10] on the basis of vaporization studies came to the conclusion that plate performance changed linearly with reciprocal of surface tension. This indirectly suggests that small droplets are produced in a system with low absolute value of surface tension because such a system will assist sheet disintegration and tend to give higher proportion of thin filaments, thus giving a range of drop sizes with predominantly more small drops. Therefore, density of the spray and its interfacial area is greater for low surface tension systems.

Dispersion density profiles (Fig. 4.5) also suggests that there is more liquid in the upper levels of the dispersion and the height at which the maximum occurs in the profile increases with decreasing surface tension. This again suggests a finer drop size at formation and the higher heights reached by small drops.

In terms of energy transfer it can be said that drops are more easily formed in a low surface tension system. Larger surface area can be formed with less expenditure of energy so that more energy is

available for droplet projection giving the droplets high projection velocities. Therefore it can be concluded that initial projection velocity and droplet diameter are both functions of surface tension.

$$V_p = f(\gamma)$$

CONCLUSION

It can be inferred from the above analysis that surface tension and viscosity affect the projection of droplets and also the size of the droplet formed. Decrease in surface tension and viscosity of a liquid will produce smaller droplets and thus increase the surface area and hence the mass transfer performance of the plate. The smaller the droplets the greater wojld be the heights reached because of the high projection velocities. This will also result in increased entrainment. Therefore

$$V_p = f(\mu_G, \mu_L, \gamma)$$

5.4.3 Projection of Droplets

5.4.3.1 Effect of Hole Diameter

Among the design parameters which have an influence on the projection velocity hole diameter is the most significant one. If the hole diameter is doubled for the same free area, the pitch increases two-fold and the number of holes decreases by a factor of four and the surface area of the liquid in contact with the gas halves. This has a significant effect on the momentum transfer process as well as on energy losses. For triangular pitch

$$\text{Free area} = 0.907 \times \left(\frac{\text{Hole diameter}}{\text{pitch}}\right)^2 \qquad (5.8)$$

As the diameter increases pitch also increases in the same proportion and the number of holes are reduced for the same free area. This means that in plates with large hole diameter jet interaction will be minimal, whereas in small hole diameter plates jet impingement will be comparatively high contributing to energy losses. Surface area of the liquid which comes into contact with the gas is twice as high as that in large hole diameter plates. This indicates more energy is dissipated in liquid shearing and this increases the turbulence on the tray which means higher energy losses. In other words, less energy is available for interfacial area formation. In large hole diameter plates a large periphery of liquid can be efficiently sheared with minimal energy losses producing more droplets. There is experimental evidence[61] to suggest that the larger the hole diameter the higher is the projection velocity. Therefore

$$V_p = f(d_H)$$

5.4.4 Momentum Transfer

The drops formed at disintegration of the ligaments acquire an initial velocity which is the velocity of the ligament at the instant of ligament breakup. The ligaments attain their velocity as a result of momentum transferred by the gas to the liquid. Once the drops are formed they follow a well defined trajectory in the intertray space where the effect of drag is negligible[44] on drop trajectory. Therefore

$$V_p = f(V_R, \rho_G, \rho_L, d_P)$$

CONCLUSION

It can be concluded therefore that

$$V_p = f(d_P, d_H, V_R, \mu_G, \mu_L, \gamma, \rho_G, \rho_L, g)$$

As discussed above, at the instant of ligament break-up drops are formed and they simultaneously acquire an initial velocity. Initial projection velocity and drop diameter are both interrelated and depend on similar parameters. In the past, because of the simplicity with which the droplet diameter could be measured, the projection velocity was always considered as a function of droplet diameter. This is clearly insufficient and a correlation for the initial projection velocity must take into account all the parameters discussed above.

5.5 Proposed Correlation

In the present work, it was found that

$$V_P = \text{const} \frac{d_H^{0.75} V_R^2}{d_P^{0.83} \mu_L^{0.2} \gamma^{0.3}} \left(\frac{\rho_G}{\rho_L}\right) \qquad (5.9)$$

The constant is equal to 0.01795 if SI units are used throughout. $d_H^{0.75}$ was taken from Fells[61] data and $d_P^{-0.83}$ from the correlation of Jeronimo and Sawistowski.

The above correlation fits the data obtained using a light probe in a small column for the different systems studied (Figs 5.1 and 5.2). It also fits the data of Fell et al[61] taken on an industrial sieve try for 6.4 mm, 12.7 mm and 19.1 mm hole diameters (Fig. 5.3). In dimensionless form equation 5.9 can be written as

$$Fr^{1/2} = 25.41\ We^{1.25}\ Re^{-0.5}\ Bo^{-0.665} \left(\frac{\rho_G}{\rho_L}\right)^{1.085} \left(\frac{\mu_G}{\mu_L}\right)^{0.7} \left(\frac{\gamma}{\gamma_W}\right)^{0.285} \qquad (5.10)$$

where $Fr = \frac{V_P^2}{g d_P}$ - Froude number; $Re = \frac{V_R \rho_L d_H}{\mu_L}$ - Reynolds number

$We = \frac{V_R^2 d_H \rho_L}{\gamma}$ - Weber number; $Bo = \frac{g d_P^2 \rho_L}{\gamma}$ - Bond number.

However, the disadvantage of equation 5.9 is that the initial projection velocity is a function of drop diameter and needs a separate correlation for drop diameter. Fane and Sawistowski[1] found Mugele's[76] equation for mean drop diameter to be applicable in their studies.

$$\frac{d_{Pm}}{d_H} = 7.846 \left(\frac{V_R d_H \rho_L}{\mu_L}\right)^{-0.35} \left(\frac{\mu_G V_R}{\gamma}\right)^{-0.20} \qquad (5.12)$$

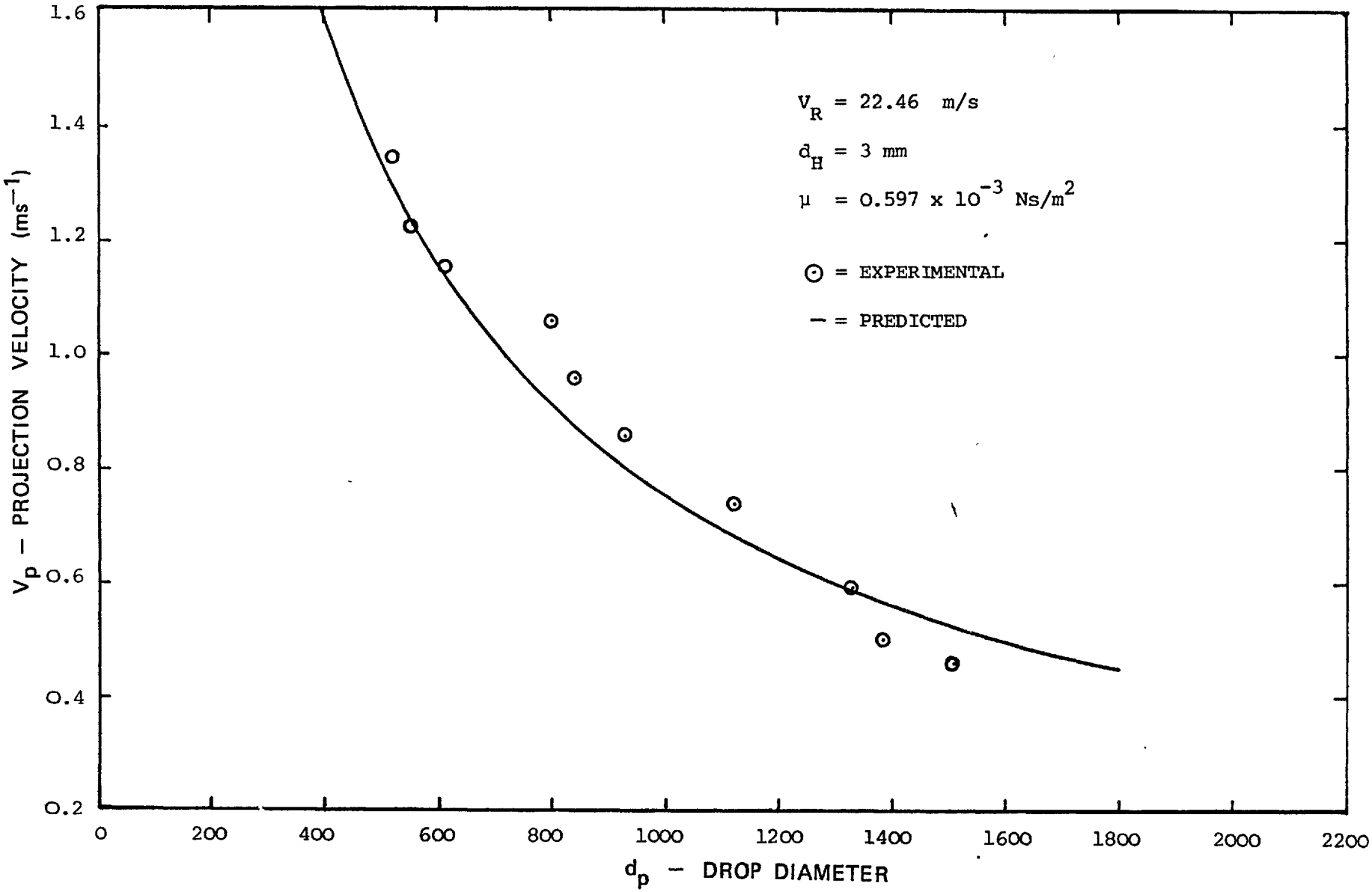


Fig. 5.1 Experimental and Predicted Droplet Projection Velocities

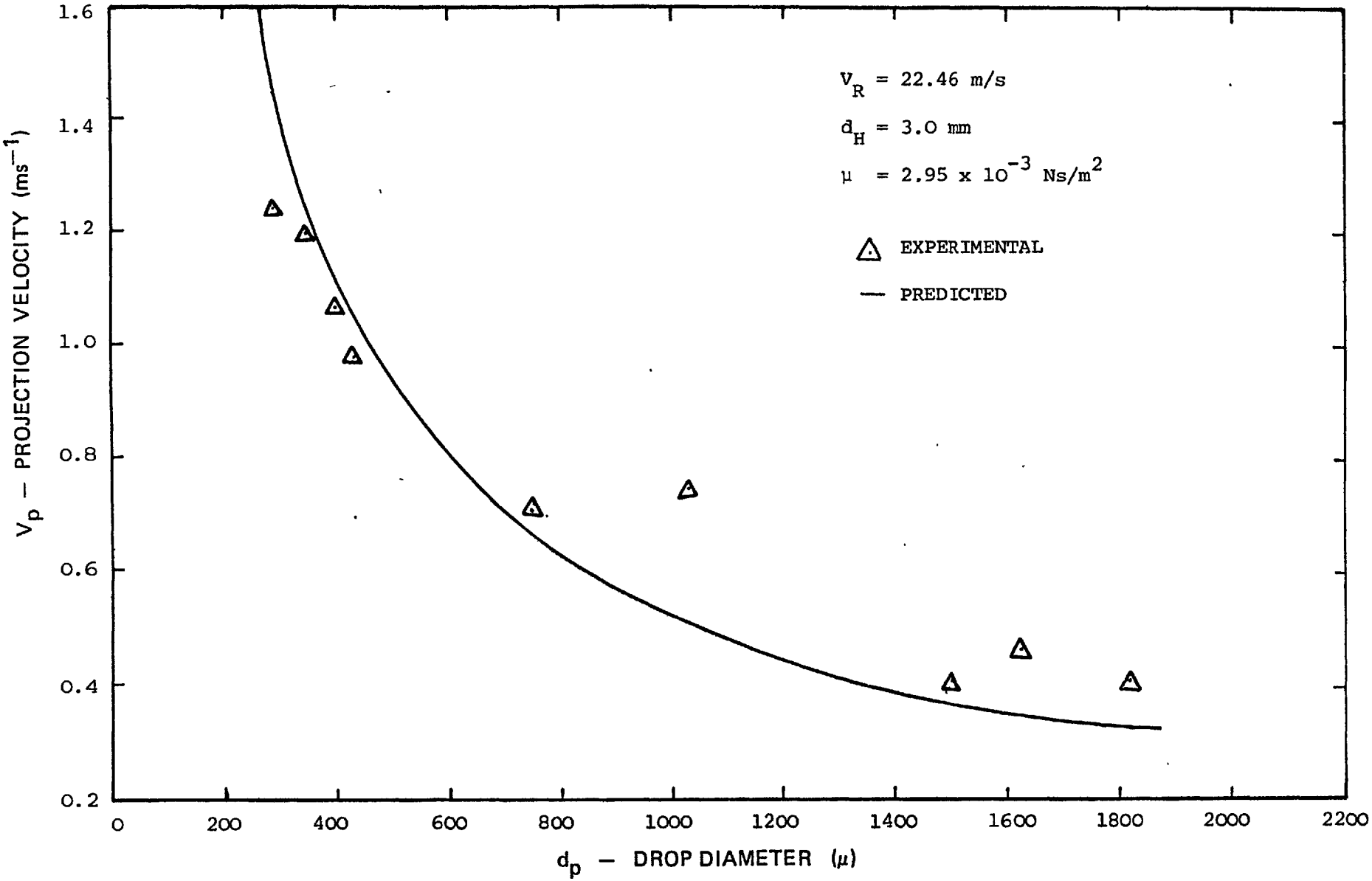


Fig. 5.2 Experimental and Predicted Droplet Projection Velocities.

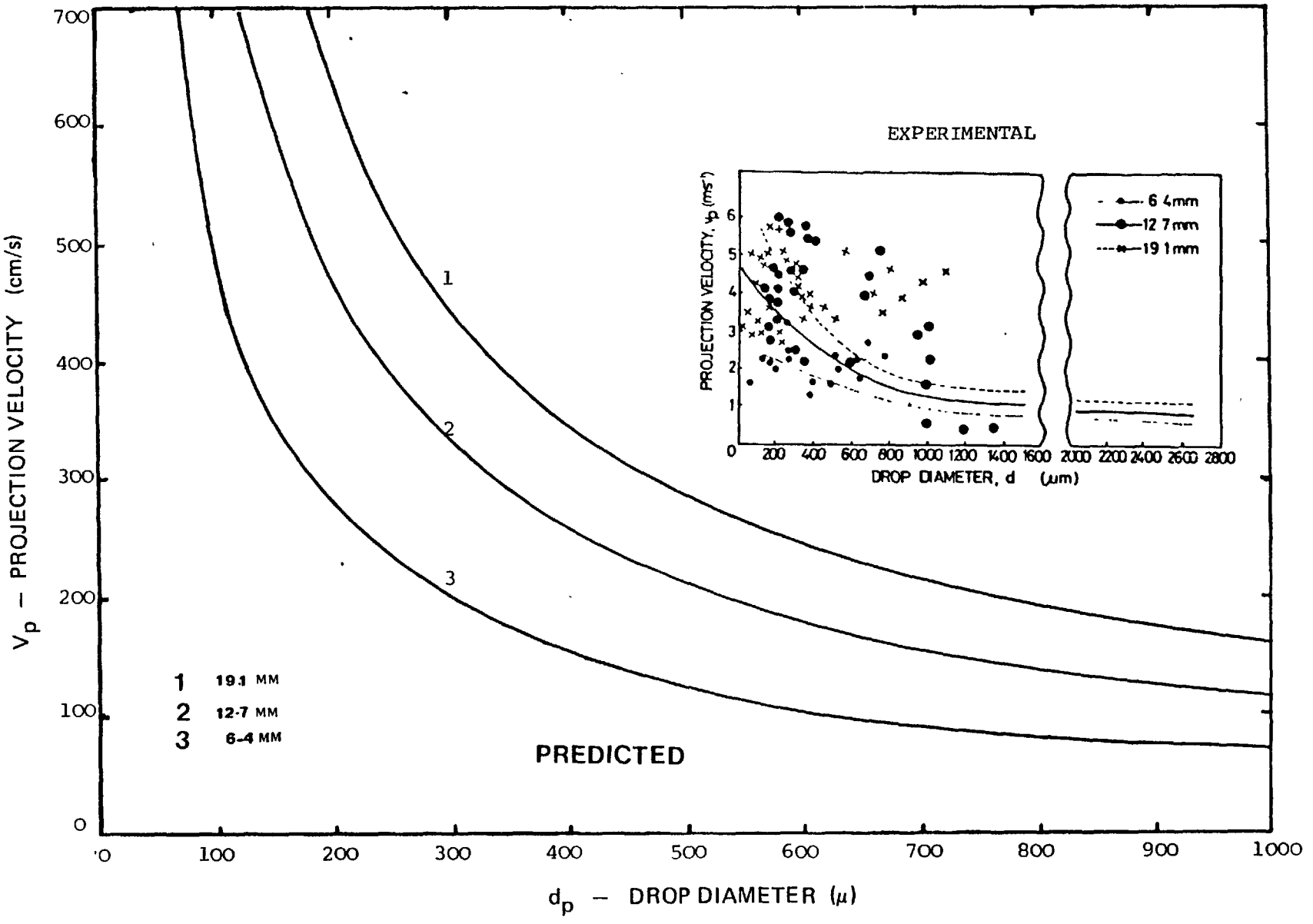


Fig. 5.3 Experimental[61] and Predicted Droplet Projection Velocities.

This can be written as

$$\frac{d_{Pm}}{d_H} = 7.846\ Re^{-0.15}\ We^{-0.2}\ \left(\frac{\mu_G}{\mu_L}\right)^{-0.2}$$

Substituting this in equation 5.9

$$(Fr)^{1/2} = 71.18\ We^{1.15}\ Re^{-0.575}\ Bo^{-0.665}\ \left(\frac{\rho_G}{\rho_L}\right)^{1.085}\left(\frac{\mu_G}{\mu_L}\right)^{0.6}\left(\frac{\gamma}{\gamma_W}\right)^{0.285}$$

where $Fr = \frac{V_P^2}{gd_H}$.

CHAPTER SIX

EFFICIENCY PREDICTION

6.1 Introduction

In the fully developed spray regime the liquid is continuously atomised at the plate floor by the high velocity vapour stream jetting through the orifice. The droplets generated follow clearly defined trajectories in the intertray space. The flow of liquid to the plate floor is supplied partly by the liquid flow onto the plate, and partly by the drops returning to the plate at the end of their trajectories for re-atomisation. Therefore, it can be said, that there are two distinct zones within the dispersion; one is a shallow pool of liquid on the plate floor serving as a liquid supply to the orifice, which is continuously replenished by the liquid feed, and the droplets returning to the plate floor. The other is the droplets zone, i.e. the actual spray. The dispersion density profiles clearly illustrate the presence of these two zones within the dispersion (Fig. 6.12). This observation, first made by Fane and Sawistowski on a small sieve plate, was later confirmed by Fell et al[72] on an industrial plate.

In general it is assumed that, in a fully developed spray regime, only the spray zone is of importance for mass transfer considerations. Starting with this assumption Fane and Sawistowski successfully modelled the spray regime and predicted the performance of a small scale sieve plate operating in this regime. In such a plate where the degree of liquid mixing is very high point efficiency was practically equal to the plate efficiency. In order to predict the mass transfer performance of a large-scale industrial sieve tray a relationship connecting the point efficiency to the plate efficiency is required.

It is obvious that the amount of liquid in the spray and the surface area of the drops are the main contributors to the mass transfer performance in the spray regime. Therefore, in order to formulate an efficiency model for the spray regime the amount of liquid in the spray must be predicted fairly accurately. This, in turn, depends on tray hydraulics and gas flowrates. In addition to handle the required liquid throughput the amount of liquid flowing along the plate floor, i.e. the first zone must be taken into account. This is particularly important for the relation between the point and plate efficiencies. Based on the hydrodynamic knowledge of the spray regime two models have been formulated to predict the mass transfer performance of a large-scale industrial sieve tray operating in the fully developed spray regime.

6.2 Description of Model

It is assumed that the dispersion in the spray regime consists of discrete droplets atomised at the plate floor and following defined trajectories in the inter-tray space. Also there exists a certain drop size distribution and each drop has associated with it its own projection velocity. Drops retain their identity during their life time in the spray, i.e. there is no coalescence or break-up in flight. The sole contribution to mass transfer area is the surface area of the droplets and there is a continuously replenished shallow pool of liquid on the plate floor. The concept used to relate the point efficiency to plate efficiency is to divide the plate into a number of pools, each pool being completely mixed. Two models have been proposed. In model 1, which is the simplified model, it is assumed

that droplets are projected upwards and return to the same pool for re-atomisation. However, a fraction of the liquid on the plate by-passes the atomisation process. In model 2 it is assumed that projected droplets return to the adjacent pool for re-atomisation. In the development of the models entrainment is neglected and a constant value of point efficiency across the tray is assumed.

6.3 Formulation of Models

6.3.1 Model 1

This is a by-pass model in which it is assumed that a fraction C of the liquid flow-rate L_m by-passes the plate and only a fraction $(1-C)L_m$ undergoes continuous atomisation during its flow along the plate floor.

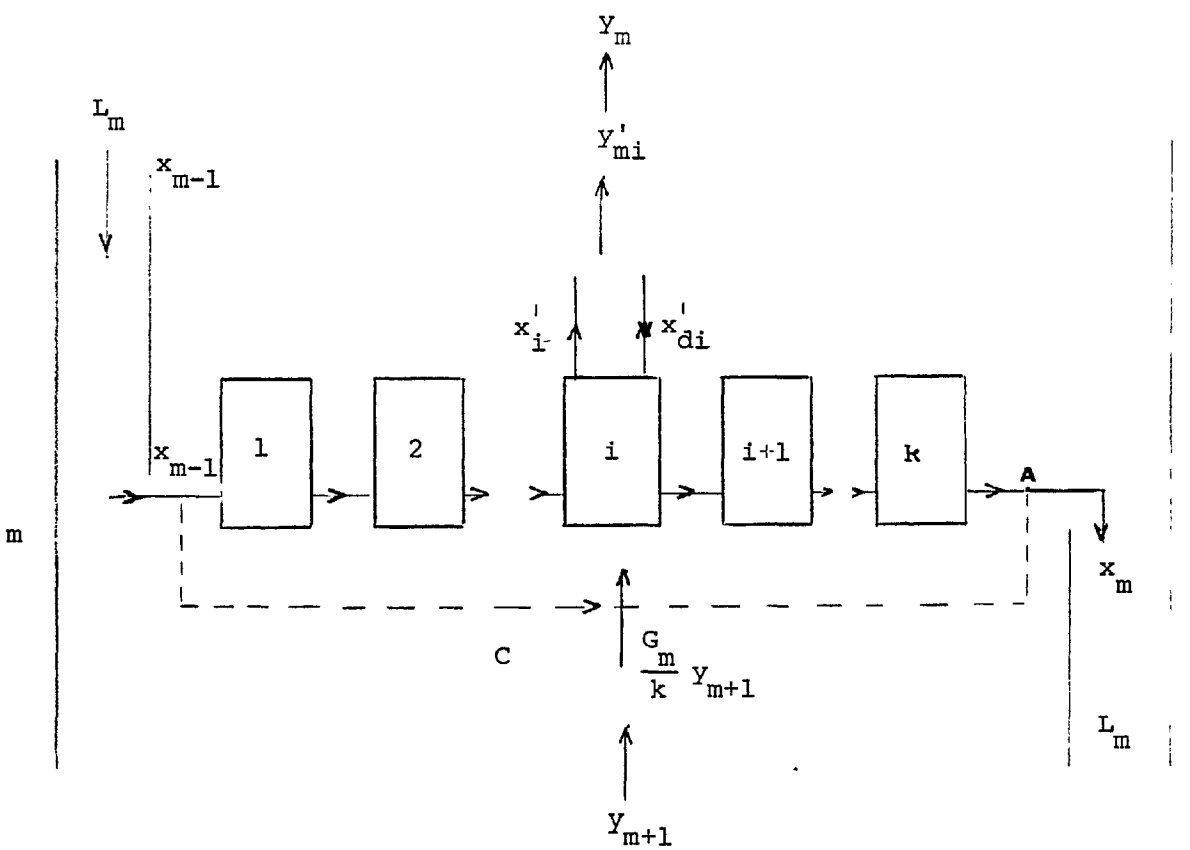


Fig. 6.1 Model 1

Consider the plate in Fig. 6.1.

Consider pool i of plate m.

k - number of pools.

x_i - concentration of droplets leaving pool i.

x_{di} - concentration of droplets returning to pool i.

y'_{mi} - gas leaving pool i.

y_{m+1} - gas approaching plate m, assumed to be perfectly mixed,

i.e. y_{m+1} = constant.

y_m - gas leaving plate m (flow average value).

From material balance on solute in pool i

$$\frac{G_m}{k}(y_{m+1} - y'_i) = (1-C)L_m(x'_{di} - x'_i) \tag{6.1}$$

Point efficiency is defined as

$$E = \frac{y_{m+1} - y'_{mi}}{y_{m+1} - mx'_{di}} \tag{6.2}$$

Mass balance at exit point A

$$CL_m x_{m-1} = -x_{dk}(1-C)L_m + L_m x_m \tag{6.3}$$

overall mass balance

$$G_m(y_{m+1} - y_m) = L_m(x_m - x_{m-1}) \tag{6.4}$$

From equations 6.1, 6.2, 6.3 and 6.4

$$E_{mV} = \frac{1}{\lambda}(1-C)\left\{\frac{\beta^k - 1}{1-C+C\beta^k}\right\} \tag{6.5}$$

where

$$\beta = 1 + \frac{m}{(1-C)} \frac{G_m}{L_m} \frac{E}{k}$$

For C = 0 the equation 6.5 reduces to

$$E_{mV} = \frac{1}{\lambda} \{(1 + \lambda \frac{E'}{k})^k - 1\} \qquad (6.6)$$

which is the standard form of pool model expression relating point efficiency to plate efficiency.

6.3.2 Model 2

It is assumed that the plate is divided into k number of completely mixed pools and the droplets generated in a given pool return to the adjacent pool for re-atomisation at the end of their trajectories. The model will be referred to as the forward jump model. Consider the plate in Fig. 6.2

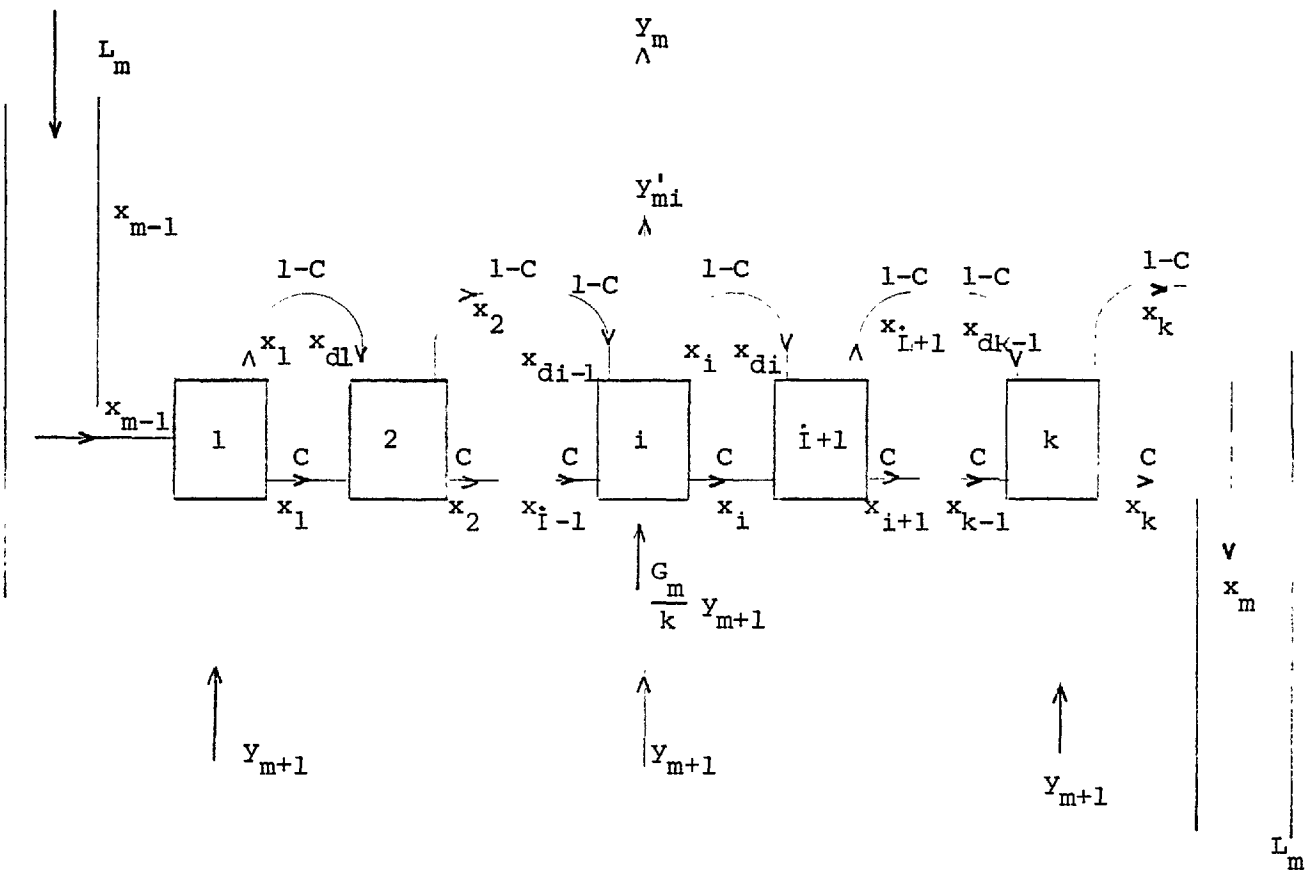


Fig. 6.2 **Model 2**

Fraction C of liquid flowrate L_m is on the tray floor and the fraction (1-C) is in the spray.

x_i = concentration of liquid leaving the pool i

x_{di} = concentration of droplets entering the pool i+1

y'_{mi} = gas leaving the pool i

y_{m+1} = gas approaching the plate m

y_m = gas leaving the plate m.

From balance on pool i+1

Assumption (1): Entrainment is neglected.

Assumption (2): Constant value of point efficiency exists across the tray

$$(1-C)x_{di} + Cx_i = (1-C)x_{i+1} + Cx_{i+1} \tag{6.7}$$

Assumption (3): Gas approaching the plate is perfectly mixed, i.e. y_{m+1} = constant

Assumption (4): Liquid on plate floor does not contribute to separation.

$$(1-C)(x_{di}-x_i)L_m = \frac{G_m}{k}(y_{m+1} - y'_{mi}) \tag{6.8}$$

Point efficiency

$$E = \frac{y_{m+1} - y'_{mi}}{y_{m+1} - mx_{di}} \tag{6.9}$$

$$(1-C)(x_{di}-x_i) = \frac{G_m}{L_m}\frac{E}{k}(y_{m+1} - mx_{di}) \tag{6.10}$$

From equation 6.7

$$x_{di} = \frac{x_{i+1} - Cx_i}{1 - C}$$

Substitute into (6.10)

$$(1-C)\left(\frac{x_{i+1}-Cx_i}{1-C}\,x_i\right) = \frac{G_m}{L_m}\frac{E}{k}\left(y_{m+1} - m\,\frac{x_{i+1}-Cx_i}{1-C}\right)$$

$$x_{i+1} - Cx_i - x_i + Cx_i = \frac{G_m}{L_m}\frac{E}{k}\,y_{m+1} - \frac{mG_m}{L_m}\frac{E'}{k}\,\frac{x_{i+1}}{1-C}$$

$$+ \frac{C}{1-C}\,\lambda\,\frac{E}{k}\,x_i$$

where $\lambda = \dfrac{mG_m}{L_m}$

$$x_i\left(\frac{C}{1-C}\,\lambda\,\frac{E}{k} + 1\right) = \left(1 + \frac{1}{1-C}\,\lambda\,\frac{E}{k}\right)x_{i+1} - \frac{G_m}{L_m}\frac{E}{k}\,y_{m+1}$$

$$x_i = \frac{1 + \frac{1}{1-C}\,\lambda\,\frac{E}{k}}{1 + \frac{C}{1-C}\,\lambda\,\frac{E}{k}}\,x_{i+1} - \frac{\frac{G_m}{L_m}\frac{E}{k}\,y_{m+1}}{1 + \frac{C}{1-C}\,\lambda\,\frac{E}{k}} = ax_{i+1} - b \qquad (6.11)$$

For pool k: $x_{k-1} = ax_k - b$

k-1: $x_{k-2} = ax_{k-1} - b = a^2x_k - b(1+a)$

k-2: $x_{k-3} = a^3x_k - b(1+a+a^2)$

2: $x_{k-(k-1)} = x_1 = a^{k-1}x_k - b(1+a+\ldots.a^{k-2})$

$$= a^{k-1}x_k - b\,\frac{a^{k-1}-1}{a-1}$$

But from pool 1: $x_1 = x_{m-1}$ also $x_k = x_m$.

$$x_{m-1} = a^{k-1}x_m - b\,\frac{a^{k-1} - 1}{a - 1} \tag{6.12}$$

$$a = \frac{1 + \frac{1}{1-C}\lambda\frac{E}{k}}{1 + \frac{C}{1-C}\lambda\frac{E}{k}} \qquad b = \frac{\frac{G_m}{L_m}\frac{E}{k}y_{m+1}}{1 + \frac{C}{1-C}\lambda\frac{E}{k}}$$

$$a-1 = \frac{1 + \frac{1}{1-C}\lambda\frac{E}{k} - 1 - \frac{C}{1-C}\lambda\frac{E}{k}}{1 + \frac{1}{1-C}\lambda\frac{E}{k}} = \frac{\lambda\frac{E}{k}}{1 + \frac{C}{1-C}\lambda\frac{E}{k}}$$

$$\frac{b}{a-1} = \frac{y_{m+1}}{m}$$

$$\therefore\ x_{m-1} = a^{k-1}x_m - \frac{y_{m+1}}{m}(a^{k-1} - 1) \tag{6.13}$$

$$\text{But}\quad x_{m-1} = x_m - \frac{G_m}{L_m}(y_{m+1} - y_m) \tag{6.14}$$

$$x_m - \frac{G_m}{L_m}(y_{m+1} - y_m) = a^{k-1}x_m - \frac{y_{m+1}}{m}(a^{k-1} - 1)$$

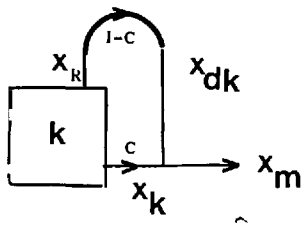
$$(y_{m+1} - mx_m)a^{k-1} - (y_{m+1} - mx_m) = m\frac{G_m}{L_m}(y_{m+1} - y_m)$$

$$= \lambda(y_{m+1} - y_m)$$

$$\therefore\quad E_{mV} = \frac{a^{k-1} - 1}{\lambda} \tag{6.15}$$

$$E_{mV} = \frac{1}{\lambda}\left(\left(\frac{1 + \frac{1}{1-C}\lambda\frac{E}{k}}{1 + \frac{C}{1-C}\lambda\frac{E}{k}}\right)^{k-1} - 1\right) \tag{6.16}$$

Strictly speaking, there is an extra stage between pool k and the downcomer. This counteracts the neutral character of pool 1 thus



$$E_{mV} = \frac{1}{\lambda}\left(\left(\frac{1 + \frac{1}{1-C}\lambda\frac{E}{k}}{1 + \frac{C}{1-C}\lambda\frac{E}{k}}\right)^{k} - 1\right) \qquad (6.17)$$

For C = 0 as expected

$$E_{mV} = \frac{1}{\lambda}\{(1 + \lambda\frac{E'}{k})^{k} - 1\} \qquad (6.18)$$

i.e. the normal relation between point and plate efficiency for the pool model is obtained.

The upper limit for C is the transition from spray to froth regine.

6.4 Discussion of Models

Graphical representations of equations 6.5 and 6.17 are given in Figures 6.4-6.11 respectively for models 1 and 2. Figures show the dependence of plate efficiency on various parameters and these are discussed below. Fig. 6.3 is for C = 0, drawn as reference value.

Fig. 6.4
Effect of number of pools on efficiency
Fig. 6.5

Fig. 6.6 Effect of change in non-atomised fraction
Fig. 6.7 of liquid flow on efficiency

Fig. 6.8 Effect of variation in mG/L on
Fig. 6.9 efficiency
Fig. 6.10

6.4.1 Effect of Varying the Number of Pools on Efficiency

It is clear from Figs 6.4 and 6.5 that the effect of the number of pools on efficiency is more pronounced up to the first six stages and tends to assume an asymptotic value with increasing number of stages (plug-flow equivalent). This is shown in Table 6.1 for models 1 and 2.

Table 6.1

$E = 0.65 \quad C = 0.1 \quad \lambda = 1$

MODEL 1		MODEL 2	
k	E_{mG}	k	E_{mG}
2	0.63	2	0.73
3	0.67	3	0.78
4	0.69	4	0.81
5	0.70	5	0.83
10	0.73	10	0.87
15	0.74	15	0.88
20	0.74	20	0.89
α	0.75	α	0.92

For a constant number of pools, the efficiency increases with increasing λ, and decreases with increasing liquid flowrate on the tray. For the same number of pools Model 2 predicts higher plate efficiency than Model 1.

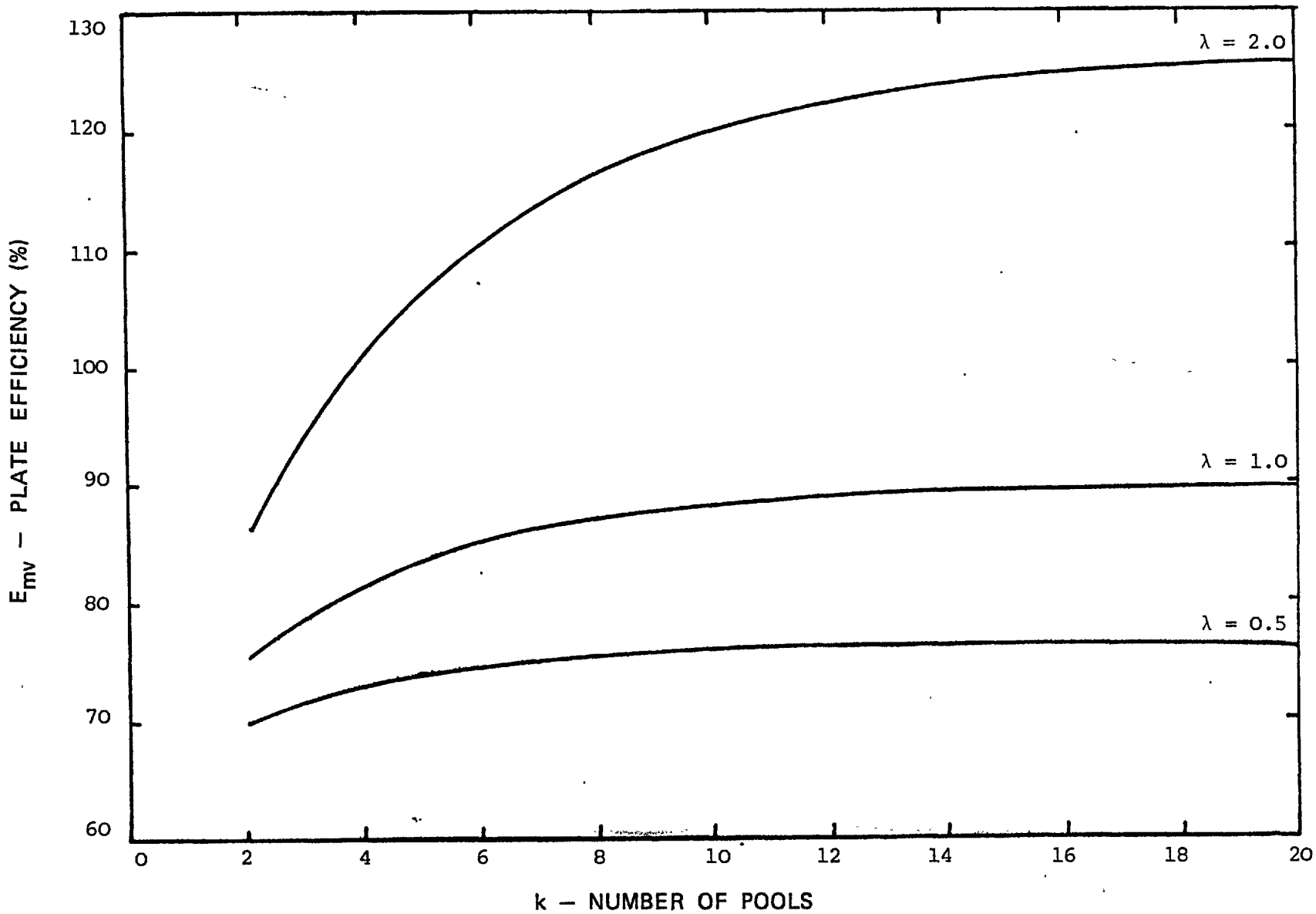


Fig. 6.3 Variation of plate efficiency with number of pools for C = 0.

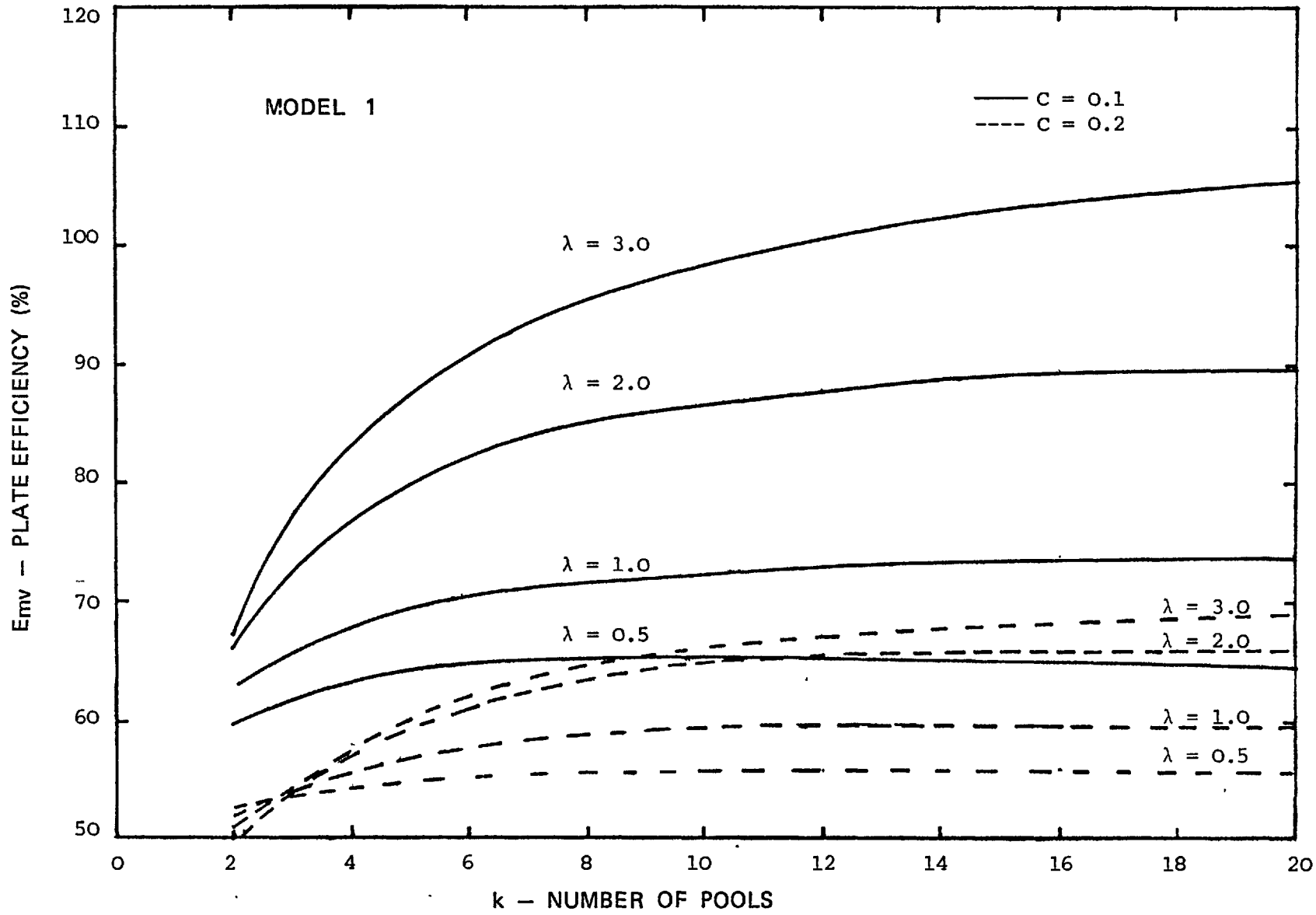


Fig. 6.4 Variation of plate efficiency with number of pools.

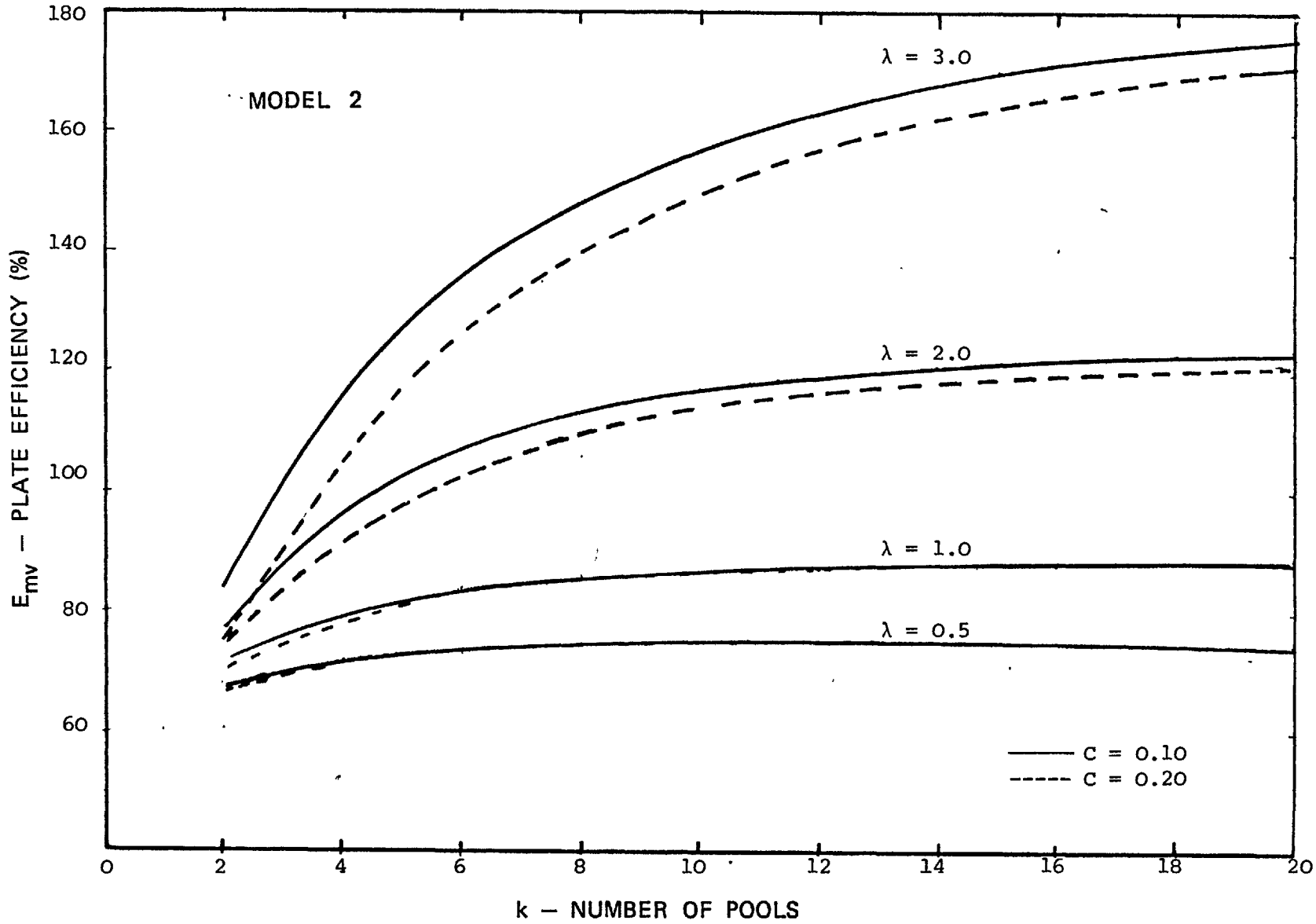


Fig. 6.5 Variation of plate efficiency with number of pools for E = 0.65.

6.4.2 Effect of Change in Non-Atomised Fraction of Liquid Flow on Efficiency

Figures 6.6 and 6.7 clearly indicate the effect of fraction C on plate efficiency. Efficiency decreases with increasing C in both cases but the trend is different. In model 1 there is a steep decrease over the significant range of C. This can be explained by the diluting effect of the liquid by-pass. In model 2 for low and moderate point efficiencies up to about 80%, the increase in C does not affect the plate efficiency appreciably over the practically relevant values of C. However, for higher point efficiencies the effect becomes significant. It can be concluded from this that for industrial columns operating in the spray regime the liquid-handling capacity of the tray does not affect the plate efficiency provided the point efficiency remains unchanged, which also implies that the plate continues to operate in the spray regime. This is shown in Table 6.2

Table 6.2

$\lambda = 1, \quad k = 10, \quad E = 0.8$

MODEL 1		MODEL 2	
C	E_{mV}	C	E_{mV}
0.1	0.93	0.1	1.15
0.3	0.60	0.3	1.10
0.5	0.36	0.5	1.04

6.4.3 Effect of Variation in mG/L on Efficiency

Figures 6.8-6.11 show the effect of varying λ on efficiency. For a constant point efficiency plate efficiency increases with increasing λ and the plate efficiency increases with increasing point efficiency. This is shown in Table 6.3 for models 1 and 2.

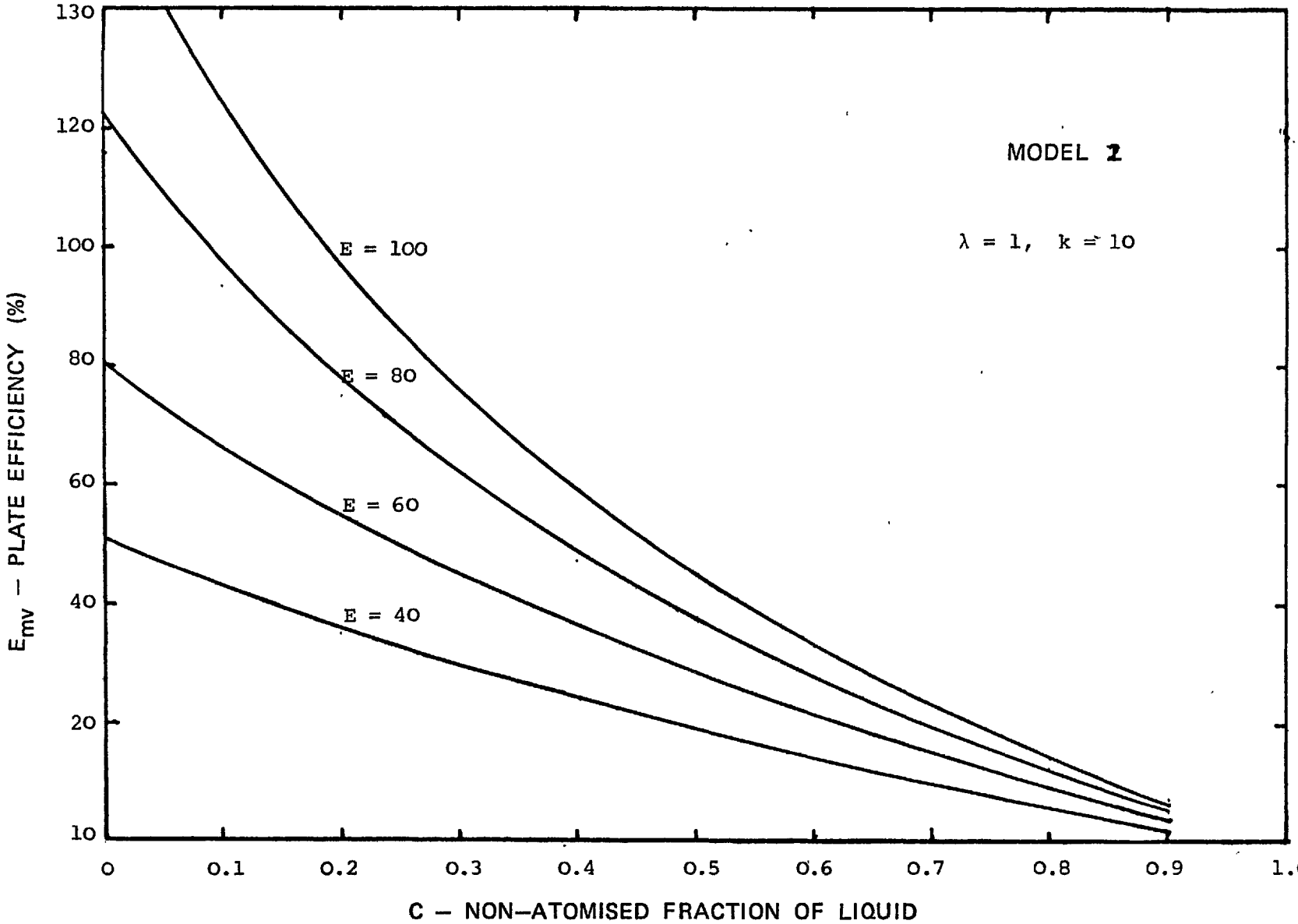


Fig. 6.6 Variation of plate efficiency with non-atomised fraction of liquid.

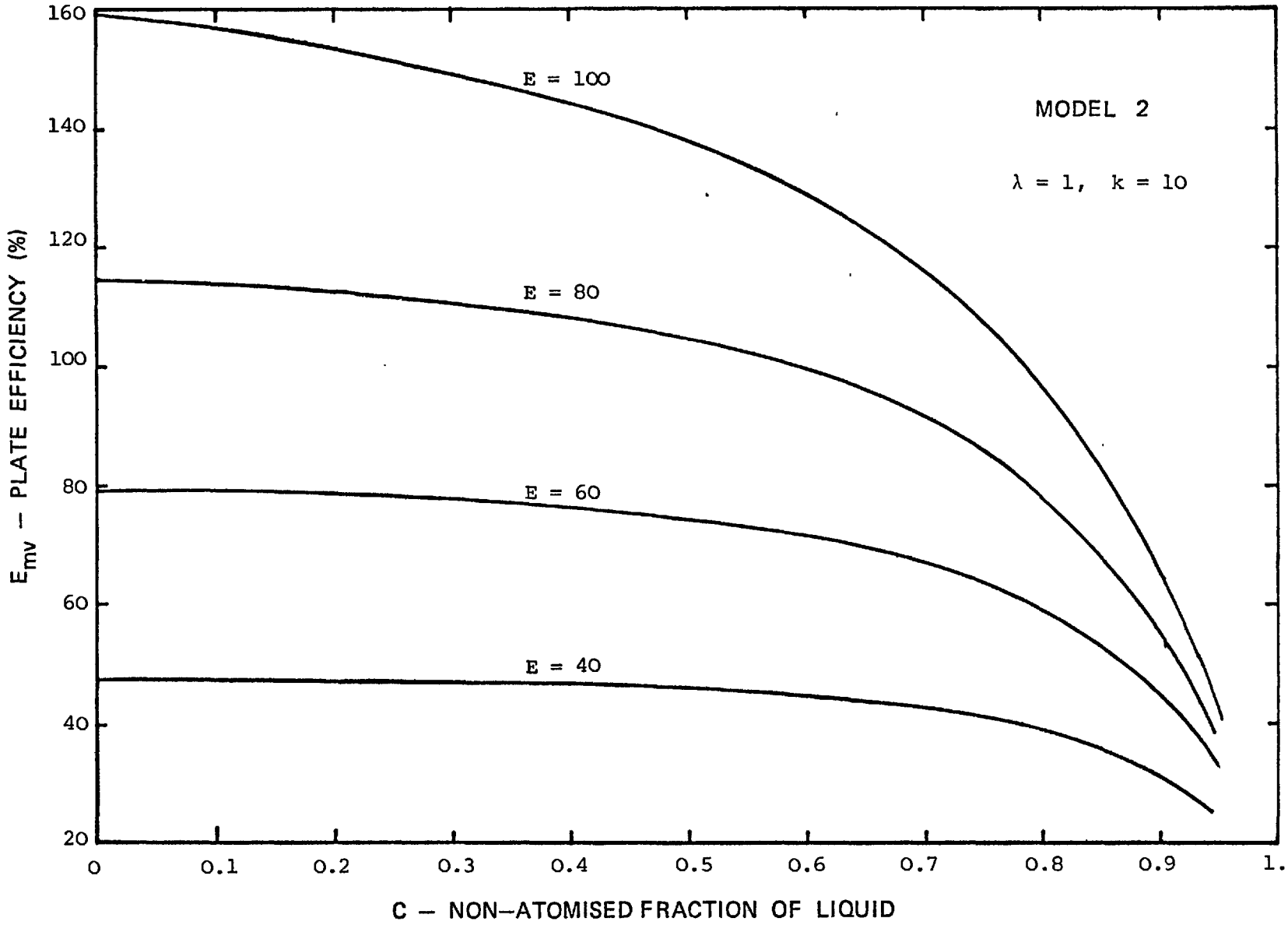


Fig. 6.7 Variation of plate efficiency with non-atomised fraction of liquid.

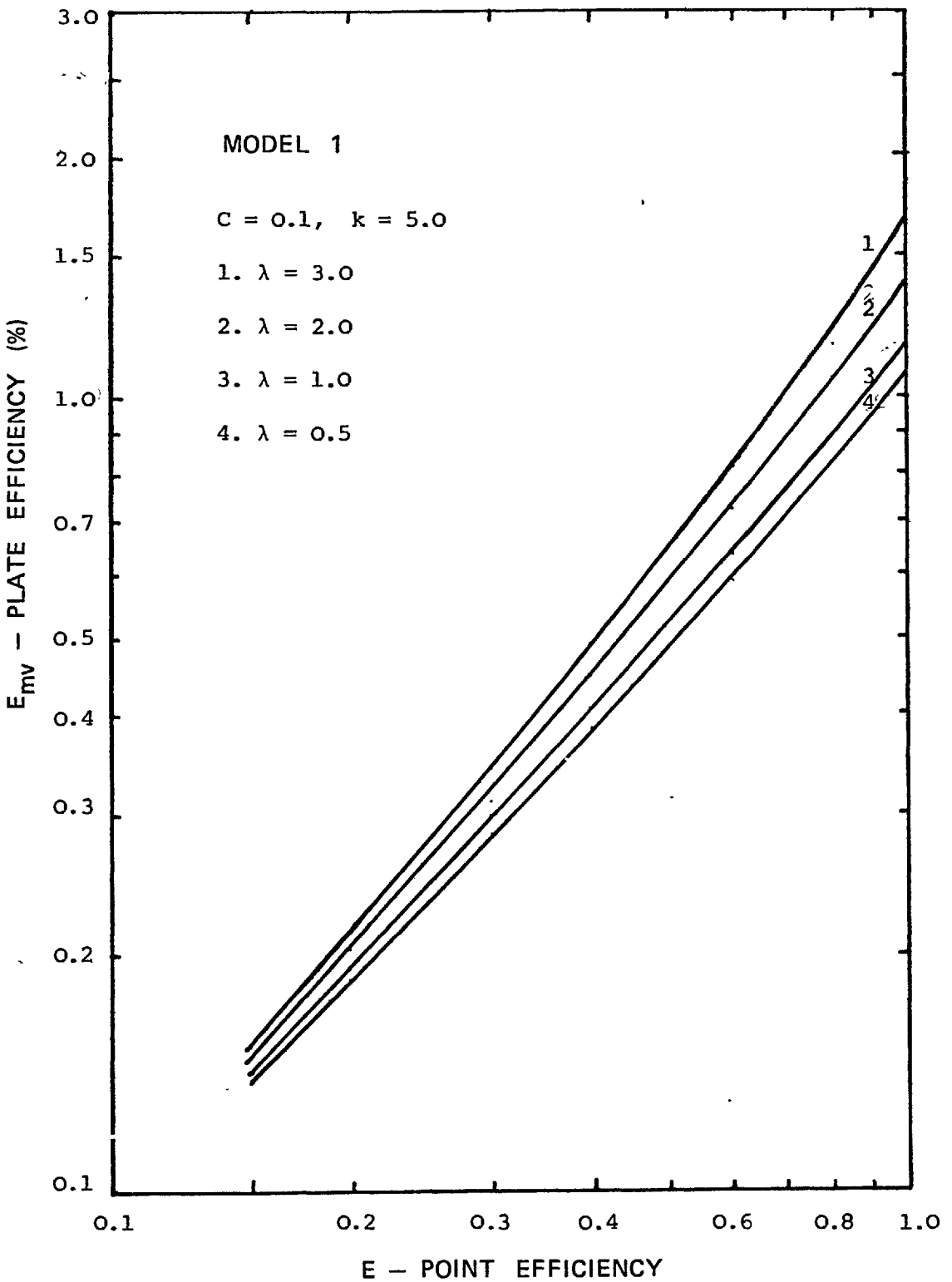


Fig. 6.8 Variation of plate efficiency with point efficiency and mG/L.

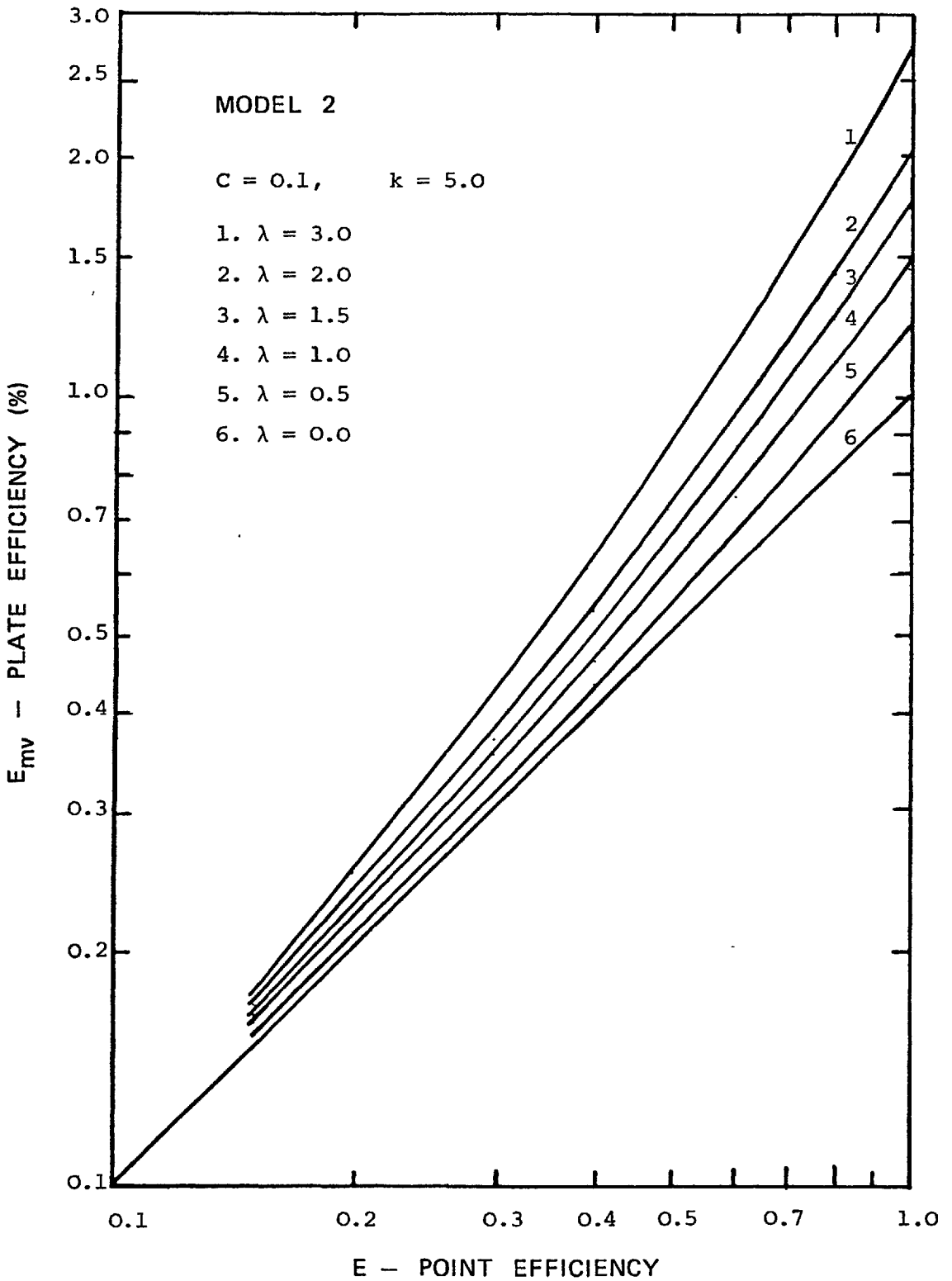


Fig. 6.9 Variation of plate efficiency with point efficiency and mG/L.

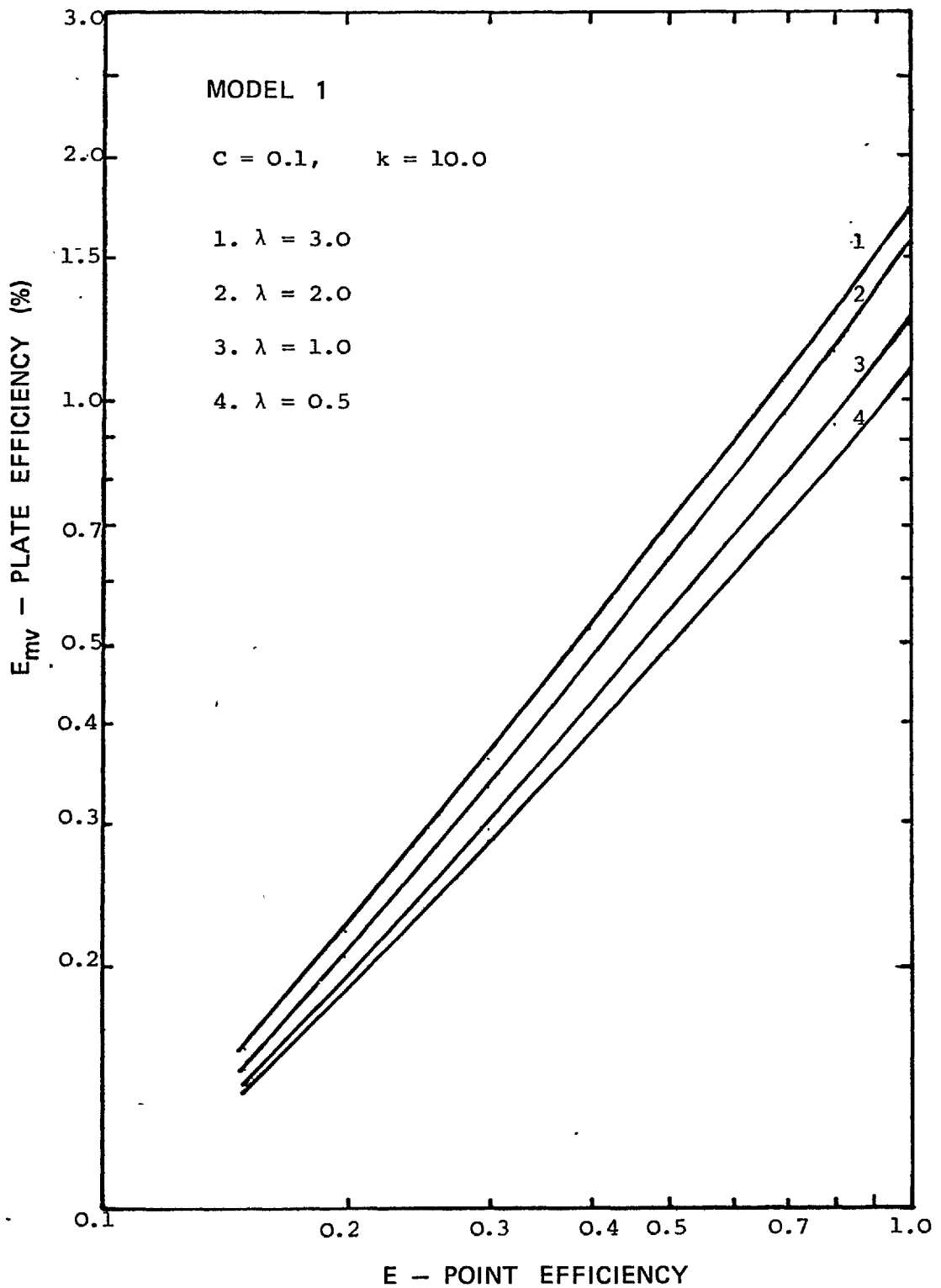


Fig. 6.10 Variation of plate efficiency with point efficiency and mG/L.

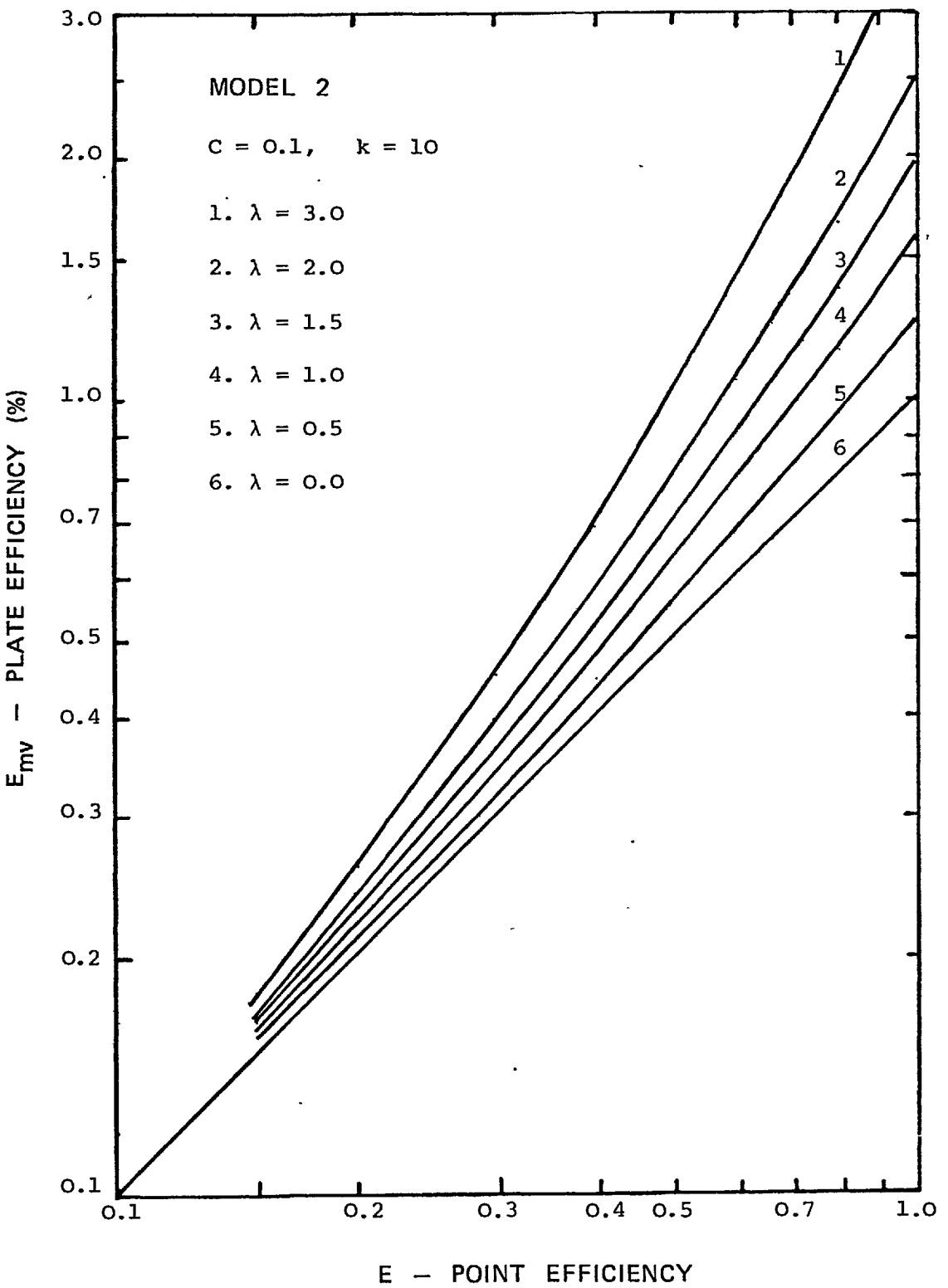


Fig. 6.11 Variation of plate efficiency with point efficiency and mG/L.

Table 6.3

k = 5, C = 0.1 E = 0.8

MODEL 1			MODEL 2		
λ	E_{mV}		λ	E_{mV}	
	k = 5	k = 10		k = 5	k = 10
0.5	0.807	0.824	0.5	0.929	0.955
1	0.892	0.935	1	1.075	1.145
2	1.040	1.145	2	1.422	1.653
3	1.136	1.295	3	1.846	2.391

CONCLUSION

It is clear from the above analysis model 2 gives higher efficiencies than for model 1 under the same conditions.

6.5 Determination of the Volumetric Flowrate of Liquid Leaving the Plate in the Form of Droplets

First step towards the prediction of efficiency is the determination of the volumetric liquid flowrate of liquid leaving the plate in the form of droplets. This can be determined from the knowledge of the Height-Velocity-Residence time relation of each drop and the experimental dispersion density profile.

6.5.1 Droplet Trajectories

Fore balance on a droplet in the rising vapour stream is given by For motion upwards

$$\frac{\pi d_p^3}{6} \rho_p V \frac{dv}{dh} = \frac{\pi d_p^3}{6} \rho_G g \pm C \frac{\pi d_p^2}{4} \rho_G \frac{(v-v_s)^2}{2} - \frac{\pi d_p^3}{6} \rho_p g \qquad (6.19)$$

Jeronimo and Sawistowski[84] has shown that effect of C_D is negligible. This was confirmed by Zuiderweg[3]. Neglecting drag equation 6.19 reduces to

$$\int_{h_1}^{h_2} dh = \pm \frac{1}{g} \left(\frac{\rho_p}{\rho_G - \rho_p}\right) \int_{v_1}^{v_2} v dv \qquad (6.20)$$

$$h_{max} = \pm \frac{1}{g} \left(\frac{\rho_p}{\rho_G - \rho_p}\right) \int_{v_p}^{0} v dv \qquad (6.21)$$

6.5.2 Experimental Dispersion Density Profile

In principle the dispersion density profile should straighten out at higher levels above the plate floor indicating entrainment as shown in the Fig. 6.12 (point A). Let the corresponding height be h_{max}.

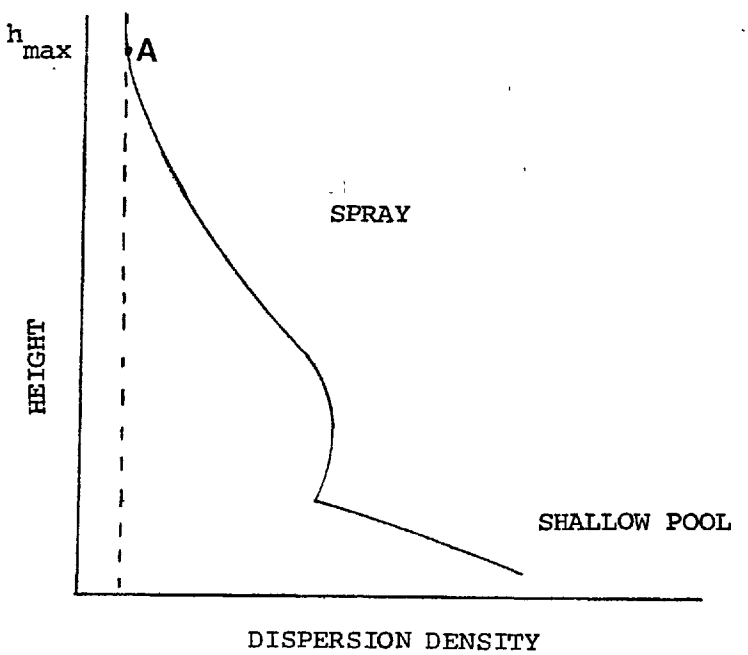


Fig. 6.12

The diameter of the droplet which reaches the height h_{max} fixes the boundary of the droplets which properly belong to the spray, i.e., will have complete trajectories. Drops with diameter less than this will be entrained. Projection velocity of the droplet reaching the height h_{max} can be calculated from equation 6.21. Corresponding diameter can be determined from the correlation

$$V_p = \frac{0.01795\, d_H^{0.75} V_h^2}{d_p^{0.83}\, \mu_L^{0.2}\, \gamma^{0.3}} \left(\frac{\rho_G}{\rho_L}\right) \qquad (6.22)$$

where V_p is the initial projection velocity.

6.5.3 Height-Velocity-Residence Time Relation

For a particular drop size j the velocity profile is shown diagrammatically in Fig. 6.13.

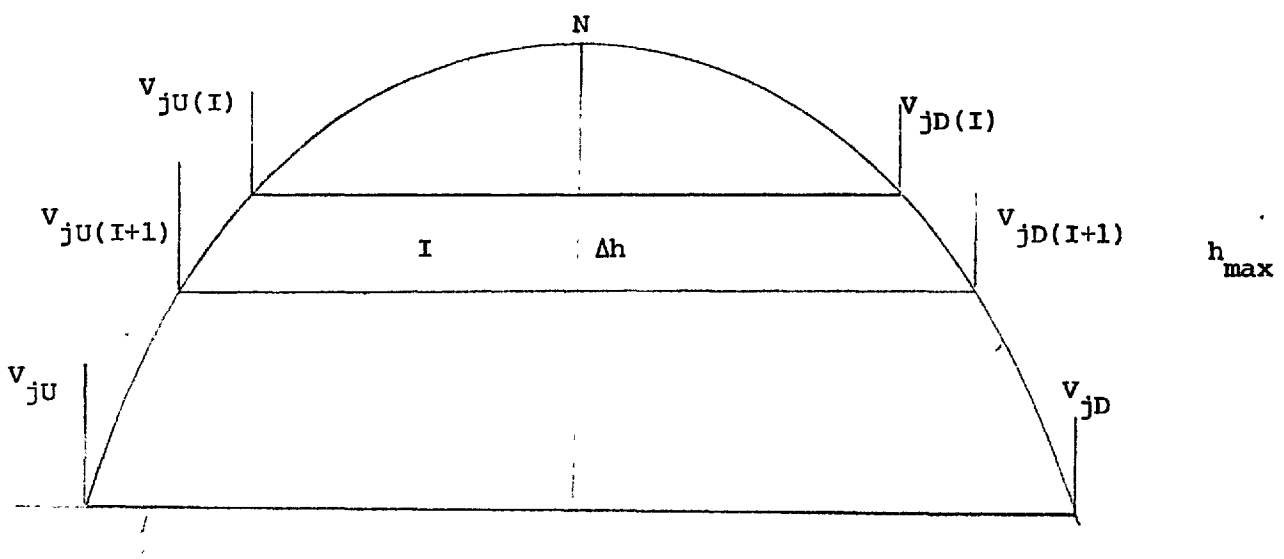


Fig. 6.13

Let the intertray space up to h_{max} be divided into N equal height increments. Consider a drop of size d_j. This has a vertical component velocity V_{jU} in the upward direction and V_{jD} in the downward direction. Initial projection velocity V_{jU} is calculated as stated earlier from equation 6.21. In order to determine the residence time of the drop in each height increment, the velocity of the drop at each level has to be determined. This is done using equation 6.20. The value V_2 which satisfies the chosen height increment is calculated. This value is stored and the procedure continued till h_{max} is reached. From then onwards the equation for motion downwards is used to calculate the velocities at each level in the downward direction. From this information residence time of the drop in each increment can be evaluated. Let T_{jU} be the residence time of the drop in a particular increment I in the upward direction and T_{jD} the residence time in the downward direction. T_j the time spent by the drop in the I^{th} increment is given by

$$T_{jU} = \frac{\Delta h}{\left(\frac{V_{jU(I)} + V_{jU(I+1)}}{2}\right)} \tag{6.23}$$

$$T_{jD} = \frac{\Delta h}{\left(\frac{V_{jD(I)} + V_{jD(I+1)}}{2}\right)} \tag{6.24}$$

$$T_j = T_{jU} + T_{jD} \tag{6.25}$$

6.5.4 Volume Flowrate in Spray

Consider Fig. 6.14.

Starting from the terminal increment N and working downwards, the drop size range in the N^{th} increment is d_N.

Volumetric liquid flowrate due to drop size range d_N in the N^{th} increment, $Q_{dN,N}$

$$Q_{dN,N} = \frac{\phi_{dN,N}}{T_{dN,N}} \tag{6.26}$$

where

$\phi_{dN,N}$ - Holdup due to drop size range d_N in the N^{th} increment obtained by the integration of the dispersion density profile.

$T_{dN,N}$ - Residence time due to drop size range d_N in the N^{th} increment.

Now consider increment I

$$Q_{dN,N} = Q_{dN,N-1} = Q_{dN,N-2} = \cdots\cdots Q_{dN,I} \tag{6.27}$$

$$\phi_I = \phi_{dN,I} + \phi_{dN-1,I} + \cdots\cdots \phi_{dI+1,I} + \phi_{dI,I} + \phi_E \tag{6.28}$$

Therefore

$$\phi_I = \sum_{j=I+1}^{N} \phi_{dj,I} + \phi_{dI,I} + \phi_E \tag{6.29}$$

where ϕ_I - Total holdup in the I^{th} increment. (Experimental Value)

ϕ_{En} - Entrainment holdup

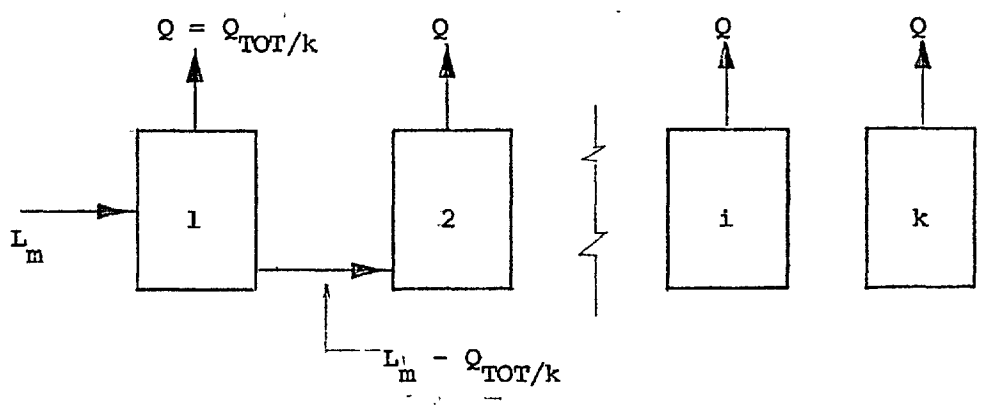
$$\phi_{dI,I} = \phi_I - \phi_{EN} - \sum_{j=I+1}^{N} \phi_{dj,I} \tag{6.30}$$

$$Q_{dI,I} = \frac{\phi_{dI,I}}{T_{dI,I}} \tag{6.31}$$

Volume flowrate due to all the drop size ranges, Q_{TOT}

$$Q_{TOT} = \sum_{j=1}^{N} Q_{dj,j} \tag{6.32}$$

6.5.5 Volume Flowrate on Tray Floor



The plate is divided into k number of pools. Therefore volumetric liquid flowrate leaving each pool in the form of droplets

$$Q = \frac{Q_{TOT}}{k} \tag{6.33}$$

Volume flowrate on the tray floor = $L_m - \frac{Q_{TOT}}{k}$.

6.5.6 Mass Transfer

From this information it is now possible to calculate the mass transfer performance of the plate.

Surface area of the droplet in increment I, S_I

$$S_I = 6 \left(\frac{\phi_{dN,I}}{d_N} + \frac{\phi_{dN-1,I}}{d_{N-1}} \cdots\cdots \frac{\phi_{dI,I}}{d_I} \right)$$

$$= 6 \sum_{j=I}^{N} \frac{\phi_{dj,I}}{d_j} \qquad (6.34)$$

Number of transfer units in increment I

$$N_{OG_I} = \frac{\sum_{j=I}^{N} (K_{OG_{dj,I}} \times S_{dj,I})_u + (K_{OG_{dj,I}} \times S_{dj,I})_D}{G_m} \qquad (6.35)$$

where

U denotes ascending drops

D denotes descending drops.

Total number of transfer unit

$$N_{OG} = \frac{\sum_{I=1}^{N} \sum_{j=1}^{N} (K_{OG_{dj,I}} \times S_{dj,I})_u + (K_{OG_{dj,I}} \times S_{dj,I})_D}{G_m} \qquad (6.36)$$

6.6 Testing of the Models

It is clear that success of predicting the efficiency depends on the accurate evaluation of the volumetric flowrate of liquid leaving the tray in the form of droplets, and their surface area. This in turn depends on the initial projection velocity of the droplets. Each flowrate has associated with it its unique dispersion density profile. Data on dispersion density profile and accurate prediction of initial projection velocity are the two prerequisites for testing the model. From the knowledge of the initial projection velocity the maximum height reached by the droplets can be calculated. Since the objective of the present work is to predict the mass transfer performance of a large scale industrial sieve tray, the data of Fell et al[61] were used to test the model.

Fell et al studied the mass transfer efficiency for the absorption of small amount of ammonia from air into water. Because of the high solubility of ammonia in water the system studied is gas phase controlled. The gas phase mass transfer coefficient was evaluated from the equation of Ranz and Marshall[74]

$$Sh_G = 2\{1 + 0.276\ Re^{1/2}\ Sc^{1/3}\} \qquad (6.37)$$

It is clear that the gas phase mass transfer coefficient is a function of Reynolds number, i.e. drop size and relative velocity. The models were tested using Fell's data obtained on an industrial-size sieve tray. Fig. 6.14 is a schematic representation of the calculation procedure to determine the volumetric liquid flowrate. A computer program has been written to determine the volumetric liquid flowrate and to predict the plate efficiency. This is given in Appendix 3 and the results are given below in Table 6.4.

Table 6.4

Fell's data

Hole size	=	12.7 mm
Hole area %	=	10.7
Tray active area	=	0.182 m^2
Tray thickness	=	1.7 mm
Tray dimensions	=	0.3 × 0.6 m
Liquid cross flow	=	8.6 m^3/h - m weir
F_s	=	2.8 ms^{-1} $(kg/m^3)^{1/2}$
Number of mixing pools	=	9
Calculated point efficiency	=	66%
Calculated plate efficiency	=	74%
Experimental plate efficiency	=	88.5%

It is clear that there is a discrepancy between the experimental values and the predicted plate efficiency although the number of pools was selected to fit the existing conditions. This was attributed by Fell to using a constant characteristic drop size over the whole of the dispersion and neglecting the mass transfer during droplet formation.

Calculated Results

Volume flowrate of liquid in the spray = 5.675 × 10^{-3} m^3/s

Fraction of liquid on plate floor = 0.1346

Table 6.5

Predicted Values			Fell's Results		
Point efficiency	Model 1 Plate efficiency	Model 2 Plate efficiency	Point efficiency	Calculated Plate efficiency	Experimental Plate efficiency
78.3	73.5	88	66	74	88.5

The point efficiency calculated using the model is higher than Fell's value but the plate efficiency predicted by model 2 is in good agreement with his experimental results. Efficiency predicted by model 1 is lower than that of model 2 because of the assumed by-pass effect.

Schematic Representation of the Determination of Liquid Flowrate

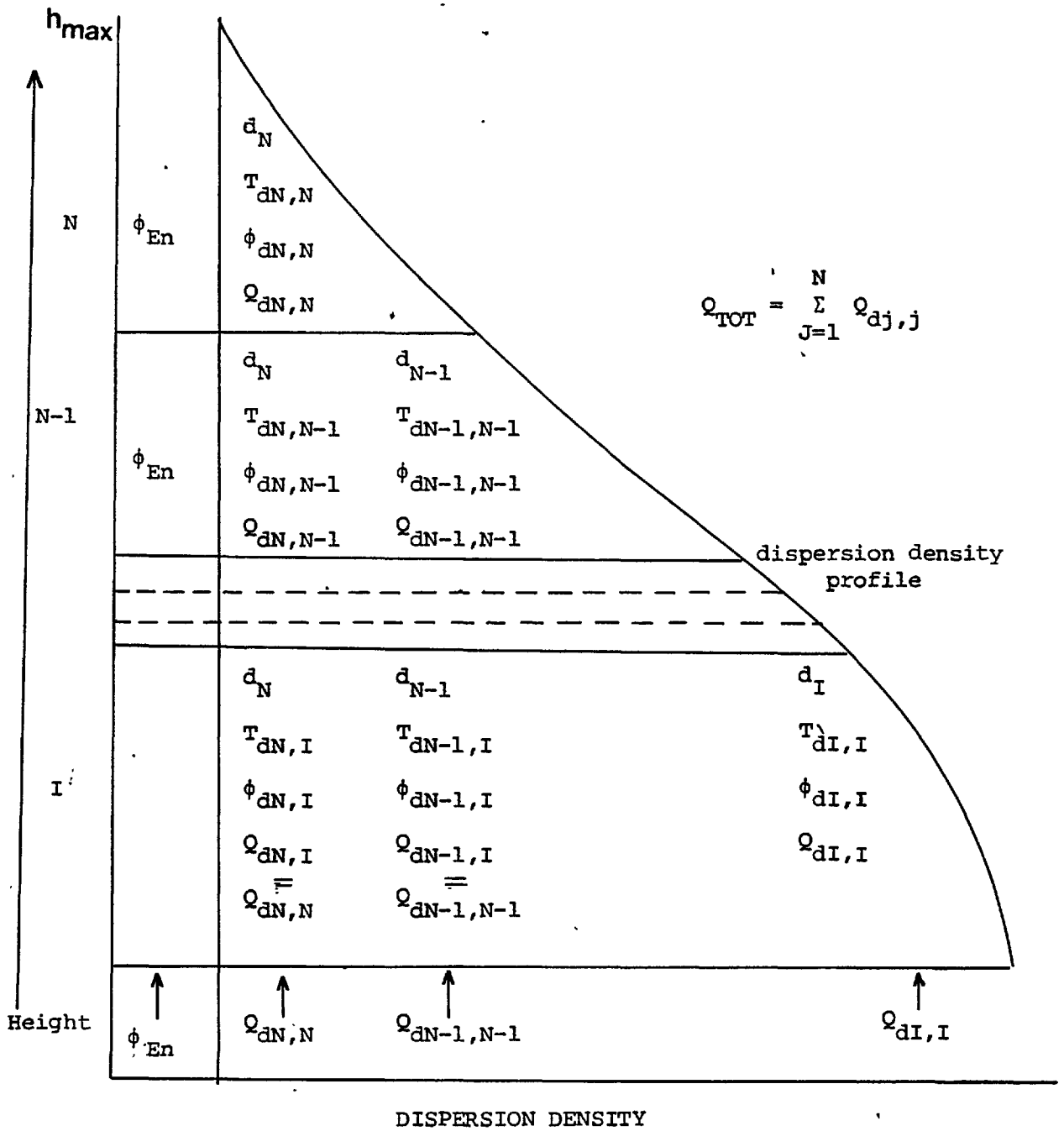


FIG. 6.14

CHAPTER SEVEN

DISCUSSION

7.1 Introduction

It is well known that the nature of the dispersion formed on a sieve plate changes from liquid continuous/gas dispersed to gas continuous/liquid dispersed with increasing gas flowrate. Design parameter, operating variables, physical properties of the system and presence of colloids are expected to have an influence on the nature of the dispersion formed and the effect of these parameters will be discussed.

Spray regime has associated with it a unique dispersion density profile with a distinct maximum and a minimum. This is discussed in relation to ligament break-up process.

Prediction of the mass transfer performance depends on a sound knowledge of the hydrodynamics of the spray regime. Once the hydrodynamic behaviour is understood, point efficiency can be calculated and plate efficiency predicted from a relationship connecting the point efficiency to the plate efficiency. Such a relationship was developed in Chapter 6 and will be discussed in Section 7.5.

7.2 Factors Affecting the Dispersion in the Foam Regime

The effect of the presence of colloidal suspensions on the operation of sieve plates proved to be negligible. Surface tension measurements indicated that the surface tension of the two colloidal suspensions were marginally greater than that of pure water. There was no thermodynamic reason for foam formation. It would also seem

that the concentrations employed were too small to affect the viscosity of the continuous phase and hence the rate of film drainage. However it was thought that solid particles trapped in the film may weaken it locally and accelerate coalescence.

The pure colloids used in this work were hydrophilic in nature and did not form a finite contact angle with the surface of the air bubble. These results contradicted previous work[66] which positively indicated that the presence of colloids introduced a tendency to foam. This was due to the water insoluble dyes used in these experiments. The dyes were hydrophobic in nature (formed a finite and positive contact angle with the gas bubble) and acted as profoamers. In addition it was suspected that they contained organic materials acting as surfactants.

In theory hydrophobic colloidal suspensions act in a similar way to surfactants in that the solute after being transferred to the interface slows down drainage by mechanical means and not by surface chemical means and stabilizes the film. Work required to transfer the solute from the interface to the bulk would be less than that corresponding to the decrease in area, thus making the foam thermodynamically stable.

The opposite behaviour would apply to a foam inhibiting agent. It is therefore possible that, in the case of hydrophilic colloids, which are unable even to enter the surface, there is no work to be done to transfer the solute from the surface to the bulk. Hence according to Chapter 2, foaming should not have been expected with the colloidal suspensions employed.

On the basis of experimental evidence obtained so far it seems safe to conclude that hydrophilic colloidal suspensions of low

concentrations do not promote foaming. Similarly as was shown later they had little effect on spray behaviour.

7.3 Factors Affecting Phase Transition

Attention was mainly focussed on the spray regime and as a first step towards this objective spray regime was delineated in terms of operating variables using a light transmission technique. As discussed previously the transition from froth to spray is a gradual process starting with one hole jetting and ending up with all the holes jetting. Based on the criteria formulated by Sawistowski[20] the transition point was taken midway of the sudden increase in transmittivity. This corresponds to a condition in which the contribution to the total interfacial area presented by the surface of liquid drops is significantly greater than the simultaneous contribution provided by the surface of gas bubbles.

Main conclusion drawn from these studies is that viscosity has a significant influence on the transition point. The results suggest that for the same liquid flowrate transition occurs at a lower gas flowrate for butanol than for methanol. This could be explained in terms of bubble break-up as in the case of higher viscosity liquids large bubbles are formed in the froth. A small increase in gas velocity will then lead to chain bubbling and jetting, i.e. entering into the spray regime. In methanol, however, large number of small bubbles are formed requiring a higher gas velocity to break through the dispersion.

Payne and Prince[71] found viscosity to have no effect on transition on a static sieve plate. This could be due to the fact that the systems chosen to study the effect of viscosity by the above

investigators were not selected properly. To study the effect of viscosity other physical properties such as surface tension and density must be kept constant.

It is not possible to compare the author's results with the data of Fell et al[31] on an industrial sieve tray because a splash baffle was not used in the experiments carried out and therefore it is not representative of a large industrial tray as pointed out by Jeronimo and Sawistowski[84].

7.4 Factors Affecting Dispersion in the Spray Regime

In the fully developed spray regime, where the bulk of the dispersion is in the form of droplets dispersed in a continuous gas phase, the hydrodynamic behaviour of the plate is different from that observed when the liquid represent continuous phase.

Generally, the shape of the experimental dispersion density profile which characterises the dispersion is in agreement with that of previous workers[1][44]. There is a distinct maximum in the profile some distance above the plate floor which is the unique feature of the spray regime. It was found for surface tension and viscosity to have an effect on dispersion and hence on the dispersion density profile. Generally, the lower the surface tension and viscosity of a liquid the more liquid is held at upper levels of the dispersion and the maximum in the profile also increases. It can be inferred from the surface area profile that decrease in surface tension and viscosity will produce larger surface area. This means that the lower the surface tension and viscosity, the higher proportion of small drops are formed explaining the higher surface area. The smaller the drops the greater are the heights reached because of higher projection

velocities explaining the higher liquid holdup at upper layers of the dispersion. This suggests that liquids of lower surface tension and viscosity would give higher mass transfer performance of the plate because of the higher interfacial area. However, this would also increase entrainment and hence the statement is only valid up to a critical gas velocity. In terms of energy transfer it can be explained that, if the system is less viscous, less energy is needed for shearing making more energy available for formation of interfacial area and droplet projection. In a system with low surface tension larger surface area can be formed with minimum expenditure of energy thus making available more energy for droplet projection.

Considering the effect of the operating variables on the profile, the maximum in the profile decreases with increasing gas flowrate but the height at which this maximum occurs increases at constant liquid flowrate. The net effect is to bring about a redistribution of the liquid hold-up with more liquid being held at higher levels of the dispersion. From the energy transfer point of view there is more energy available for liquid shearing, formation of interfacial area and droplet projection. There is experimental evidence[81] to support the fact that, with increasing gas flowrate, the drop size distribution shifts in favour of smaller droplets. For increasing liquid flowrate the maximum and the height both increase, at constant gas flowrate, due to more liquid being atomised.

In addition to more liquid being present on the tray floor more droplets are returned at the end of their trajectories for re-atomisation. This increases the energy need for shearing and therefore less energy is available for projection. This would decrease entrainment. Jeronimo and Sawistowski[84] found entrainment to decrease with increasing liquid flowrate.

Provided that the tray continues to operate in the spray regime this should produce higher point efficiencies. However, a critical point will be reached when the amount of energy available from the gas is not enough to atomise the increasing liquid load. At this point the dispersion will change to froth.

Among the design parameters hole diameter and free area have an effect on the dispersion. The maximum in the profile is at a higher level for large diameter holes, high free area trays. Liquid can be efficiently sheared in large hole diameter trays with minimum of energy losses making more energy available for droplet projection. Weir height was found by Fane and Sawistowski[1] to have no effect in the fully developed spray regime.

It was found that the presence of colloids did not have an appreciable effect on the dispersion density profile or on the transition point.

A correlation was developed for initial projection velocity based on energy and momentum transfer. In the development of the correlation significant factors affecting the dispersion density profile were considered. They are surface tension, viscosity, density, tray design parameters and operating variables. The correlation fits the data of an industrial sieve tray operating in the spray regime.

There is a distinct maximum and minimum in the dispersion density profile which is the characteristic feature of the spray regime. The maximum in the profile is attributed to the presence of a maxima in the drop size distribution curve by Fane and Sawistowski[1]. Fell[72] has explained that the minimum represents the point at which droplets acquire their projection velocity, i.e. the point at which ligaments breakup into droplets.

7.5 Efficiency Prediction

Hydrodynamics of the spray regime is fairly well understood now and the free trajectory model gives a plausible explanation of the spray regime. Of the two hydrodynamic models proposed the fluidisation model is no longer regarded as realistic. There is strong evidence to support the free trajectory model. The free trajectory model was first formulated by Fane and Sawistowski and successfully employed to predict point efficiency. Since then there has been considerable interest in the spray regime, but only limited attempts to predict plate efficiency.

Fell et al[60-61] assumed that the passage of liquid across the tray takes the form of a number of kangaroo-like hops and divided the tray into number of mixing pools. The extent of mass transfer in a given pool is calculated using the free trajectory model and related to the tray efficiency by summing the gas output from the mixing pools.

In the model proposed by Lockett et al[73] it is assumed that liquid is transported across the tray by the random movement of liquid particles, described by the equation of diffusion. Droplet concentration is the driving force for diffusion. Magnitude of the diffusion coefficient accounts for the size and frequency of the random movement of the liquid droplets.

Both models break down on account of the fact that they do not allow for sufficient liquid flow across the plate floor. Visual observation, photographic evidence and the dispersion density profile clearly suggest that there is a shallow pool of liquid on the plate floor supplied partly by the liquid flowing to the plate, and partly by the droplets returning to the plate at the end of their trajectories. This liquid pool, although contributing little to mass transfer

effects but significantly to the capacity of the tray for liquid flow.

Therefore in the model developed to relate the point efficiency to plate efficiency the shallow pool of liquid on the plate floor was taken into consideration. Calculated plate efficiency is in good agreement with experimental values.

CHAPTER EIGHT

CONCLUSIONS

8.1 Conclusions

The present work was mainly concerned with the nature of the dispersion formed on sieve plates, particularly with the spray regime. In the course of this work the following conclusions were reached:

1. Viscosity has a strong, previously unnoticed effect on hydrodynamics of spray regime through its influence on the drop formation stage.

2. Similar conclusions apply to the effect of surface tension. Speculative predictions of Jeronimo and Sawistowski on the proportionality between transition point and surface tension has been confirmed.

3. Much stronger effect was found of liquid flow-rate on transition point than previously expected.

4. Empirical correlations were established for the initial projection velocity, transition point and entrainment which correlate well the data obtained in this work and as well those of Pinczewski and Fell.

5. It has been confirmed that the maximum in the dispersion density profile decreases with increasing gas flowrate but the height at which this maximum occurs above the plate floor increases.

6. It has been found that the maximum in the profile and the height both increase with increasing liquid flowrate.

7. The effect of the presence of colloidal suspensions were found to be negligible both in the foam and spray regime.

8. Two models have been formulated to relate point efficiency to plate efficiency. Of these the forward-jump model when applied to the data of Fell et al proved superior to that of their kangaroo-jump model.

8.2 Future Work

Spray regime has received considerable attention in the past few years but most of the work carried out so far has been on the system air/water. Further investigation is needed in systems other than air/water to study the effect of physical properties on the nature of dispersion formed. It is evident from the above experimental studies that viscosity and surface tension have an effect on the dispersion and further work along this line would strengthen the above findings. Furthermore, the effect of viscosity on transition and entrainment needs further investigation to complete the hydrodynamic knowledge of the spray regime.

However, the most important aspect is the formation of a jet formation-liquid disintegration model to give a sound basis for initial projection velocity and drop size correlations. In addition, further work is needed on large scale columns to relate the number of pools to operating and geometrical parameters in order to predict plate efficiency.

NOMENCLATURE

A	Constant
A_f	fractional free area of the plate
a	surface area per unit volume of dispersion
B	constant
B_O	Bond Number $(\frac{g\rho_L d_H^2}{\gamma})$
C	non-atomised fraction of liquid
C_D	drag coefficient
d_H	hole diameter
d_P	drop diameter
d_{Pm}	man drop diameter
$\bar{d}$	Sauter mean diameter
E	point efficiency
E_O	overall column efficiency
E_{mv}	Murphree plate efficiency based on gas phase
E_{mL}	Murphree plate efficiency based on liquid phase
F_C	correction factor for crossflow of liquid
F_H	F-factor $(U_h\sqrt{\rho_g})$ based on hole velocity
F_s	F-factor $(U_s\sqrt{\rho_g})$ based on superficial velocity
f	fraction of light transmitted through the dispersion
G	gas rate (kg/s)
G_m	gas flowrate per bubbling area (kg mol/s)
g	gravitational acceleration (9.81 ms^{-2})
H	plate spacing
h	height above plate floor
I	intensity of the transmitted radiation
I_O	intensity of the incident radiation

K_G	gas-phase mass-transfer coefficient
K_{OG}	overall mass-transfer coefficient based on the gas phase
K_L	liquid-phase mass-transfer coefficient
K_{OL}	overall mass-transfer coefficient based on the liquid phase
k	number of pools
L	liquid rate (kg/s)
L_m	liquid flowrate per bubbling area (kg mol/s)
L_v	volumetric liquid flowrate (m^3/s)
ℓ	optical path length
M	value of the maximum in the profile
m	slope of the equilibrium line
N	count for column filled with liquid
N_O	empty column count
N_{OG}	number of overall gas-phase transfer unit
P	pressure
Re	Reynolds number
Sc	Schmidt number ($\mu/\rho D$)
Sh	Sherwood number ($K_G d_p/D$)
T	temperature
t	residence time
t_d	dead time
U_h^t	hole velocity at transition
U_G	gas velocity
U_L	liquid velocity
V_h	hole velocity
V_p	projection velocity
V_R	relative velocity

We_G	Weber number-gas phase $(F_s^2 d_H/\gamma)$
We_L	Weber number-liquid phase $(V_p^2 \rho_L d_H/\gamma)$
We_t	Weber number at transition $(d\rho_G U_t^{h\,2}/\gamma)$
x_m	maximum dropsize in the spray
x_{n+1}	liquid concentration entering the plate
x_n	liquid concentration leaving the plate
x_n^*	liquid concentration in equilibrium with exit vapour y_n
x_i	concentration of droplets leaving pool i
x_{di}	concentration of droplets returning to pool i
y_{mi}	gas leaving pool i
y_{m+1}	gas approaching plate m
y_m	gas leaving plate m
y_n	composition of vapour entering the plate leaving the plate
y_n^*	composition of the vapour in equilibrium with the exit liquid concentration x_n
y_{n-1}	composition of vapour leaving the plate
γ	surface tension
γ_W	surface tension of water
μ	mass absorption coefficient
μ_G	gas viscosity
μ_L	liquid viscosity
ρ_G	gas density
ρ_L	liquid density
σ	standard deviation
ϕ	holdup

BIBLIOGRAPHY

1. Fane, A.G. and Sawistowski, H.
   In "Distillation 1969", I. chem. E. Symp. Ser. No. 32, 1, 8. (London: The Institution of Chemical Engineers).

2. Sawistowski, H.
   Chemie - Ing - Techn. 45, 1093, 1973.

3. Hofhuis, P.A.M. and Zuiderweg, F.J.
   In "Distillation 1979", I. chem. E. Symp. Ser. No. 56, 2, 1. (London: The Institution of Chemical Engineers).

4. Macmillan, W.P.
   Ph.D. Thesis. University of London, 1962.

5. Bernard, J.D.T. and Sargent, R.W.H.
   Trans. Instn. Chem. Engrs. 44, 314, 1966.

6. Fell, C.J.D. and Pinczewski, W.V.
   Chem. Engr. Jan. 45, 1977.

7. Calderbank, P.H. and Rennie, J.
   Trans. Instn. Chem. Engrs. 40, 3, 1962.

8. Ross, S.
   Chem. Eng. Prog. 63, 41, 1967.

9. Kitchner, J.A. and Cooper, C.F.
   Quart. Rev. (London) 13, 71, 1959.

10. de Goederen, C.W.J.
    Chem. Eng. Sci. 20, 1115, 1965.

11. Rennie, J. and Evans, F.

Brit. Chem. Eng. 7, 498, 1962.

12. Schroter, R.C.

Ph.D. Thesis. University of London, 1967.

13. Dancwerts, P.V. and Smith, W. and Sawistowski, H.

In Rottenburg, "International Symposium on Distillation", 9, 1960. (London: The Institution of Chemical Engineers).

14. Sawistowski, H.

Private Communication.

15. Calderbank, P.H.

Trans. Instn. Chem. Engrs. 37, 173, 1959.

16. Calderbank, P.H., Evans, F. and Rennie, J.

In Rottenburg, "International Symposium on Distillation". (London: The Institution of Chemical Engineers). 51, 1960.

17. Calderbank, P.H. and Moo-Young, M.B.

Ibid., 59.

18. Ditnerski, Y.I.

Intl. Chem. Engng. 6, 204, 1966.

19. Porter, K.E., Davies, B.T. and Wong, P.F.Y.

Trans. Instn. Chem. Engrs. 45, 265, 1967.

20. Sawistowski, H.

Private Communication.

21. Ashley, M.J. and Haselden, G.G.

Trans. Instn. Chem. Engrs. 50, 119, 1972.

22. Sawistowski, H.

Chemie - Ing - Techn. 45, 1114, 1973.

23. Lindsey, J.K.

Ph.D. Thesis. University of London. 1972.

24. Muller, R.L. and Prince, R.G.H.

Chem. Eng. Sci. 27, 1583, 1972.

25. Spells, K.E. and Bakowski, S.

Trans. Instn. Chem. Engrs. 28, 38, 1950.

26. Spells, K.E. and Bakowski, S.

Trans. Instn. Chem. Engrs. 30, 189, 1952.

27. Spells, K.E.

Trans. Instn. Chem. Engrs. 32, 167, 1954.

28. Nielsen, R.D., Tek, M.R. and York, J.L.

In "Proceedings of Symposium on Two-Phase Flow",

Exeter, 1, F201, 1965.

29. Newitt, D.M., Dombrowski, N. and Knelman, F.H.

Trans. Inst. Chem. Engrs. 32, 244, 1954.

30. Teller, A.J. and Rood, R.D.

A.I.Ch.E.J. 8, 369, 1961.

31. Pinczewski, W.V. and Fell, C.J.D.

Trans. Instn. Chem. Engrs. 50, 102, 1972.

32. Banerjee, T.S., Roy, N.K. and Rao, M.N.

Indian Journal of Technology, 7, 301, 1969.

33. Banerjee, T.S., Roy, N.K. and Rao, M.N.

Indian Journal of Technology, 7, 308, 1969.

34. Aiba, S. and Yamada, T.

A.I.Ch.E.J. 5, 506, 1959.

35. Akselrod, L.S. and Yusova, G.M.

J. Appl. Chem. (U.S.S.R.) 30, 740, 1957.

36. Cheng, S.I. and Teller, A.J.

A.I.Ch.E.J. 7, 282, 1961.

37. Pinczewski, W.V. and Fell, C.J.D.

The Can. J. of Chem. Eng. 49, 548, 1971.

38. Jeronimo, M.A. da S. and Sawistowski, H.

Trans. Instn. Chem. Engrs. 52, 291, 1974.

39. Hughes, R.R. and Gilliland, E.R.

Chem. Eng. Prog. 48, 497, 1952.

40. Marshall, W.R.

Chem. Eng. Progr. Monograph. Ser. No. 2, 50, 1954.

41. Mugele, R.A. and Evans, H.D.

Ind. Eng. Chem. 43, 1317, 1951.

42. Sawistowski, H.

Private Communication.

43. Porter, K.E. and Wong, P.F.Y.

In "Distillation 1969", I.Chem.E.Symp. Ser. No. 32, 2, 22.

(London: The Institution of Chemical Engineers).

44. Jeronimo, M.A. da S.

Ph.D. Thesis. University of London, 1976.

45. Shakhov, Yu.A., Noskov, A.A. and Romankov, P.G.

Zh. prikl. Khim. 37, 2074, 1964.

46. Burgess, R.G. and Robinson, K.

In "Distillation 1969", I.Chem.E.Symp. Ser. No. 32, 2, 34 (London: The Institution of Chemical Engineers).

47. Payne, G.J.

Ph.D. Thesis. University of Sydney. 1974.

48. Pinczewski, W.V., Benke, N.D., Fell, C.J.D.

A.I.Ch.E.J. 21, No. 6, 1210, 1975.

49. Ho, G.E., Muller, R.L. and Prince, R.G.H.

In "Distillation 1969", I.Chem.E.Symp. Ser. No. 32, 2, 10. (London: The Institution of Chemical Engineers).

50. Kutateladze, S.S. and Sorokin, Y.L.

"Problems of Heat Transfer and Hydraulics of Two-Phase Media", P.385, 1969. (Oxford: Pergamon Press).

51. Andrew, S.P.S.

In "Distillation 1969", I.Chem.E.Symp. Ser. No. 32. 2, 49. (London: The Institution of Chemical Engineers).

52. Jeronimo, M.A.daS. and Sawistowski, H.

Trans. Instn. Chem. Engrs. 51, 265, 1973.

53. Porter, K.E. and Jenkins, J.D.

In "Distillation 1979". I.Chem.E.Symp. Ser. No. 56. Discussion Volume. P.75. (London: The Institution of

Chemical Engineers).

54. Murphree, E.V.

Ind. Eng. Chem. 17, 747, 1925.

55. Whitman, W.G.

Chem. Met. Eng. 29, 4, 1923.

56. Chilton, T.H. and Colburn, A.P.

Ind. Eng. Chem. 26, 1183, 1934.

57. Lewis, W.K.

Ind. Eng. Chem. 28, 399, 1936.

58. Zuiderweg, F.J. and Harmens, A.

Chem. Eng. Sci. 9, 89, 1958.

59. Bainbridge, G.S. and Sawistowski, H.

Chem. Engng. Sci. 19, 992, 1964.

60. Hai, N.T., Burges, J.M., Pinczewski, W.V. and Fell, C.J.D.

Second Australasian Conference on Heat and Mass Transfer. The University of Sydney. P.377, 1977.

61. Raper, J.A., Hai, N.T., Pinczewski, W.V. and Fell, C.J.D.

In "Distillation 1979", I.Chem.E.Symp. Ser. No. 56. 2, 57. (London: The Institution of Chemical Engineers).

62. Friend, L., Lemieux, E.J. and Schreiner, W.C.

Chem. Eng. 101, 1960 (Oct.).

63. Hunt, C. d'A., Hanson, D.N. and Wilke, C.R.

A.I.Ch.E.J. 1, 441, 1955.

64. Lemieux, E.J. and Scotti, L.J.

Chem. Eng. Progr. 65, No. 3, 52, 1969.

65. Colburn, A.P.

Ind. Eng. Chem. 28, 526, 1936.

66. Siddique,

M.Sc. Thesis. University of London, 1976.

67. Hauser, E.A. and Lynn, J.E.

"Experiments in Colloid Chemistry". p.25, 1940.

68. Fane, A.G.

Ph.D. Thesis. University of London, 1968.

69. Sargent, R.W.H., Bernard, J.D.T., Macmillan, W.P. and Schroter, R.C.

In Sawistowski, H. (Ed.). "Distillation. Final Report by ABCM. BCPMA Distillation Panel" 1964, P.145. (London: Chemical Industries Association).

70. McLaughlin, C.M. and Rushton, J.H.

A.I.Ch.E.J. 19, No. 4, 817, 1973.

71. Payne, G.J. and Prince, R.G.H.

Trans. Instn. Chem. Engrs. 53, 209, 1975.

72. Pinczewski, W.V. and Fell, C.J.D.

Trans. Instn. Chem. Engrs. 52, 294, 1974.

73. Porter, K.E., Safekourdi. and Lockett, M.J.

Trans. Instn. Chem. Engrs. 55, 190, 1977.

74. Ranz, W.E. and Marshall, W.R.

Chem. Eng. Prog. 48, 141, 173, 1952.

75. Kolodzie, P.A. and Winkle, M.V.

A.I.Ch.E.J. 3, No. 3, 305, 1957.

76. Mugele, R.A.

A.I.Ch.E.J. 6, No. 1, 3, 1960.

77. Hinze, J.O.

Appl. Sci. Res. A1, 273, 1949.

78. Garner, F.H., Ellis, S.R.M. and Lacey, J.A.

Trans. Instn. Chem. Engrs. 32, 222, 1954.

79. Levich, V.G.

In "Physiocochemical Hydrodynamics" P.644. 1962.

(New Jersey: Prentice Hall).

80. Pinczewski, W.V.

Ph.D. Thesis. The University of New South Wales. 1973.

81. Pinczewski, W.V. and Fell, C.J.D.

Trans. Instn. Chem. Engrs. 55, 46, 1977.

82. Yoshida, F., Nishibe, T. and Nagai, S.

In Rottenburg, P.A. (Ed.). "Transport Phenomena", P. 34.

1965. (London: The Institution of Chemical Engineers).

83. Standart, G.L., Rahman, M.A. and Arastafar, M.B.

4th Annual Research Meeting. The Institution of Chemical

Engineers.

84. Jeronimo, M.A. and Sawistowski, H.

In "Distillation 1979", I. Chem. E. Symp. Ser. No. 56. 2.2.41. (London: The Institution of Chemical Engineers).

85. Fane, A.G., Lindsey, J.K. and Sawistowski, H.

Indian. Chem. Engr. XV, No. 4., 1973.

86. Jeronimo, M.A. and Sawistowski, H.

4th Annual Research Meeting. The Institution of Chemical Engineers.

APPENDIX 1

Apparent Foam Density by the γ-radiation Absorption Technique

The basic law for the absorption of γ-radiation is:

$$\frac{dI}{dx} = -\mu\rho I \qquad \text{(A1)}$$

where I is the radiation intensity in the x-direction, ρ is the density and μ the mass absorption coefficient for the medium.

Integrating over x, we obtain:

$$\int_{I_o}^{I} \frac{dI}{I} = -\int_{o}^{x} \mu\rho dx$$

$$\log_e \frac{I}{I_o} = -\mu\bar{\rho}x$$

or

$$I = I_o\, e^{-\mu\bar{\rho}x} \qquad \text{(A2)}$$

where $\bar{\bar{\rho}}$ is the space-mean density.

Now $\bar{\rho}$ fluctuates with time, so we write:

$$\bar{\rho} = \bar{\bar{\rho}} + r(t) \qquad \text{(A3)}$$

where $\bar{\bar{\rho}}$ is the time-mean value of $\bar{\rho}$ and r(t) is the instantaneous deviation from the mean at time t.

Now using (A2) and (A3), we obtain an expression for the time-mean intensity, $\bar{I}$:

$$\bar{I} = \frac{1}{\tau}\int_0^\tau I\,dt = \frac{1}{\tau}\int_0^\tau I_0 e^{-\mu x(\bar{\bar{\rho}}+r)}dt$$

$$\bar{I} = \frac{I_0 e^{-\mu x \bar{\bar{\rho}}}}{\tau}\int_0^\tau e^{-\mu x r}dt \qquad \text{(A4)}$$

Now, for sufficiently long count-time, τ, we may assume that time-means approximate closely the statistical means of the various quantities (denoted by $< >$).

Thus, from (A3):

$$< r > = \frac{1}{\tau}\int_0^\tau r\,dt = 0 \qquad \text{(A5)}$$

Also:

$$< e^{-\mu x r} > = \frac{1}{\tau}\int_0^\tau e^{-\mu x r}dt$$

so that from (A4):

$$\bar{I} = \bar{I}_0 < e^{-\mu x r} > e^{-\mu x \bar{\bar{\rho}}} \qquad \text{(A6)}$$

If we assume that r is a Gaussian noise, of variance σ^2:

$$< e^{-\mu x r} > = \int_{-\infty}^{+\infty} e^{-\mu x r}\,\frac{1}{\sqrt{2\pi\sigma^2}}\exp(-\frac{r^2}{2\sigma^2})dr$$

$$= \exp(\frac{\sigma^2\mu^2x^2}{2})\int_{-\infty}^{+\infty}\frac{1}{\sqrt{2\pi\sigma^2}}\exp[-\frac{(r+\sigma^2\mu x)^2}{2\sigma^2}]\,d(r+\sigma^2\mu x)$$

$$\text{i.e. } < e^{-\mu x r} > = \exp(\frac{\sigma^2\mu^2x^2}{2}) \qquad \text{(A7)}$$

Now the apparent density, ρ', calculated on the assumption that ρ is constant, is given by substituting in equation (A2):

$$\bar{I} = I_o e^{-\mu\rho x} \qquad \text{(A8)}$$

From (A6), (A7) and (A8):

$$I_o e^{-\mu\rho x} = I_o e^{\frac{\sigma^2\mu^2x^2}{2}} \cdot e^{-\mu x\bar{\rho}}$$

Hence:

$$\rho = \bar{\rho} - \frac{\sigma^2\mu x}{2} \qquad \text{(A9)}$$

If a Poisson distribution is assumed for r, (with distribution function proportional to $r^a e^{-br}$), we obtain:

$$\rho' = \bar{\rho}\,\frac{b}{\mu x}\log_e\left(1 - \frac{\mu x}{b}\right) \qquad \text{(A9a)}$$

and for a regular sinusoidal variation, of amplitude r_o

$$\rho' = \bar{\rho} - \frac{r_o^2\mu x}{4} \qquad \text{(A9b)}$$

APPENDIX 2

EXPERIMENTAL RESULTS

TABLE 2 DISPERSION DENSITY DATA

2.1 System A: Butanol

2.2 System B: Methanol

2.3 System C: Water

2.4 System D: 1000 ppm Hydrous ferric oside in water.

2.5 System E: 1000 ppm Hydrous aluminium oxide in water.

TABLE 3 SURFACE AREA DATA

TABLE 2.1

DISPERSION DENSITY DATA

SYSTEM : BUTANOL

Run A101

$L_v = 0.12 \times 10^{-5}$ $F_s = 0.82$ $N_o = 17868$ $N = 4021$ $\phi = 0.103$

h	1.000	1.500	2.000	2.500	3.000	3.500	4.000	4.500	5.000
ϕ	0.081	0.037	0.038	0.032	0.028	0.023	0.019	0.015	0.011
h	6.000	7.000	8.000	9.000					
ϕ	0.005	0.003	0.001	0.001					

Run A102

$L_v = 0.12 \times 10^{-5}$ $F_s = 0.98$ $N_o = 17868$ $N = 4021$ $\phi = 0.111$

1.000	1.500	2.000	2.500	3.000	3.500	4.000	4.500	5.000
0.076	0.034	0.039	0.035	0.030	0.025	0.020	0.016	0.012
6.000	7.000	8.000	9.000					
0.006	0.004	0.002	0.001					

Run A103

$L_v = 0.12 \times 10^{-5}$ $F_s = 1.13$ $N_o = 17868$ $N = 4021$ $\phi = 0.108$

1.000	1.500	2.000	2.500	3.000	3.500	4.000	4.500	5.000
0.061	0.030	0.034	0.032	0.029	0.025	0.021	0.018	0.015
6.000	7.000	8.000						
0.008	0.004	0.001						

Run A104

$L_v = 0.12 \times 10^{-5}$ $F_s = 1.41$ $N_o = 17868$ $N = 4021$ $\phi = 0.106$

1.000	1.500	2.000	2.500	3.000	3.500	4.000	4.500	5.000
0.069	0.027	0.031	0.030	0.027	0.023	0.020	0.017	0.014
6.000	7.000	8.000	9.000					
0.009	0.005	0.002	0.001					

Run A201

$L_v = 0.16 \times 10^{-5}$ $F_s = 0.82$ $N_o = 17868$ $N = 4021$ $\phi = 0.114$

1.000	1.500	2.000	2.500	3.000	3.500	4.000	4.500	5.000
0.097	0.039	0.042	0.036	0.030	0.025	0.019	0.015	0.012
6.000	7.000	8.000						
0.006	0.003	0.001						

Run A202

$L_v = 0.16 \times 10^{-5}$ $F_s = 0.98$ $N_o = 17868$ $N = 4021$ $\phi = 0.114$

1.000	1.500	2.000	2.500	3.000	3.500	4.000	4.500	5.000
0.086	0.036	0.040	0.039	0.032	0.027	0.021	0.016	0.012
6.000	7.000	8.000	9.000					
0.008	0.004	0.002	0.001					

Run A203

$L_v = 0.16 \times 10^{-5}$ $F_s = 1.13$ $N_o = 17868$ $N = 4021$ $\phi = 0.116$

1.000	1.500	2.000	2.500	3.000	3.500	4.000	4.500	5.000
0.079	0.032	0.036	0.035	0.030	0.027	0.023	0.018	0.015
6.000	7.000	8.000	9.000					
0.009	0.005	0.002	0.002					

Run A204

$L_v = 0.16 \times 10^{-5}$ $F_s = 1.41$ $N_o = 17868$ $N = 4021$ $\phi = 0.116$

1.000	1.500	2.000	2.500	3.000	3.500	4.000	4.500	5.000
0.071	0.026	0.032	0.032	0.029	0.026	0.022	0.019	0.016
6.000	7.000	8.000	9.000					
0.010	0.006	0.003	0.002					

Run A301

$L_v = 0.19 \times 10^{-5}$ $F_s = 0.82$ $N_o = 17868$ $N = 4021$ $\phi = 0.121$

1.000	1.500	2.000	2.500	3.000	3.500	4.000	4.500	5.000
0.097	0.040	0.045	0.040	0.031	0.025	0.020	0.016	0.013
6.000	7.000	8.000						
0.008	0.008	0.001						

Run A302

$L_v = 0.19 \times 10^{-5}$ $F_s = 0.98$ $N_o = 17868$ $N = 4021$ $\phi = 0.127$

1.000	1.500	2.000	2.500	3.000	3.500	4.000	4.500	5.000
0.084	0.037	0.043	0.041	0.033	0.028	0.023	0.018	0.015
6.000	7.000	8.000						
0.009	0.005	0.002						

Run A303

$L_v = 0.19 \times 10^{-5}$ $F_s = 1.13$ $N_o = 17868$ $N = 4021$ $\phi = 0.128$

1.000	1.500	2.000	2.500	3.000	3.500	4.000	4.500	5.000
0.081	0.034	0.038	0.040	0.035	0.029	0.024	0.019	0.016
6.000	7.000	8.000	9.000	10.000				
0.009	0.005	0.003	0.002	0.001				

Run A304

$L_v = 0.19 \times 10^{-5}$ $F_s = 1.41$ $N_o = 17868$ N = 4021 $\phi = 0.130$

1.000	1.500	2.000	2.500	3.000	3.500	4.000	4.500	5.000
0.076	0.028	0.033	0.038	0.035	0.030	0.025	0.020	0.017
6.000	7.000	8.000	9.000	10.000				
0.010	0.006	0.003	0.003	0.002				

Run A401

$L_v = 0.27 \times 10^{-5}$ $F_s = 0.98$ $N_o = 17775$ N = 4021 $\phi = 0.141$

1.000	1.500	2.000	2.500	3.000	3.500	4.000	4.500	5.000
0.079	0.040	0.045	0.046	0.035	0.030	0.025	0.020	0.016
6.000	7.000	8.000	9.000					
0.010	0.006	0.003	0.001					

Run A402

$L_v = 0.27 \times 10^{-5}$ $F_s = 1.13$ $N_o = 17775$ N = 4021 $\phi = 0.144$

1.000	1.500	2.000	2.500	3.000	3.500	4.000	4.500	5.000
0.056	0.037	0.040	0.043	0.039	0.032	0.026	0.022	0.018
6.000	7.000	8.000	9.000					
0.012	0.007	0.004	0.002					

Run A403

$L_v = 0.27 \times 10^{-5}$ $F_s = 1.41$ $N_o = 17708$ N = 4013 $\phi = 0.148$

1.000	1.500	2.000	2.500	3.000	3.500	4.000	4.500	5.000
0.071	0.028	0.032	0.037	0.039	0.035	0.029	0.024	0.020
6.000	7.000	8.000	9.000	10.000	11.000	12.000		
0.013	0.008	0.005	0.003	0.003	0.002	0.001		

Run A501

$L_v = 0.35 \times 10^{-5}$ $F_s = 0.98$ $N_o = 17708$ $N = 4013$ $\phi = 0.157$

1.000	1.500	2.000	2.500	3.000	3.500	4.000	4.500	5.000
0.103	0.036	0.044	0.049	0.043	0.035	0.028	0.023	0.018
6.000	7.000	8.000	9.000					
0.012	0.007	0.003	0.001					

Run A502

$L_v = 0.35 \times 10^{-5}$ $F_s = 1.13$ $N_o = 17708$ $N = 4013$ $\phi = 0.169$

1.000	1.500	2.000	2.500	3.000	3.500	4.000	4.500	5.000
0.071	0.036	0.043	0.048	0.045	0.036	0.030	0.026	0.021
6.000	7.000	8.000	9.000	10.000				
0.014	0.009	0.005	0.003	0.001				

Run A503

$L_v = 0.35 \times 10^{-5}$ $F_s = 1.41$ $N_o = 17708$ $N = 4013$ $\phi = 0.185$

1.000	1.500	2.000	2.500	3.000	3.500	4.000	4.500	5.000
0.073	0.032	0.038	0.043	0.045	0.041	0.035	0.030	0.025
6.000	7.000	8.000	9.000	10.000	11.000			
0.018	0.010	0.006	0.004	0.003	0.002			

Run A601

$L_v = 0.44 \times 10^{-5}$ $F_s = 1.13$ $N_o = 17708$ $N = 4013$ $\phi = 0.195$

1.000	1.500	2.000	2.500	3.000	3.500	4.000	4.500	5.000
0.113	0.040	0.047	0.051	0.053	0.045	0.037	0.030	0.024
6.000	7.000	8.000	9.000	10.000				
0.015	0.010	0.006	0.003	0.002				

Run A602

$L_v = 0.44 \times 10^{-5}$ $F_s = 1.41$ $N_o = 17708$ $N = 4013$ $\phi = 0.197$

1.000	1.500	2.000	2.500	3.000	3.500	4.000	4.500	5.000
0.082	0.036	0.042	0.045	0.048	0.048	0.040	0.032	0.026
6.000	7.000	8.000	9.000	10.000	11.000	12.000		
0.018	0.012	0.008	0.005	0.004	0.003	0.003		

Run A701

$L_v = 0.53 \times 10^{-5}$ $F_s = 1.41$ $N_o = 17708$ $N = 4013$ $\phi = 0.225$

1.000	1.500	2.000	2.500	3.000	3.500	4.000	4.500	5.000
0.096	0.036	0.043	0.048	0.052	0.053	0.046	0.037	0.030
6.000	7.000	8.000	9.000	10.000	11.000	12.000		
0.020	0.014	0.009	0.006	0.005	0.004	0.003		

Run A801

$L_v = 0.62 \times 10^{-5}$ $F_s = 1.41$ $N_o = 17708$ $N = 4013$ $\phi = 0.249$

1.500	2.000	2.500	3.000	3.500	4.000	4.500	5.000	6.000
0.040	0.044	0.048	0.051	0.053	0.053	0.045	0.035	0.023
7.000	8.000	9.000	10.000	11.000	12.000			
0.015	0.010	0.007	0.005	0.004	0.003			

TABLE 2.2

SYSTEM METHANOL

Run B101

$L_v = 0.12 \times 10^{-5}$ m^3/s $F_s = 1.22$ $N_o = 18247$ $N = 4165$ $\phi = 0.123$

0.500	0.750	1.000	1.500	2.00	2.500	3.00	3.500	4.000
0.687	0.321	0.122	0.024	0.030	0.032	0.029	0.026	0.018
4.500	5.000	6.000	7.000	8.000	9.000	10.000	11.000	12.000
0.019	0.014	0.012	0.006	0.005	0.007	0.002	0.002	0.001

Run B102

$L_v = 0.12 \times 10^{-5}$ $F_s = 1.413$ $N_o = 18247$ $N = 4165$ $\phi = 0.114$

0.500	0.750	1.000	1.500	2.000	2.500	3.000	3.500	4.000
0.748	0.261	0.110	0.015	0.022	0.027	0.030	0.026	0.019
4.500	5.000	6.000	7.000	8.000	9.000	10.000	11.000	12.000
0.019	0.022	0.013	0.007	0.006	0.002	0.003	0.002	0.001

Run B103

$L_v = 0.12_x 10^{-5}$ $F_s = 1.51$ $N_o = 18247$ $N = 4165$ $\phi = 0.118$

0.500	0.750	1.000	1.500	2.000	2.500	3.000	3.500	4.000
0.781	0.312	0.138	0.012	0.018	0.023	0.023	0.023	0.019
4.500	5.000	6.000	7.000	8.000	9.000	10.000	11.000	12.000
0.017	0.015	0.012	0.009	0.008	0.005	0.006	0.003	0.003

Run B104

$L_v = 0.12 \times 10^{-5}$ $F_s = 1.61$ $N_o = 18247$ $N = 4165$ $\phi = 0.110$

0.500	0.750	1.000	1.500	2.000	2.500	3.000	3.500	4.000
0.673	0.310	0.147	0.007	0.013	0.017	0.023	0.020	0.019
4.500	5.000	6.000	7.000	8.000	9.000	10.000	11.000	12.000
0.015	0.013	0.011	0.009	0.008	0.007	0.005	0.005	0.004

Run B201

$L_v = 0.16 \times 10^{-5}$ $F_s = 1.22$ $N_o = 16407$ $N = 3894$ $\phi = 0.134$

0.500	0.750	1.000	1.500	2.000	2.500	3.000	3.500	4.000
0.800	0.314	0.123	0.022	0.031	0.035	0.034	0.030	0.023
4.500	5.000	6.000	7.000	8.000	9.000	10.000	11.000	12.000
0.020	0.016	0.010	0.007	0.005	0.003	0.003	0.002	0.001

Run B202

$L_v = 0.16 \times 10^{-5}$ $F_s = 1.41$ $N_o = 16047$ $N = 3894$ $\phi = 0.136$

0.500	0.750	1.000	1.500	2.000	2.500	3.000	3.500	4.000
0.600	0.269	0.129	0.013	0.022	0.027	0.026	0.027	0.024
4.500	5.000	6.000	7.000	8.000	9.000	10.000	11.000	12.000
0.022	0.018	0.012	0.009	0.006	0.005	0.005	0.003	0.002

Run B203

$L_v = 0.16 \times 10^{-5}$ $F_s = 1.51$ $N_o = 18060$ $N = 4165$ $\phi = 0.14$

0.500	0.750	1.000	1.500	2.000	2.500	3.000	3.500	4.000
0.640	0.200	0.123	0.016	0.022	0.025	0.028	0.026	0.024
4.500	5.000	6.000	7.000	8.000	9.000	10.000	11.000	12.000
0.021	0.018	0.015	0.011	0.008	0.006	0.005	0.004	0.003

Run B204

$L_v = 0.16 \times 10^{-5}$ $F_s = 1.61$ $N_o = 18060$ $N = 4165$ $\phi = 0.130$

0.500	0.750	1.000	1.500	2.000	2.500	3.000	3.500	4.000
0.730	0.300	0.150	0.010	0.015	0.020	0.023	0.023	0.022
4.500	5.000	6.000	7.000	8.000	9.000	10.000	11.000	12.000
0.020	0.018	0.014	0.011	0.009	0.008	0.006	0.005	0.005

Run B301

$L_v = 0.19 \times 10^{-5}$ $F_s = 1.22$ $N_o = 18060$ $N = 4165$ $\phi = 0.174$

0.500	0.750	1.000	1.500	2.000	2.500	3.000	3.500	4.000
0.710	0.520	0.340	0.027	0.030	0.038	0.039	0.035	0.030
4.500	5.000	6.000	7.000	8.000	9.000	10.000	11.000	12.000
0.027	0.022	0.016	0.014	0.009	0.007	0.005	0.004	0.003

Run B302

$L_v = 0.19 \times 10^{-5}$ $F_s = 1.41$ $N_o = 18060$ $N = 4165$ $\phi = 0.174$

0.500	0.750	1.000	1.500	2.000	2.500	3.000	3.500	4.000
0.630	0.413	0.270	0.018	0.030	0.029	0.033	0.033	0.032
4.500	5.000	6.000	7.000	8.000	9.000	10.000	11.000	12.000
0.028	0.021	0.018	0.0125	0.009	0.009	0.005	0.004	0.004

Run B303

$L_v = 0.19 \times 10^{-5}$ $F_s = 1.51$ $N_o = 18065$ $N = 4165$ $\phi = 0.163$

0.500	0.750	1.000	1.500	2.000	2.500	3.000	3.500	4.000
0.470	0.380	0.173	0.015	0.020	0.025	0.028	0.031	0.029
4.500	5.000	6.000	7.000	8.000	9.000	10.000	11.000	12.000
0.025	0.021	0.017	0.013	0.010	0.007	0.005	0.004	0.003

Run B304

$L_v = 0.19 \times 10^{-5}$ $F_s = 1.61$ $N_o = 18060$ $N = 4165$ $\phi = 0.159$

0.500	0.750	1.000	1.500	2.000	2.500	3.000	3.500	4.000
0.513	0.478	0.032	0.014	0.018	0.021	0.024	0.027	0.027
4.500	5.000	6.000	7.000	8.000	9.000	10.000	11.000	12.000
0.024	0.023	0.018	0.015	0.012	0.010	0.008	0.007	0.006

Run B401

$L_v = 0.23 \times 10^{-5}$ $F_s = 1.32$ $N_o = 16355$ $N = 3894$ $\phi = 0.176$

0.750	1.000	1.500	2.000	2.500	3.000	3.500	4.000	4.500
0.400	0.038	0.025	0.030	0.033	0.035	0.033	0.030	0.026
5.000	6.000	7.000	8.000	9.000	10.000	11.000	12.000	
0.024	0.018	0.015	0.011	0.008	0.005	0.003	0.002	

Run B402

$L_v = 0.23 \times 10^{-5}$ $F_s = 1.41$ $N_o = 16355$ $N = 3894$ $\phi = 0.183$

0.750	1.000	1.500	2.000	2.500	3.000	3.500	4.000	4.500
0.332	0.039	0.021	0.026	0.030	0.033	0.036	0.032	0.028
5.000	6.000	7.000	8.000	9.000	10.000	11.000	12.000	
0.021	0.018	0.016	0.012	0.009	0.006	0.004	0.003	

Run B403

$L_v = 0.23 \times 10^{-5}$ $F_s = 1.51$ $N_o = 16355$ $N = 3894$ $\phi = 0.192$

1.000	1.500	2.000	2.500	3.000	3.500	4.000	4.500	5.000
0.104	0.018	0.022	0.026	0.029	0.033	0.032	0.027	0.025
6.000	7.000	8.000	9.000	10.000	11.000	12.000		
0.021	0.015	0.013	0.011	0.009	0.007	0.005		

Run B404

$L_v = 0.23 \times 10^{-5}$ $F_s = 1.61$ $N_o = 16355$ $N = 3894$ $\phi = 0.197$

1.000	1.500	2.000	2.500	3.000	3.500	4.000	4.500	5.000
0.103	0.015	0.020	0.024	0.027	0.030	0.030	0.030	0.025
6.000	7.000	8.000	9.000	10.000	11.000	12.000		
0.022	0.022	0.013	0.013	0.010	0.008	0.006		

Run B501

$L_v = 0.27 \times 10^{-5}$ $F_s = 1.32$ $N_o = 16355$ $N = 3894$ $\phi = 0.208$

1.000	1.500	2.000	2.500	3.000	3.500	4.000	4.500	5.000
0.116	0.028	0.031	0.037	0.041	0.040	0.035	0.030	0.028
6.000	7.000	8.000	9.000	10.000	11.000	12.000		
0.021	0.017	0.011	0.009	0.007	0.006	0.005		

Run B502

$L_v = 0.27 \times 10^{-5}$ $F_s = 1.41$ $N_o = 16355$ $N = 3894$ $\phi = 0.209$

1.000	1.500	2.000	2.500	3.000	3.500	4.000	4.500	5.000
0.103	0.023	0.027	0.032	0.035	0.037	0.037	0.032	0.031
6.000	7.000	8.000	9.000	10.000	11.000	12.000		
0.022	0.017	0.014	0.011	0.007	0.006	0.004		

Run B503

$L_v = 0.27 \times 10^{-5}$ $F_2 = 1.51$ $N_o = 16355$ $N = 3894$ $\phi = 0.206$

1.000	1.500	2.000	2.500	3.000	3.500	4.000	4.500	5.000
0.117	0.022	0.028	0.029	0.031	0.036	0.036	0.033	0.031
6.000	7.000	8.000	9.000	10.000	11.000	12.000		
0.025	0.020	0.015	0.011	0.009	0.006	0.007		

Run B504

$L_v = 0.27 \times 10^{-5}$ $F_s = 1.61$ $N_o = 16355$ $N = 3894$ $\phi = 0.217$

1.000	1.500	2.000	2.500	3.000	3.500	4.000	4.500	5.000
0.139	0.022	0.028	0.030	0.032	0.033	0.035	0.034	0.030
6.000	7.000	8.000	9.000	10.000	11.000	12.000		
0.026	0.020	0.016	0.015	0.009	0.007	0.006		

Run B601

$L_v = 0.31 \times 10^{-5}$ $F_s = 1.41$ $N_o = 18145$ $N = 4165$ $\phi = 0.226$

1.000	1.500	2.000	2.500	3.000	3.500	4.000	4.500	5.000
0.027	0.029	0.032	0.034	0.037	0.038	0.040	0.032	0.030
6.000	7.000	8.000	9.000	10.000	11.000	12.000		
0.024	0.019	0.015	0.012	0.008	0.006	0.006		

Run B602

$L_v = 0.031 \times 10^{-5}$ $F_s = 1.51$ $N_o = 18145$ $N = 4165$ $\phi = 0.229$

1.000	1.500	2.000	2.500	3.000	3.500	4.000	4.500	5.000
0.113	0.024	0.030	0.032	0.034	0.038	0.037	0.038	0.031
6.000	7.000	8.000	9.000	10.000	11.000	12.000		
0.026	0.020	0.016	0.013	0.009	0.007	0.007		

Run B603

$L_v = 0.031 \times 10^{-5}$ $F_s = 1.61$ $N_o = 18145$ $N = 4165$ $\phi = 0.234$

1.000	1.500	2.000	2.500	3.000	3.500	4.000	4.500	5.000
0.095	0.022	0.026	0.028	0.031	0.035	0.034	0.036	0.033
6.000	7.000	8.000	9.000	10.000	11.000	12.000		
0.027	0.023	0.017	0.011	0.012	0.008	0.007		

Run B701

$L_v = 0.35 \times 10^{-5}$ $F_s = 1.51$ $N_o = 17819$ $N = 4165$ $\phi = 0.256$

1.000	1.500	2.000	2.500	3.000	3.500	4.000	4.500	5.000
0.224	0.023	0.026	0.035	0.038	0.039	0.042	0.044	0.042
6.000	7.000	8.000	9.000	10.000	11.000	12.000		
0.032	0.025	0.017	0.012	0.010	0.009	0.008		

Run B702

$L_v = 0.35 \times 10^{-5}$ $F_s = 1.61$ $N_o = 17819$ $N = 4165$ $\phi = 0.259$

1.000	1.500	2.000	2.500	3.000	3.500	4.000	4.500	5.000
0.165	0.024	0.029	0.033	0.038	0.040	0.040	0.041	0.037
6.000	7.000	8.000	9.000	10.000	11.000	12.000		
0.028	0.022	0.019	0.015	0.012	0.011	0.008		

Run B801

$L_v = 0.4 \times 10^{-5}$ $F_s = 1.61$ $N_o = 17141$ $N = 3894$ $\phi = 0.255$

1.000	1.500	2.000	2.500	3.000	3.500	4.000	4.500	5.000
0.279	0.019	0.027	0.032	0.036	0.035	0.039	0.038	0.040
6.000	7.000	8.000	9.000	10.000	11.000			
0.030	0.026	0.020	0.014	0.011	0.010			

TABLE 2.3

SYSTEM: WATER

Run C101

$L_v = 0.12 \times 10^{-5}$ $F_s = 1.41$ $N_o = 14783$ $N = 4089$ $\phi = 0.109$

1.000	1.500	2.000	2.500	3.000	3.500	4.000	4.500	5.000
0.065	0.028	0.035	0.033	0.029	0.024	0.019	0.015	0.012
6.000	7.000	8.000						
0.006	0.003	0.001						

Run C102

$L_v = 0.12 \times 10^{-5}$ $F_s = 1.89$ $N_o = 14783$ $N = 4089$ $\phi = 0.102$

1.000	1.500	2.000	2.500	3.000	3.500	4.000	4.500	5.000
0.055	0.025	0.031	0.030	0.028	0.024	0.020	0.016	0.013
6.000	7.000	8.000						
0.007	0.003	0.002						

Run C103

$L_v = 0.12 \times 10^{-5}$ $F_s = 2.12$ $N_o = 14783$ $N = 4089$ $\phi = 0.115$

1.000	1.500	2.000	2.500	3.000	3.500	4.000	4.500	5.000
0.048	0.018	0.025	0.030	0.029	0.026	0.022	0.018	0.015
6.000	7.000	8.000	9.000	10.000				
0.010	0.006	0.004	0.002	0.001				

Run C104

$L_v = 0.12 \times 10^{-5}$ $F_s = 2.41$ $N_o = 14783$ N = 4089 $\phi = 0.118$

1.000	1.500	2.000	2.500	3.000	3.500	4.000	4.500	5.000
0.058	0.015	0.021	0.025	0.027	0.025	0.023	0.020	0.017
6.000	7.000	8.000	9.000	10.000				
0.012	0.008	0.006	0.003	0.002				

Run C201

$L_v = 0.19 \times 10^{-5}$ $F_s = 1.41$ $N_o = 14783$ N = 4089 $\phi = 0.121$

1.000	1.500	2.000	2.500	3.000	3.500	4.000	4.500	5.000
0.060	0.030	0.037	0.036	0.031	0.026	0.021	0.017	0.013
6.000	7.000	8.000	9.000	10.000				
0.008	0.003	0.002	0.002	0.001				

Run C202

$L_v = 0.19 \times 10^{-5}$ $F_s = 1.89$ $N_o = 14783$ N = 4089 $\phi = 0.123$

1.000	1.500	2.000	2.500	3.000	3.500	4.000	4.500	5.000
0.062	0.029	0.033	0.036	0.032	0.028	0.024	0.019	0.015
6.000	7.000	8.000	9.000	10.000				
0.010	0.005	0.003	0.002	0.001				

Run C203

$L_v = 0.19 \times 10^{-5}$ $F_s = 2.12$ $N_o = 14783$ N = 4089 $\phi = 0.141$

1.000	1.500	2.000	2.500	3.000	3.500	4.000	4.500	5.000
0.048	0.025	0.029	0.032	0.032	0.029	0.026	0.023	0.019
6.000	7.000	8.000	9.000	10.000				
0.014	0.008	0.004	0.003	0.002				

Run C204

$L_v = 0.19\times10^{-5}$ $F_s = 2.41$ $N_o = 14783$ $N = 4089$ $\phi = 0.124$

1.000	1.500	2.000	2.500	3.000	3.500	4.000	4.500	5.000
0.044	0.020	0.025	0.028	0.029	0.026	0.023	0.020	0.018
6.000	7.000	8.000	9.000	10.000				
0.013	0.009	0.006	0.004	0.002				

Run C301

$L_v = 0.27\times10^{-5}$ $F_s = 1.89$ $N_o = 14783$ $N = 4089$ $\phi = 0.143$

1.000	1.500	2.000	2.500	3.000	3.500	4.000	4.500	5.000
0.062	0.033	0.039	0.041	0.038	0.033	0.028	0.023	0.019
6.000	7.000	8.000	9.000	10.000				
0.011	0.006	0.004	0.002	0.002				

Run C302

$L_v = 0.27\times10^{-5}$ $F_s = 2,12$ $N_o = 14783$ $N = 4089$ $\phi = 0.156$

1.000	1.500	2.000	2.500	3.000	3.500	4.000	4.500	5.000
0.054	0.030	0.033	0.035	0.036	0.033	0.028	0.024	0.021
6.000	7.000	8.000	9.000	10.000				
0.015	0.010	0.006	0.004	0.003				

Run C303

$L_v = 0.27\times10^{-5}$ $F_s = 2.41$ $N_o = 14783$ $N = 4089$ $\phi = 0.166$

1.000	1.500	2.000	2.500	3.000	3.500	4.000	4.500	5.000
0.051	0.023	0.028	0.033	0.035	0.034	0.030	0.028	0.024
6.000	7.000	8.000	9.000	10.000	11.000			
0.018	0.013	0.008	0.006	0.004	0.002			

Run C401

$L_v = 0.35 \times 10^{-5}$ $F_s = 1.89$ $N_o = 14783$ $N = 4089$ $\phi = 0.157$

1.000	1.500	2.000	2.500	3.000	3.500	4.000	4.500	5.000
0.072	0.033	0.040	0.043	0.042	0.036	0.031	0.025	0.021
6.000	7.000	8.000	9.000	10.000	11.000			
0.013	0.008	0.005	0.004	0.003	0.001			

Run C402

$L_v = 0.35 \times 10^{-5}$ $F_s = 2.12$ $N_o = 14783$ $N = 4089$ $\phi = 0.178$

1.000	1.500	2.000	2.500	3.000	3.500	4.000	4.500	5.000
0.059	0.028	0.036	0.041	0.044	0.045	0.039	0.034	0.030
6.000	7.000	8.000	9.000	10.000	11.000			
0.021	0.014	0.010	0.007	0.006	0.005			

Run C403

$L_v = 0.35 \times 10^{-5}$ $F_s = 2.41$ $N_o = 14783$ $N = 4089$ $\phi = 0.181$

1.000	1.500	2.000	2.500	3.000	3.500	4.000	4.500	5.000
0.046	0.023	0.027	0.031	0.035	0.036	0.033	0.030	0.027
6.000	7.000	8.000	9.000	10.000	11.000			
0.021	0.015	0.010	0.008	0.006	0.002			

Run C501

$L_v = 0.4 \times 10^{-5}$ $F_s = 2.12$ $N_o = 14783$ $N = 4089$ $\phi = 0.209$

1.000	1.500	2.000	2.500	3.000	3.500	4.000	4.500	5.000
0.053	0.023	0.037	0.041	0.044	0.045	0.039	0.034	0.030
6.000	7.000	8.000	9.000	10.000	11.000			
0.022	0.014	0.010	0.007	0.007	0.005			

Run C502

$L_v = 0.4 \times 10^{-5}$ $F_s = 2.41$ $N_o = 14783$ $N = 4089$ $\phi = 0.206$

1.000	1.500	2.000	2.500	3.000	3.500	4.000	4.500	5.000
0.046	0.028	0.031	0.035	0.039	0.041	0.039	0.036	0.032
6.000	7.000	8.000	9.000	10.000	11.000			
0.024	0.018	0.012	0.009	0.007	0.006			

TABLE 2.4

SYSTEM: 1000 ppm HYDROUS FERRIC OXIDE SOL.

Run D101

$L_v = 0.27 \times 10^{-5}$ $F_s = 1.90$ $N_o = 14849$ $N = 4113$ $\phi = 0.143$

1.000	1.500	2.000	2.500	3.000	3.500	4.000	4.500	5.000
0.059	0.031	0.037	0.042	0.035	0.030	0.025	0.023	0.020
6.000	7.000	8.000	9.000	10.000				
0.013	0.010	0.007	0.003	0.002				

Run D102

$L_v = 0.35 \times 10^{-5}$ $F_s = 1.89$ $N_o = 14849$ $N = 4113$ $\phi = 0.158$

1.000	1.500	2.000	2.500	3.000	3.500	4.000	4.500	5.000
0.074	0.038	0.042	0.044	0.045	0.037	0.029	0.025	0.016
6.000	7.000	8.000	9.000	10.000				
0.012	0.008	0.004	0.005	0.003				

TABLE 2.5

SYSTEM: 1000 ppm HYDROUS ALUMINIUM OXIDE SOL.

Run E101

$L_v = 0.27 \times 10^{-5}$ $F_s = 1.90$ $N_o = 14731$ N = 4068 $\phi = 0.143$

1.000	1.500	2.000	2.500	3.000	3.500	4.000	4.500	5.000
0.063	0.030	0.036	0.041	0.037	0.030	0.025	0.023	0.020
6.000	7.000	8.000	9.000	10.000				
0.015	0.007	0.006	0.005	0.003				

Run E102

$L_v = 0.35 \times 10^{-5}$ $F_s = 1.89$ $N_o = 14731$ N = 4068 $\phi = 0.157$

1.000	1.500	2.000	2.500	3.000	3.500	4.000	4.500	5.000
0.069	0.036	0.040	0.043	0.039	0.033	0.030	0.025	0.023
6.000	7.000	8.000	9.000	10.000				
0.013	0.011	0.004	0.004	0.003				

TABLE 3

SPECIFIC SURFACE AREA DATA

l = 7-25 CM

Run No.	h	4.000	4.500	5.000	6.000	7.000	8.000	9.000	10.000	12.000
A101		0.479	0.428	0.382	0.330	0.255	0.205	0.174	0.144	0.116
A103		0.579	0.520	0.492	0.394	0.330	0.273	0.238	0.205	0.159
A201		0.549	0.492	0.441	0.330	0.273	0.229	0.189	0.166	0.123
A202		0.743	0.629	0.564	0.441	0.372	0.301	0.273	0.229	0.177
A301		0.664	0.579	0.492	0.405	0.340	0.282	0.238	0.213	0.166
A303		0.765	0.702	0.646	0.534	0.453	0.382	0.340	0.282	0.238
A304		0.823	0.743	0.683	0.579	0.479	0.417	0.372	0.340	0.282
A402		0.888	0.787	0.702	0.579	0.492	0.405	0.356	0.330	0.238
A502		0.962	0.916	0.888	0.722	0.620	0.506	0.441	0.372	0.301
A602		1.270	1.220	1.126	0.978	0.787	0.664	0.564	0.506	0.394
B101		0.888	0.835	0.787	0.683	0.549	0.441	0.382	0.330	0.246
B102		1.047	0.978	0.916	0.787	0.664	0.579	0.506	0.453	0.372
B103		1.085	1.047	0.977	0.861	0.765	0.646	0.534	0.492	0.417

	4.000	4.500	5.000	6.000	7.000	8.000	9.000	10.000	12.000
B104	1.147	1.085	1.047	0.916	0.787	0.683	0.595	0.534	0.441
B301	0.962	0.888	0.811	0.683	0.579	0.441	0.405	0.361	0.282
B302	1.270	1.218	1.126	0.962	0.811	0.646	0.564	0.492	0.405
B303	2.923	2.823	2.700	1.126	1.011	0.811	0.664	0.595	0.472
B304	2.664	2.664	2.599	1.218	1.047	0.861	0.743	0.646	0.506
B502	2.822	2.738	2.664	1.218	0.978	0.835	0.712	0.612	0.492
B503	2.823	2.738	2.738	2.599	1.085	0.946	0.787	0.683	0.541
C103	0.765	0.743	0.712	0.620	0.520	0.428	0.361	0.310	0.238
C104	0.962	0.916	0.888	0.743	0.629	0.520	0.453	0.405	0.320
C202	1.270	1.170	1.085	0.978	0.835	0.712	0.617	0.534	0.417
C203	2.600	1.270	1.169	1.085	0.888	0.811	0.722	0.646	0.506
C204	2.664	2.599	1.270	1.085	0.978	0.888	0.787	0.712	0.564

```
0001:  C
0002:  C
0003:  C                          PROGRAM  MODEL
0004:  C
0005:  C
0006:  C      THIS  PROGRAM
0007:  C                    1.  DETERMINES  THE  VOLUMETRIC  FLOW  RATE  OF
0008:  C                        LIQUID  LEAVING  THE  PLATE  IN  THE  FORM
0009:  C                        SPRAY,
0010:  C
0011:  C                    2.  PARAMETER  FITTING  OF  DISPERSION  DENSITY
0012:  C                        PROFILES  USING  POWELL,S  MINIMISATION
0013:  C                        SUBROUTINE
0014:  C
0015:  C
0016:         PROGRAM MODEL(INPUT,OUTPUT,TAPE5=INPUT,TAPE6=OUTPUT)
0017:         COMMON DENPAR, DENGAS, VIS, NO, NO1, DIF, GRAD, GM, FRATE, IND
0018:         COMMON TOTNOG, CT, ICNT, JK, J, US, NDU, SC, QTOT, AMDA
0019:         COMMON GRTOT, RATEF
0020:  C
0021:         ISW     =  0
0022:         CALL READIN
0023:         IF (ISW .EQ. 1) GO  TO  20
0024:         DO 10 J = 1, NO
0025:         CALL UPWARD
0026:         CALL DOWN
0027:         CALL VOLUME
0028:  10     CONTINUE
0029:         GO  TO  30
0030:  20     CALL FRQCY
0031:  C
0032:  C      NUMBER  OF  POOLS  =  9,  SELECTED  BY  FELL
0033:  C
0034:  30     PK      =  9.
0035:         C       =  (RATEF - QTOT/PK) / RATEF
0036:         EOG     =  1 - EXP(-TOTNOG)
0037:         ALPHA   =  AMDA * EOG / ((1 - C) * PK)
0038:         BETA    =  1 + ALPHA
0039:         EMG1    =  ( (1 - C) / AMDA) * ((BETA**PK - 1)/(1-C+C*BETA**PK))
0040:         A       =  BETA / ( 1 + C * ALPHA)
0041:         EMG2    =  (1/AMDA) * (A ** (PK - 1) - 1)
0042:         STOP
0043:         END
0044:         SUBROUTINE READIN
0045:         COMMON DENPAR, DENGAS, VIS, NO, NO1, DIF, GRAD, GM, FRATE, IND
0046:         COMMON TOTNOG, CT, ICNT, JK, J, US, NDU, SC, QTOT, AMDA
0047:         COMMON GRTOT, RATEF
0048:         COMMON /SET1/ V(100)
0049:         COMMON /SET2/ DMAV(100)
0050:         COMMON /SET5/ HOLD(100)
0051:         COMMON /SET4/ DISP(100), HT(100), DM(100), EXHOLD(100)
0052:         COMMON /SET15/ AREA, XA, EXDIS(100)
0053:         COMMON /SET20/ HLOTOT(100), HL(100)
0054:         COMMON /SET31/ DPM, STDV
0055:  C
0056:         READ,          DENPAR, DENGAS, VIS, NO, NO1, ENHOLD, VISL, ST
0057:         READ,          FS, FA, XA, FLOW, HEIGHT, GRAD, DIF
0058:         READ, ULIM, BLIM, GMOL, FMOL, DPM, STDV, HDM
0059:         READ (5, 30) (DISP(I), I = 1, NO)
0060:  30     FORMAT (F10.8)
```

```
0061:  C
0062:         IND     =  0
0063:         TOTNOG  =  0.0
0064:         QTOT    =  0.0
0065:         GRTOT   =  0.0
0066:         ICNT    =  0
0067:         N       =  30
0068:         IF (IND .EQ. 1 ) GO TO 950
0069:         DO 900 I = 1, 100
0070:         HT(I)   =  0.0
0071:         DM(I)   =  0.0
0072:         HOLD(I) =  0.0
0073:         DMAV(I)     =  0.0
0074:         EXHOLD(I)   =  0.0
0075:         HL(I)   =  0.0
0076:  900    CONTINUE
0077:  C
0078:  C      SUPERFICIAL  VELOCITY
0079:  C
0080:  950    US      =  FS / SQRT(DENGAS)
0081:  C
0082:  C      HOLE  VELOCITY
0083:  C
0084:         UH      =  US / FA
0085:         GM      =  US * XA * DENGAS / GMOL
0086:         FRATE   =  FLOW * 0.305 * DENPAR / 3600/ FMOL
0087:         AMDA    =  GRAD * GM / FRATE
0088:         RATEF   =  FLOW * 0.305 / 3600
```

```
0001:  C
0002:  C
0003:  C      SET  HEIGHT
0004:  C
0005:         HT(1)    =  HEIGHT
0006:         DO 1000  I = 2, NO1
0007:         HT(I)    =  HT(I - 1) - 0.005
0008:  1000   CONTINUE
0009:         HT(NO1) =  .001
0010:  C
0011:  C      INITIAL  PROJECTION  VELOCITY
0012:  C
0013:         DO  1050  I = 1, NO1
0014:         V(I)     =  SQRT(2. * 9.81 * HT(I))
0015:  1050   CONTINUE
0016:  C
0017:  C      DIAMETER
0018:  C
0019:         DO 1100  I = 1, NO1
0020:         DM(I)    =  (0.01795 * (HDM ** 0.75) *(UH ** 2) * DENGAS /
0021:        1            (V(I) * (VISL**0.2) * (ST**0.3) * DENPAR)) **(1/0.83)
0022:  1100   C ONTINUE
0023:         DO 1150 I = 1, NO
0024:         DMAV(I) =  (DM(I) + DM(I + 1) )/ 2.
0025:         V(I)     =  0.01795 * (HDM ** 0.75) * (UH ** 2 ) * DENGAS /
0026:        1            ((DMAV(I) ** 0.83) * (VISL ** 0.2) *(ST ** 0.3) *
0027:        2            DENPAR )
0028:  1150   CONTINUE
0029:  C
0030:  C      EXPERIMENTAL  HOLDUP  IN  EACH  INCREMENT
0031:  C
0032:         EXTOT    =  0.0
0033:         DO 1200 I = 1, NO
0034:         EXHOLD(I)  =  DISP(I) / 100. * XA
0035:         HOLD(I) =  EXHOLD(I) - ENHOLD
0036:         EXTOT    =  EXTOT + EXHOLD(I)
0037:  1200   CONTINUE
0038:         AREA     =  SINT(N, ULIM, BLIM)
0039:         DO 1250 I = 1, NO
0040:         EXDIS(I)    =  HOLD(I)
0041:  1250   CONTINUE
0042:         RETURN
0043:         END
0044:  C
0045:  C      UPWARD  TRAJECTORY
0046:  C
0047:         SUBROUTINE  UPWARD
0048:         COMMON DENPAR, DENGAS, VIS, NO, NO1, DIF, GRAD, GM, FRATE, IND
0049:         COMMON TOTHOG, CT, ICNT, JK, J, US, NDU, SC, QTOT, AMDA
0050:         COMMON /SET1/ V(100)
0051:         COMMON /SET2/ DMAV(100)
0052:         COMMON /SET5/ V2(100), DHDIFF(100), VU(100), HU(100), REU(100)
0053:         COMMON /SET6/ RESUP(100), AKGU(100)
0054:         COMMON /SET7/ VUP(100), HUP(100)
0055:  C
0056:         IF (IND .EQ. 1) GO TO 5000
0057:         DO 4950 I = 1, 100
0058:         HU(I)    =  0.0
0059:         VU(I)    =  0.0
0060:         VUP(I)   =  0.0
0061:         HUP(I)   =  0.0
0062:         V2(I)    =  0.0
0063:         REU(I)   =  0.0
0064:         AKGU(I) =  0.0
0065:         RESUP(I)    =  0.0
0066:         DHDIFF(I)   =  0.0
0067:  4950   CONTINUE
0068:  5000   V1       =  V(J) * 100.
0069:         VUP(1)   =  V1
0070:         HUP(1)   =  0.0
0071:         NDU      =  0
0072:         CT       =  - DENPAR / ((DENPAR - DENGAS) * 981. * 2.0)
0073:         DO 5100 K = 2, 100
0074:         V2(1)    =  V1 - 0.5
0075:         DO  5050  I = 1,100
0076:         IF (V2(I)) 5150,5150,5110
0077:  5110   DHDIFF(I)  = CT * (V2(I) ** 2 - V1 ** 2)
0078:         IF (DHDIFF(I) .GT. 0.5) GO TO 5060
0079:         V2(I + 1)  =  V2(I) - 0.5
0080:  5050   CONTINUE
0081:  5060   C        =  0.5
0082:         M        =  I
0083:         D        =  0
0084:         N        =  1
0085:         Y        =  TPLN(M, DHDIFF, V2, C, D, N)
0086:         V1       =  Y
0087:         VUP(K)   =  Y
0088:         HUP(K)   =  HUP(K - 1) + 0.5
0089:         NDU      =  NDU + 1
```

```
0001:  C
0002:  C
0003:  C      NEGATIVE  VELOCITY  -  FIND  TERMINAL  INCREMENT
0004:  C
0005:  C
0006:  5150   V2(I)    =  0.0
0007:         DHDIFF(I)  = CT * (V2(I) ** 2 - V1 ** 2)
0008:         DF       =  DHDIFF(I)
0009:         NDU      =  NDU + 1
0010:         VUP(K)   =  0.0
0011:         HUP(K)   =  HUP(K - 1) + DF
0012:         JAN      =  K
0013:         JN       =  JAN
0014:         DO  5200  ITN  = 1,JAN
0015:         HU(ITN) =  HUP(JN)
0016:         VU(ITN) =  VUP(JN)
0017:         JN       =  JN - 1
0018:  5200   CONTINUE
0019:  C
0020:  C      RESIDENCE  TIME
0021:  C
0022:         DO 5250 I = 1, NDU
0023:         RESUP(I)    =  (HU(I) - HU(I + 1)) * 2. / (VU(I) + VU(I+ 1))
0024:  5250   CONTINUE
0025:  C
0026:  C      REYNOLDS  NUMBER
0027:  C
0028:         DO  5300  I = 1, NDU
0029:         REU(I)   =  ( DENGAS * DMAV(J) * ABS ((VU(I) + VU(I+1))/200. - US))
0030:        1          / VIS
0031:  5300   CONTINUE
0032:  C
0033:  C      MASS  TRANSFER  COEFFICIENT
0034:  C
0035:         SC       =  0.61
0036:         DO 5350 I = 1, NDU
0037:         AKGU(I) =  (DENGAS * DIF * 2. / DMAV(J)) * ( 1 + 0.276
0038:        1           * REU(I) ** 0.5 * SC ** 0.333)
0039:  5350   CONTINUE
0040:         RETURN
0041:         END
0042:  C
0043:  C      DOWNWARD  TRAJECTORY
0044:  C
0045:         SUBROUTINE DOWN
0046:         COMMON DENPAR, DENGAS, VIS, NU, NOI, DIF, GRAD, GM, FRATE, IND
0047:         COMMON TOTNOG, CT, ICNT, JK, J, US, NDU, SC, QTOT, AMDA
0048:         COMMON /SET2/ DMAV(100)
0049:         COMMON /SET5/ V2(100), DHDIFF(100), VD(100), HU(100), RED(100)
0050:         COMMON /SET7/ RESDWN(100), AKGD(100)
0051:  C
0052:         IV = 1
0053:         NDD = NDU
0054:         IF (IV .EQ. 1) GO TO 8250
0055:         CT       =  -CT
0056:         IF (IND .EQ. 1) GO TO 7950
0057:         DO 7900 I = 1, 100
0058:         RED(I)   =  0.0
0059:         RESDWN(I)  =  0.0
0060:         AKGD(I) =  0.0
0061:  7900   CONTINUE
0062:  7950   NDD      =  0
0063:         DF       =  HU(1) - HU(2)
0064:         VD(1)    =  0.0
0065:         V1       =  0.0
0066:         DO  8200  K = 2, 100
0067:         V2(1)    =  V1 + 0.5
0068:         IF (DF .LT. 0.5) GO TO 8050
0069:         DO 8000 I = 1, 99
0070:         DHDIFF(I)  =  CT * (V2(I) ** 2 - V1 ** 2)
0071:         V2(I + 1)  =  V2(I) + 0.5
0072:  8000   CONTINUE
0073:         GO TO 8150
0074:  8050   DO 8100 I = 1, 99
0075:         DHDIFF(I)  =  CT * (V2(I) ** 2 - V1 ** 2)
0076:         V2(I + 1) = V2(I) + 0.5
0077:         KN       = I
0078:  8100   CONTINUE
0079:         I        =  KN
0080:  8150   C        =  DF
0081:         M        =  I
0082:         D        =  0
0083:         N        =  1
0084:         Y        =  TPLN(M, DHDIFF, V2, C, D, N)
0085:         V1       =  Y
0086:         VD(K)    =  Y
0087:         NDD      =  NDD + 1
0088:         IF (NDD .EQ. NDU) GO TO 8250
0089:         DF       = 0.5
```

```
0002:  C      RESIDENCE  TIME
0003:  C
0004:  8250   DO 8300 I = 1, NDD
0005:         RESDWN(I)  =  (HU(I) - HU(I + 1))  * 2. / (VD(I) + VD(I + 1))
0006:  8300   CONTINUE
0007:  C
0008:  C      REYNOLDS  NUMBER
0009:  C
0010:         DO 8350 I = 1, NDD
0011:         RED(I)  =  ( DENGAS * DMAV(J) * ABS ((VD(I) + VD(I+1))/200. - US))
0012:        1          / VIS
0013:  8350   CONTINUE
0014:  C
0015:  C      MASS  TRANSFER  COEFFICIENT
0016:  C
0017:         DO 8400 I = 1, NDD
0018:         AKGD(I) =  (DENGAS * DIF * 2. / DMAV(J)) * ( 1 + 0.276
0019:        1           * RED(I) ** 0.5 * SC ** 0.333)
0020:  8400   CONTINUE
0021:         RETURN
0022:         END
0023:  C
0024:  C      VOLUME  FLOW  RATE  OF  LIQUID  LEAVING  THE  PLATE
0025:  C
0026:         SUBROUTINE VOLUME
0027:         COMMON DENPAR, DENGAS, VIS, NO, NO1, DIF, GRAD, GM, FRATE, IND
0028:         COMMON TOTNOG, CT, ICNT, JK, J, US, NDU, SC, QTOT, AMDA
0029:         COMMON /SET2/ DMAV(100)
0030:         COMMON /SET3/ HOLD(100)
0031:         COMMON /SET5/ V2(100), DHDIFF(100), VD(100), HU(100), RED(100)
0032:         COMMON /SET6/ RESUP(100), AKGU(100)
0033:         COMMON /SET7/ RESDWN(100), AKGD(100)
0034:         COMMON /SET8/ ACC(100), Q(100), VOL(100), AREA(100), ARACC(100)
0035:         COMMON /SET9/ ANOG(100), AKGT(100), TME(100)
0036:         COMMON /SET10/ AKGUP(100), AKGDW(100), AREAU(100), AREAD(100)
0037:         COMMON /SET20/ HLDTOT(100), HL(100)
0038:         COMMON /SET23/ STD(100), CDF(100), STDSE(100), HLD(100)
0039:  C
0040:         REAL    NUM(100)
0041:         IF (IND .EQ. 1) GO TO 8950
0042:         DO 8900 I = 1, 100
0043:         AREAU(I)   =  0.0
0044:         AREAU(I)   =  0.0
0045:         AKGDW(I)   =  0.0
0046:         AKGUP(I)   =  0.0
0047:         AKGT(I) =  0.0
0048:         Q(I)    =  0.0
0049:         TME(I)  =  0.0
0050:         ACC(I)  =  0.0
0051:         VOL(I)  =  1.0
0052:         ARACC(I)   =  0.0
0053:         AREA(I)    =  0.0
0054:  8900   CONTINUE
0055:  8950   ICNT    =  ICNT + 1
0056:         IC      =  ICNT - 1
0057:         IF (IND .EQ. 0 )NOC = NDU
0058:         IND     = 1
0059:         DO 9000 I = 1, NDU
0060:         TME(IC + I)  =  RESUP(I) + RESDWN(I)

0061:         AKGT(IC + I) =  AKGU(I) + AKGU(I)
0062:         AKGUP(IC + I) =  AKGU(I)
0063:         AKGDW(IC + I ) =  AKGD(I)
0064:  9000   CONTINUE
0065:         Q1      = (HOLD(ICNT) - ACC(ICNT))/ TME(ICNT)
0066:         Q(ICNT) =  Q1
0067:         QTOT    =  QTOT + Q(ICNT)
0068:         DO 9050 I = ICNT, NOC
0069:         VOL(I)  =  Q1 * TME(I)
0070:         ACC(I)  =  ACC(I) + VOL(I)
0071:         AREA(I) =  6 * VOL(I) / DMAV(J)
0072:         AREAU(I)=  6. * VOL(I) / (DMAV(J) * 2.)
0073:         AREAU(I)=  6. * VOL(I) / (DMAV(J) * 2.)
0074:         ARACC(I)   =  ARACC(I) + AREA(I)
0075:         ANOG(I) =  ( AKGUP(I) * AREAU(I) + AKGDW(I) * AREAD(I) ) / GM
0076:         TOTNOG  =  TOTNOG + ANOG(I)
0077:         HLDTOT(I)  = (3.1415927 * DMAV(J) ** 3 *STDSE(J) *TME(I) ) / 6.
0078:         HL(I)   =  HL(I) + HLTOT(I)
0079:  9050   CONTINUE
0080:         DO 9100 I = 1, 100
0081:         VOL(I)  =  0.0
0082:         RESUP(I)   =  0.0
0083:         RESDWN(I)  =  0.0
0084:         TME(I)  = 0.0
0085:         RED(I)  =  0.0
0086:         AKGU(I) =  0.0
0087:         AKGD(I) =  0.0
0088:         AKGT(I) =  0.0
0089:         AREAU(I)   =  0.0
0090:         AREAU(I)   =  0.0
0091:         AKGUP(I)   =  0.0
0092:         AKGDW(I)   =  0.0
0093:         AREA(I) =  0.0
0094:         HLDTOT(I)  =  0.0
0095:  9100   CONTINUE
0096:         RETURN
00 7:          ND
```

```
0001:  C
0002:  C      POLYNOMIAL  FITTING
0003:  C
0004:         SUBROUTINE CURVE
0005:         COMMON DENPAR, DENGAS, VIS, NO, ND1, DIF, GRAD, GM, FRATE, IND
0006:         COMMON /SET4/ Y(100), X(100), DM(100), EXHOLD(100)
0007:         COMMON /SET21/ COR(10,2), TAB(51,2), G(10), C(10)
0008:  C
0009:         READ (5, 9) N
0010:  9      FORMAT (I3)
0011:         READ (5, 1) (Y(I), X(I), I= 1, 9)
0012:  1      FORMAT (2F9.4)
0013:         J1       =  10
0014:         M        =  9
0015:         CALL POLYA(X,Y,N,XSC,XSH,M,J1,TAB,COR,G)
0016:         SHIFT1 = 0.
0017:         SCALE  = 1.
0018:         DO 6 M = 1,9
0019:         CALL POLYB(C,SHIFT1,SCALE,N,XSC,XSH,M,J1,TAB,COR,G)
0020:         MPLUS1 = M+1
0021:         WRITE(6,2) M, (C(I),I=1,MPLUS1)
0022:       2 FORMAT(/ 18H ORDER OF FIT.....,I2//(1X, 9E14.5))
0023:         DO 5 I =1,N
0024:         CALL POLYC(X(I),YY,XSC,XSH,M,J1,COR,G)
0025:         WRITE(6,4) X(I),YY
0026:       4 FORMAT(1X, 2E12.4)
0027:       5 CONTINUE
0028:       6 CONTINUE
0029:         RETURN
0030:         END
0031:  C
0032:  C      TWO  PARAMETER  FIT  OF  DISPERSION  DENSITY  PROFILES
0033:  C
0034:         SUBROUTINE FRQCY
0035:         DIMENSION X(2), R(19), W(132)
0036:         COMMON /SET51/ DPM, STDV
0037:         EXTERNAL RESID, MONIT
0038:         M1       =  19
0039:         N1       =  2
0040:         X(1)     =  DPM
0041:         X(2)     =  STDV
0042:         FTOL     =  X02AAF(RR)
0043:         DELTA    =  SQRT(FTOL)
0044:         STEPMX   =  0.01
0045:         IW       =  2 * N1 * (M1 + N1) + 2 * M1 + 5 * N1
0046:         IPRINT   =  1
0047:         MAXCAL    = 100
0048:         IFAIL    =  1
0049:         CALL  E04FBF (M1, N1, X, R, F, FTOL, DELTA, STEPMX, W, IW, RESID
0050:        *, MONIT, IPRINT, MAXCAL, IFAIL)
0051:         WRITE (6, 9992) F
0052:  9992   FORMAT (25H FINAL SUM OF SQUARES IS , F12.4)
0053:         WRITE (6, 9993) (X(I), I = 1,N1)
0054:  9993   FORMAT (13H AT THE POINT, 2F12.4)
0055:         WRITE (6,9994) (R(I), I = 1,M1)
0056:  9994   FORMAT (13H WITH RESIDS , 3F12.4)
0057:         WRITE (6,9995) IFAIL
0058:  9995   FORMAT (21H   THIS HAS ERROR NO , I3)
0059:         RETURN
0060:         END
```

```
0061:  C
0062:  C      CALCULATE  RESIDUALS
0063:  C
0064:         SUBROUTINE RESID(M1, N1, X, R)
0065:         DIMENSION X(2), R(19), W(132)
0066:         COMMON DENPAR, DENGAS, VIS, NO, NO1, DIF, GRAD, GM, FRATE, IND
0067:         COMMON GRTOT
0068:         COMMON /SET2/ DMAV(100)
0069:         COMMON /SET4/ DISP(100), HT(100), DM(100), EXHOLD(100)
0070:         COMMON /SET15/ AREA, XA, EXDIS(100)
0071:         COMMON /SET20/ HLDTOT(100), HL(100)
0072:         COMMON /SET23/ STD(100), CDF(100), STDSE(100), HLD(100)
0073:         COMMON /SET22/ THDIS(100), FRCT(100)
0074:         COMMON /SET31/ DPM, STDV
0075:         DPM      =  X(1)
0076:         STDV     =  X(2)
0077:         DO 5585 I = 1,50
0078:         STD(1)   =   (DM(I) - DPM) / STDV
0079:  5585   CONTINUE
0080:         IFAIL = 0
0081:         DO 5600 I = 1,50
0082:         IF (IFAIL .LT. 0) PRINT, "IFAIL"
0083:         CDF(I)   =  S15ABF(STD(I), IFAIL)
0084:  5600   CONTINUE
0085:         FRTOT    = 0.0
0086:         FRCT(1) =  CDF(1)
0087:         DO 5610 I = 2,49
0088:         FRCT(I) = CDF(I + 1) - CDF(I)
0089:         FRTOT    =  FRTOT + FRCT(I)
0090:  5610   CONTINUE
0091:         DO 5620 I = 1,49
0092:         STDSE(I) =FRCT(I)/ FRTOT
0093:  5620   CONTINUE
0094:         DO 10 J = 1, NO
0095:         CALL UPWARD
0096:         CALL DOWN
0097:         CALL VOLUME
0098:  10     CONTINUE
0099:         DO 6050 I = 1, NO
0100:         GRTOT    =  GRTOT + HL(I)
0101:  6050   CONTINUE
0102:         DO 6100 I = 1, NO
0103:         HLD(I)   =  HL(I) * AREA / GRTOT
0104:         THDIS(I)=  HLD(I) /( 0.5 * XA)
0105:  6100   CONTINUE
0106:         DO 6200 I = 1, NO
0107:         R(I)     =  EXDIS(I) - THDIS(I)
0108:  6200   CONTINUE
0109:         RETURN
0110:         END
0111:         SUBROUTINE MONIT(M1, N1, X, R, FC, NCALL)
0112:         DIMENSION X(2), R(19), W(132)
0113:         WRITE (6, 9991) NCALL, FC
0114:  9991   FORMAT (6H AFTER, I4, 18H    CALLS OF RESID,, 13H'THE SUM OF S,
0115:        *9HQUARES IS, F12.4)
0116:         WRITE (6, 9996) (X(I), I = 1,N1)
0117:  9996   FORMAT (13H AT THE POINT, 2F12.4/)
0118:         RETURN
0119:         END
0120:  C
```

```
0121:  C
0122:         FUNCTION CFN(X)
0123:         CFN      =  .24123E-01 + .11350E-01*X + .21110E-02*X**2 -
0124:        1           .69794E-03 * X**3 + .64290E-04 * X **4 - .28007E-05 * X
0125:        2           **5 + .59806E - 07 *X **6 - .50468E-09 *X **7
0126:         RETURN
0127:         END
0128:  @
```